2016

A Fractal-Based Mathematical Model for Cancellous Bone Growth Considering the Hierarchical Nature of Bone

Stephanie Marie Suhr
Wright State University

A FRACTAL-BASED MATHEMATICAL MODEL FOR CANCELLOUS BONE GROWTH CONSIDERING THE HEIRARCHICAL NATURE OF BONE

A thesis submitted in partial fulfillment of the
requirements for the degree of
Master of Science in Biomedical Engineering

By

STEPHANIE MARIE SUHR
B.S.B.M.E., Wright State University, 2015

2016
Wright State University

WRIGHT STATE UNIVERSITY

GRADUATE SCHOOL

January 11, 2017

I HEREBY RECOMMEND THAT THE THESIS PREPARED UNDER MY SUPERVISION BY Stephanie Marie Suhr ENTITLED A Fractal-Based Mathematical Model for Cancellous Bone Growth Considering the Hierarchical Nature of Bone BE ACCEPTED IN PARTIAL FULFILLMENT OF THE REQUIREMENTS FOR THE DEGREE OF Master of Science in Biomedical Engineering.

_____

Tarun Goswami, D.Sc.
Thesis Director

_____

Jaime Ramirez-Vick, Ph.D. .
Chair, Department of Biomedical Engineering

Committee on
Final Examination

_____
Tarun Goswami, D.Sc.

_____
Jamie Ramirez-Vick, Ph.D.

_____
Richard Laughlin, M.D.

_____
Robert E. W. Fyffe, Ph.D.
Vice President for Research and
Dean of the Graduate School

ABSTRACT

Suhr, Stephanie Marie. M.S.B.M.E. Department of Biomedical Engineering. Wright State University, 2016. A Fractal-Based Mathematical Model for Cancellous Bone Growth Considering the Hierarchical Nature of Bone.

The hierarchical structure of bone alone is not comprehensive enough to provide morphological explanation of how the size and arrangement of the trabeculae within cancellous bone affect load distribution, particularly concerning deterioration of bone in elderly patients. The collagen network and hydroxyapatite play a large role in defining the shape of trabeculae in cancellous bone despite that the arrangement and size is seemingly random. The growth of plates and rods in cancellous bone is mainly due to loading and stress lines within the bone, but mathematical predictive models can be developed using fractal analysis to show how bone may grow under different circumstances and what fractal density infers about the arrangement of the trabeculae as well as the strength of the bone, as fractal density is a better indicator of bone strength than bone mineral density. Using a micro-CT scan of the distal end of a human radius, the plate and rod quantity and length was measured along with the angles between the plates and rods. The volume fraction of plates and rods was calculated for each slice. The fractal density was analyzed using the box-counting method, and within this method, different combinations of scaling methods, grid placement, and rotation were utilized to see which was the most accurate. Relationships

between the measured parameters were examined to see which had the greatest effect on the perceived strength of the bone.

TABLE OF CONTENTS

Page

LIST OF FIGURES

LIST OF TABLES

1. INTRODUCTION

Bone in the human body is the framework for all of the soft tissue as well as the primary load-bearing construct for day-to-day activities. Bone can withstand a significant amount of stress, and is most unique due to its remodeling capabilities and utility of varying structures in vivo at both a macro- and micro-level in order to most efficiently distribute the stresses through the bones so as not to overload them to failure. In the case of an osteoporotic patient or someone who is needing a bone implant or replacement, understanding the nuances of the bone growth is vital since the body is experiencing difficulty remodeling bone on its own; in order to maintain the delicate balance of stresses on the bone for proper bone growth, the branching of cancellous bone and the implications that both the macro-structure and micro-structure have on overall bone strength need to be analyzed very carefully to prevent failure of the bone or failure of the implant due to improper stress shielding or bony ingrowth or on-growth.

1.1 MATERIAL-BASED COMPOSITION OF BONE

At the top level, bone can be separated into two large parts: cortical bone and cancellous bone. Cortical bone, while composing 80% of the bone mass, doesn't make up the majority of the surface area of bone because it is so dense. Cancellous bone has a unique, porous, branching, honeycomb-like structure that is composed of trabeculae in the epiphyseal ends of long bones and the bodies of vertebrae, and makes up 20% of the bone mass but boasts a very high total bone surface area. However, despite differences in spatial arrangement, the micro-structural composition of cancellous and cortical bone is the same. Exact mineral compositions vary from

person to person, but it is generally accepted that bone mass is composed of 10% water, about 65% - 70% percent bone mineral (hydroxyapatite), and around 10% - 20% collagen. The presence of polysaccharides and proteoglycans is 1% or less of the total bone mass. Cortical bone is significantly denser than cancellous bone, with a density of 1.85 g/cm^3; cancellous bone has a density of 0.05 to 1.1 g/cm^3, depending on location. Density properties of the bone types vary depending on age of the subject or conditions such as osteoporosis, rheumatoid arthritis, lupus, or diabetes.

Cancellous bone density differs from tissue density, which is specific to the individual trabeculae in cancellous bone. The tissue density of trabeculae has a relatively small variation, with values from 1.6 – 2.0 g/cm^3, but the tissue density varies with a higher frequency than overall bone density (and cancellous density in particular) due to the higher turnover rate of tissue. Because cancellous bone has a higher surface-to-volume ratio than cortical bone, the rate at which old bone is resorbed is much higher, and 10% – 14% reduction in tissue density from cancellous to cortical bone can be attributed to the remodeling rate increase.

1.2 MATERIAL PROPERTIES

Cancellous bone properties, as a result of the intense and frequent remodeling process described above, can vary as much as an order of magnitude depending on the region of the skeleton being examined. A non-linear stress-strain curve is seen when cancellous bone is loaded in uniaxial compression or tension, and the Young's modulus (E) and the shear modulus have proven to have a strong correlation with the tissue density. That being said, E and the shear modulus must be evaluated on a case-by-case basis from the evaluated density, which can help determine the overall strength of the cancellous bone segment as E is strongly correlated to ultimate strength. In contrast, the ultimate strain of cancellous bone and yield strain have no

correlation with the tissue density. Yield strain by compressive forces vary from 0.72 to 0.86, depending on the skeletal region, and yield strain in tension has a range of 0.60 to 0.70, which is lower than the yield strain by compressive forces. Since the skeleton is subjected almost exclusively to compressive forces, the bone structure is better organized to distribute the compressive forces than the tension forces.

Cancellous bone does demonstrate different mechanical properties in different directions, which makes cancellous bone anisotropic; these directional differences in the mechanics of cancellous bone as a whole are primarily contributed to the alignment of the trabeculae. The Young's Modulus decreases by as much as 50% when a force is applied perpendicularly to the orientation of the trabeculae, and with the same type of force application, the ultimate strength is decreased by as much as 45%. When aligned in the transverse plane, microstructure directionally dissipates deformation energy without crack propagation. Crack propagation requires energy dependent on the alignment of the collagen fibrils; crack extension energy is seen to differ by almost two orders of magnitude between a crack that is closely aligned with the collagen fibrils and one which progressed perpendicular to the collagen orientation. Material bone is presented in an array of mineralized connective tissues that share some common structural and mechanical characteristics. Both cortical and cancellous bone begin as hyaline cartilage, a precursor to most bones in the body that is also produced as a principal material in bone lengthening and bone repair [2]. The chondroblasts, which compose the cartilage, produce a matrix that creates a rounded chondrocyte occupying a lacunar space within the matrix. The matrix contains collagen type I most commonly but also includes collagen types III, VI, and V as well as proteoglycans to hold water, making the cartilage more durable [1,3]. Bone growth begins to occur on an interstitial plane, only changing to an appositional growth as the bone reaches maturity and

Mechanical Property	n	Age	Density (g/cm3)	$Y = A \times X^B$		
				A	B	r^2
Young's modulus (MPa)[a]	142	67 ± 15 (61–68)	0.27 (0.09–0.75)	8920 (7540–10,550)	1.83 (1.72–1.94)	0.88
Shear modulus (MPa)[b]	42	Bovine	NR[b]	2.09	1.9	0.84
σy (MPa, tension)[a]	52	65 ± 14 (61–68)	0.29 (0.25–0.34)	31.35 (23.81–41.29)	1.67 (1.58–1.77)	0.86
σy (MPa, compression)[a]	68	65 ± 14 (61–68)	0.27 ± 0.17 (0.24–0.32)	51.15 (41.53–62.99)	1.85 (1.72–1.99)	0.91
σult (MPa tension)[c]	22	54 ± 11 (27–82)	0.19 ± 0.04 (0.09–0.29)	13.3	1.07	0.47
σult (MPa compression)[c]	22	54 ± 11 (27–82)	0.17 ± 0.04 (0.07–0.27)	33.2	1.53	0.68
τ_{ult} (MPa)[b]	15	Bovine	NR[b]	72.74	1.86	0.64
K_Q (MPa/$m^{1/2}$, crack oriented perpendicular to trabeculae)d	166	82 ± 6.8 (65–99)	Range: 0.25–1.10 g/cm^3	0.67	1.58	0.62
K_Q (MPa/$m^{1/2}$, crack oriented parallel to trabeculae)d	169	82 ± 6.8 (65–99)	Range: 0.25–1.10 g/cm^3	0.54	1.6	0.56

Table 1. The term *n* in this table is defined as the number of samples evaluated during the original experiment. The age is measured in years, and the density in grams per cubic centimeter. The term *A* acts as the average value for the mechanical property, with *B* as the significance placed onto the measured density value *X,* to determine the overall mechanical property *Y.* The mechanical properties in the far left column are related to the density in the fourth column by the r^2 values on the far right. Based on the r^2 values, the BMD appears to have the strongest relationship to the compressive stress in the y-direction, followed by the Young's Modulus. Through testing, these relationships will be compared later on to see if they hold similar trends with fractal density (FD).

moves toward the epiphyseal ends. The bone itself, once formed, consists of extracellular bone matrix and bone cells, but the composition of the bone matrix is ultimately responsible for the characteristics of bone. The bone matrix of mature bone is normally about 35% organic and 65% inorganic material, with the inorganic material primarily consisting of hydroxyapatite (HA): $Ca_{10}(PO_4)_6(OH)_2$ [4,5,6]. The bone draws all strength from the HA crystals while maintaining its flexibility and durability from the collagen.

2. LITERATURE REVIEW

Trabecular bone is morphologically and functionally different from compact bone at the tissue level, but both are composed of lamellae at the micrometer-scale level. As lamellar bone, trabeculae fit into an arbitrary hierarchical structure that better defines the three-dimensional characteristics of the way trabeculae branch off. Osteons are a prominent component of bone, in which alternating orientations of collagen fibrils can be seen in lamellar layers, but the adjacent layers may have a very substantial angular offset as noted by Gebhart [7]. It has also been noted in the mineral phase of bone that calcium, phosphate, and carbonate are the primary constituents of bone material; together, they make up hydroxyapatite. However, through polarized light and x-ray diffraction, it was shown that the c-axes of the HA crystals are aligned with the collagen fiber axes [8,9], and furthermore, the crystals appeared to be plate shaped and arranged onto the type I collagen fibrils. **Figure 1** shows a general visual description of the events described above [10].

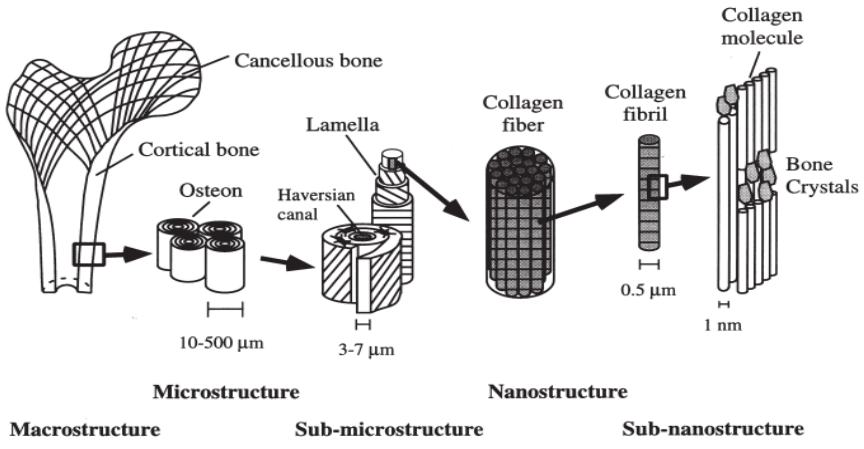

Figure 1. The hierarchy of cancellous bone from largest to smallest components.

2.1 LEVEL I: MAJOR COMPONENTS

The major components as defined by Weiner and Wagner are dahllite (carbonated apatite, or hydroxyapatite) crystals, type I collagen fibrils, and water [10,11]. Hydroxyapatite is the only mineral component present in the bone, there are more non-collagenous proteins (NCP) present in the bone besides just the type I collagen, but typically, the total protein content is made up of only 10% NCPs [12]. An overall diagram of the hierarchical nature can be seen in **Figure 2**.

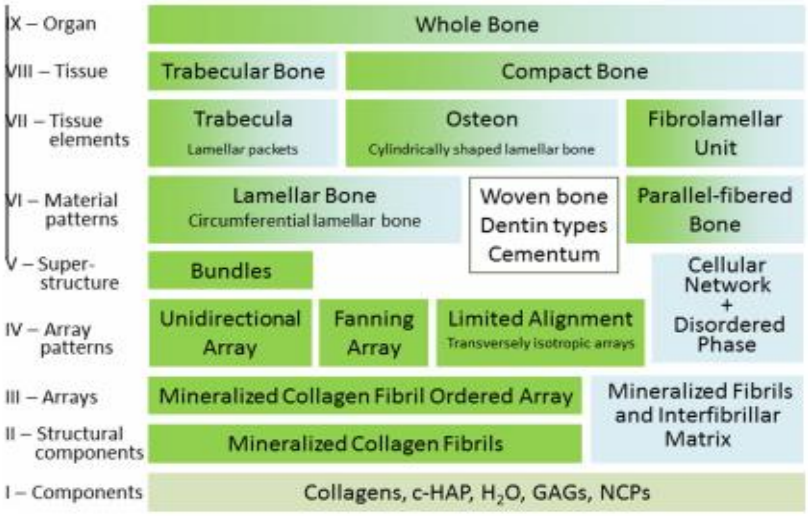

Figure 2. The ordered components for both compact and trabecular bone. Parallel chains of hierarchy can be seen between the two bone types, but collagen is the basis for both.

These crystals within the bone are of average lengths and widths of 50 x 25 nm [8-10]. The thicknesses are surprisingly uniform, but are highly disordered at an atomic level due to carbonate being a volatile additive. The crystals were measured in both transmission electron microscopy (TEM) and small angle x-ray scattering (SAXS), the latter which proved to be more reliable in measuring the smallest dimensions; the thicknesses only measured 1.5-4.0 nm [13]. The crystals plate-shape is unusual due to dahllite's hexagonal symmetry, but the octacalcium phosphate transition phase could have affected shape [14]. The Young's modulus of carbonated

HA created synthetically is 109 GPa, but for a large single crystal of HA, the Young's modulus is 114 GPa. Measurements have not been found on extracted HA crystals [15].

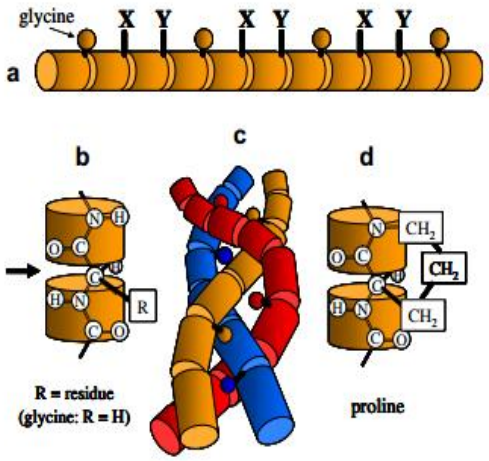

Figure 3. The triple-helix structure of collagen is a repetitive but staggered amino acid sequence that allows HA crystals to sit in and alongside it in the fibril form.

Type I collagen is the primary collagenous component, a protein, though as mentioned before, types III. VI, and V are present in much smaller quantities [16]. Type I collagen is a triple helix with molecule length of about 300 nm [17], as seen in **Figure 3**, and is a very large protein with a repetitive amino acid sequence. After the molecules go through a self-assembly process, the arrangement is so that each strand is parallel, but staggered, so that there are small holes in between the strands [18,19]. The staggered length is about 67 nm, leaving the molecules with about 5 repeating sections each, with a gap of about 35 nm to the next molecule in the axial direction. Only a few covalent links cross between the strands that mature with age [20].

The most direct measures of the mechanical properties of collagen have been obtained by studying TC monomers and fibrils formed from type I collagen. In 2006, Buehler estimated the fracture strength of a TC monomer to be 11 GPa, which is significantly greater than that of a collagen fibril (0.5 GPa) [21]. This difference is reasonable, given that fracture of a TC monomer requires unraveling of the triple helix and ultimately breaking of covalent bonds, whereas

fracture of a fibril does not necessarily require the disruption of covalent bonds. For comparison, the tensile strength of collagen in tendon is estimated to be 100 MPa [22]

The Young's modulus of a TC monomer is E = 6–7 GPa [23,24] whereas AFM measurements show that dehydrated fibrils of type I collagen from bovine Achilles tendon [22] and rat tail tendon [21]have $E \approx 5$ GPa and $E \leq 11$ GPa, respectively. Because collagen fibrils are anisotropic, the shear modulus (which is a measure of rigidity) is also an important measure of the strength of a collagen fibril. In 2008, AFM revealed that dehydrated fibrils of type I collagen from bovine Achilles tendon have G = 33 MPa [25]. Hydration of these fibrils reduced their shear modulus significantly, whereas carbodiimide-mediated cross-linking increased their shear modulus. It is noteworthy that a certain level of cross-linking is favorable for the mechanical properties of collagen fibrils, but excessive cross-linking results in extremely brittle collagen fibrils [27], a common symptom of aging.

While many non-collagenous proteins exist in the bone, none are unique to the bone itself. Many proteoglycans, however, such as biglycan and decorin, are thought to play a role with a few bone-related NCPs such as osteocalcin, matrix Gla protein, osteonectin, and more, in bone formation. The bone formation aspect of these proteins makes them valuable in that they can help define the branching nature of the trabeculae, but very little is known about their locations or specific functions [29].

The most abundant resource in the body, water, is also found in bone. Water is particularly of interest as it is found in all hierarchy levels of bone, but it is the most significant in the first level because it is of a larger size, comparatively, as components get smaller. For example, the equatorial spacing in wet collagen fibrils (non-mineralized) is about 1.6 nm, but in dried fibrils,

the spacing reduces to 1.1 nm [30]. In addition, dehydrated lamellar bone is more likely to contract perpendicular to lamellar edge than in the orthogonal direction.

All four components (hydroxyapatite, collagen, NCP's, and water) have vastly different mechanical properties individually. As a result, the material that contains all of them at once is very clearly a composite. Organically, the host framework has a triple-helical structure, but past the assemblage of the fibrils (forming fibers), within a fibril there is a crystalline structure with orthotropic symmetry as seen in **Figure 4** [31]. The bone can be considered a plate-reinforced composite, with the plates having a hexagonal atomic lattice shape despite the actual "plate" shape. These arrangements implies three planes of symmetry orthogonal to each other, as seen in Figure 5, represented by Weiner and Wagner.

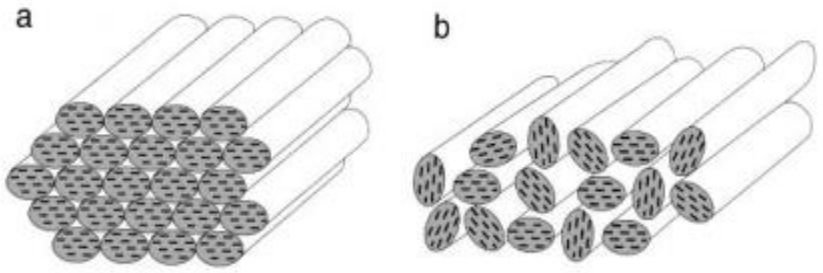

Figure 4. A demonstration of the orthotropic symmetry within a collagen fibril. The HA crystals dotted along the collagen molecule are not lined up in only one direction, as shown in (a), but rather have material properties that vary along three different (but mutually orthogonal) rotational axes of symmetry, which can be seen in (b).

2.2 LEVEL II: THE MINERALIZED COLLAGEN FIBRIL

Collagen fibrils are organized into larger fibers which run along the lamellar sections of the bone with diameters of 80-120 nm [32]. The HA crystals sit in the gaps within the fibrils in the helical structure offsets. However, as the crystals grow, they actually push out of their hole-regions and move the helical structures of the collagen. The actual interface between the collagen surface and the HA crystals is poorly understood, but the collagen framework does seem to

orient and control crystal growth does insinuate an ideally strong interface. The crystals seem to grow as a jacket around the collagen fibrils, making them much stronger as a composite than by themselves. The fibrils are separated by a thin layer only 1-2 nm thick of extrafibrillar matrix.

The assembly process of the Type I collagen arrays is complex and differs *in vivo* versus *in vitro*. The bundles are nearly always organized along their lengths, but the bundle size is not discriminate. The single, unidirectional array pattern is most common in lamellar bone, as seen in **Figure 5**. A fanning array pattern is also common in lamellar bone, but in it, the orientations of the fibril array change gradually with length, typically when collagen concentrations are high [12,18]. Finally, a disordered material is found in between the collagen layers which are more similar to arrays than individual fibers, but have no orientation. The structure is representative of woven bone, although the individual fibrils are not randomly oriented groups.

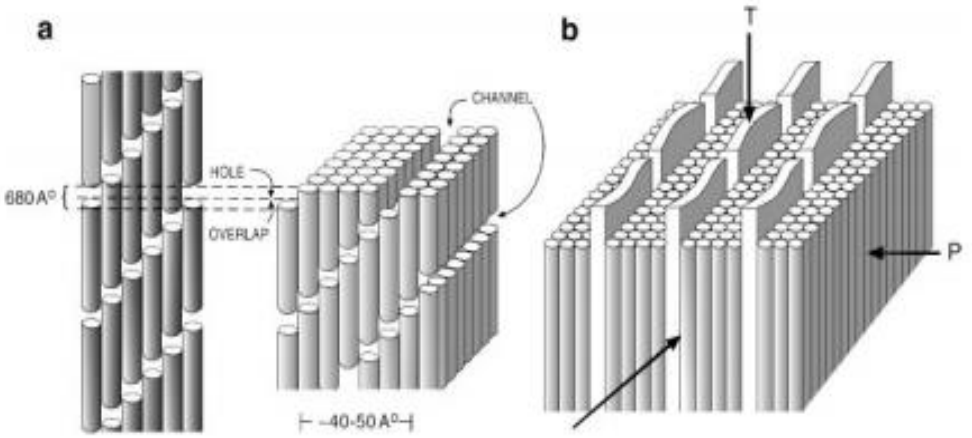

Figure 5. Offsets between the fibrils allow for a more comprehensively strengthened composite in (a). Part (b) demonstrates the disordered material found between collagen layers.

There are four overall patterns of arrays: parallel, woven fibers, plywood-like structures, and radial fibril arrays [24]. Trabecular bone is the focus of this paper, and as lamellar and assumed parallel array arrangement is the most common type of trabecular bone in the body, the other three arrangements will not be discussed.

2.3 THE COLLAGEN NETWORK IN TRABECULAE

Arrangement and mineralization are the most important considerations of trabecular bone quality. Most trabeculae are thin, 50-400 micrometers, and consist of interconnecting plates and rods. The plates are aligned longitudinally along the stress lines through the bone to bear the most weight, while the rods simply connect everything together. Several lamellae with osteocytes located in lacunae between lamellae create the bulk of trabecular bone. Each osteocyte is associated with other osteocytes through canaliculi [2]. Typically, no blood vessels can penetrate the trabeculae, so osteocytes obtain nutrients through the canaliculi. Mature trabecular bone is lamellar so that collagen fibers of one lamella lie parallel to one another, but at an angle adjacent to lamellae.

Reznikov (2014) found "an interesting correlation between the orientations of the collagen fibrils in trabecular bone matrix at one hierarchical level and the orientations of the trabeculae themselves at another hierarchical level" through the use of the inter-trabecular angle [14]. The lamellae of trabecular bone is organized into "lamellar packets" as seen in Figure 6 that all have varying angles toward each other. Unlike remodeling within compact bone which does not usually change the overall bone morphology, remodeling of trabecular elements gradually sculpts a new trabecular surface and eventually leads to re-orientation and re-shaping of individual trabeculae, and ultimately the whole trabecular network. Some of this remodeling can be seen demonstrated in **Figure 6.** Trabecular angles are typically seen at 30 and 70 degrees, but the lamellae in this case seem to be at a very low angle of 20-30 degrees. Overall, there was a strong correlation in Reznikov's work that showed the inter-trabecular angles were related to the orientation of the lamellar packets, particularly in the non-osteoporotic, young individual; with

age, the cross-linking between fibers deteriorates and there is generally less control over the growth of the collagen fibers [33].

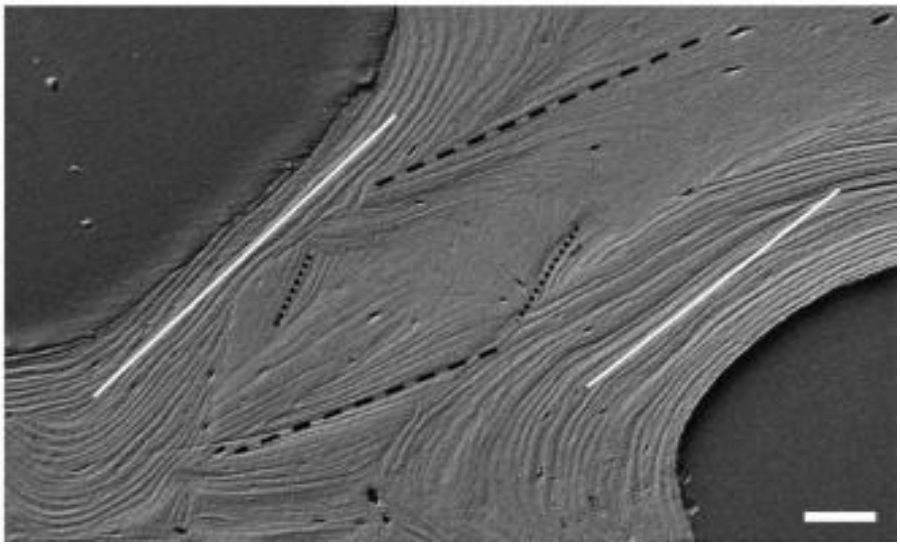

Figure 6. The near-parallel white lines show the original orientation of the lamellar packets that compose the trabecular bone, but the dotted black lines show that remodeling within the trabeculae has taken place, and these lamellar packets branch in directions different to that of the white lines.

2.4 STRENGTH OF CANCELLOUS BONE

The strength and toughness of bone can be attributed in part to its anisotropic properties, as the microstructure directionally dissipates deformation energy without crack propagation. Crack propagation requires energy dependent on the alignment of the collagen fibrils; crack extension energy is seen to differ by almost two orders of magnitude between a crack that is closely aligned with the collagen fibrils and one which progressed perpendicular to the collagen orientation. This next section will discuss overall mechanical properties of bone as a result of its microstructure.

The overarching microstructure of the fibrils is a flexible, elastic organic component that is reinforced by a very stiff inorganic component. The mineral's nanoparticles, despite their extreme toughness and brittleness, can actually be seen to deform elastically at first, in

juxtaposition to bulk apatite which is shown to reach a maximum strain of only half that of the nanoparticles. The loading results of individual fibril components is similar to the model of load transfer in the bone matrix, which reinforces the idea of hierarchical bone deformation as well as structure.

The mineralized fibrils are long, parallel, and slightly separated, but have very strong cross-linkage as evidenced by tensile testing. Tensile loads applied to the tissue resolve into tensile deformation of the mineralized fibrils and a shearing deformation in the extrafibrillar matrix, which contains the proteoglycans and NCPs. The shear stiffness was originally unanticipated, but may be explained by a series of calcium-dependent sacrificial bonds, where segments of molecules in the extrafibrillar matrix are connected by charge interactions. During deformation, the matrix and fibril interface is pushed past the yield point, and the two move past each other consequently breaking and re-forming the bonds. This movement gives this layer a glue-like texture in which the shear stiffness is increased but still relatively weak and ductile. Plastic deformation in the bone may be partially attributed to plastic deformation occurring in the "glue" layer in-between the fibrils. These two components in conjunction give the tissue stiffness from the fibers and toughness from the plastic deformation of the glue-like extrafibrillar layer.

The mineral content of bone with parallel-fibered structure is around 65%, which is representative of most bone types (except perhaps woven bone, which is premature and lacking in lamellar structure). Though stiff, the hardness values differ in the three orthogonal directions.

2.5 PREDICTING CANCELLOUS BONE GROWTH

While cancellous bone takes up much more surface area than cortical bone, it doesn't have the same strength, with a yield point in compression of only 60 GPa instead of near 200 GPa like

cortical bone. However, studies show that the bone mineral density (BMD) is less of a predictor for bone strength than originally anticipated, and fractal models of trabecular growth actually have a much stronger correlation when it comes to strength []. A stronger bone will have more networking within the cancellous portion than a trabecular section with a higher BMD and less branching [34].

While not as difficult as taking images of the individual lamellar packets, taking images of the spongy bone with a high enough resolution to determine the trabecular structure requires a 3T MRI or, preferably, a micro-CT scan or something of comparative quality. Typically sections are approximately 20-30 mm, with a Volume of Interest (VOI) region spanning 500 – 1000 micro-CT slices. Detection of the trabecular network can be done in Mimics using an auto-detection method. Trabecular growth is still a mystery as the branches, though centralized along stress lines, are inconsistent and seemingly random. The correlation between the lamellae and the trabecular osteons is very significant, but until the microstructure of the lamellar packets and the determining factor of angles is found, a better mathematical method for prediction is needed [35, 36].

Using fractal theory is the most likely way to quantify the complex structures through fractal analysis, through the examination of how a seemingly irregular object fills an empty space on multiple scales of viewing. Fractals are naturally repetitive structures that decrease in size based on a certain scale and repeat in a predictable pattern based on angles and ratios, much as trabeculae do. Fractal geometry has long been used for describing irregular patterns with self-similarity at different scales. When it comes to fractal density, cortical bone is recorded as $D \sim 3$ demonstrates a very low porosity, as a perfectly solid substance is $D = 3$. Trabecular bone is, of course, more porous, and therefore has a much lower FD.

3. MATHEMATICAL MODELING

The iteration of a very simple rule can produce shapes that are seemingly complex but with very unusual properties, including a very specific level of detail that can be analyzed on extremely small scales. The closer a shape is examined, the more detail one finds. The defining nature of fractals is that the self-similarity that is found at each smaller and smaller level of detail, indicating that each small portion, when magnified, is the exact replica of a larger section, which is invariable regardless of scale. As successive iterations are examined, more detail and more length can be found in the pattern, although it can be quite difficult to replicate with an algebraic formula that specifies points of the curve.

3.1 SELF-SIMILARITY AND DIMENSION

Fractals are generally considered a geometric shape that can be split into smaller parts, each that have the same form as the whole, but just at a reduced size. The structure is typically very fine and on a very small scale, but it is too irregular to easily be explained using Euclidean geometry. A fractal's Hausdorff dimension must also be greater than its topological dimension as well. Considered generally infinitely complex, a fractal can be found in many places in nature, including rivers, snowflakes, lightning bolts, and even clouds. In this particular case, fractals can be used to model bone growth.

Scaling, in a simplified sense, is closely connected with our intuitive understanding of dimension when parts are compared to the whole. Even in basic structures such as a line segment, scaling properties can be seen when it is divided into N identical segments. Each of

these parts can then be scaled down by a ratio $r = \frac{1}{N}$. In a two-dimensional object, divided once again into *N* identical segments, can be scaled down by a ratio $r = \frac{1}{\sqrt{N}}$. With three-dimensional objects such as a solid cube, the self-similar segments *N* are smaller cubes, which can be scaled down by a ratio $r = \frac{1}{\sqrt[3]{N}}$.

A self-similar object with dimension *D* is also able to be divided into *N* smaller copies of itself and scaled down by a factor of *r*, in which

$$r = \frac{1}{\sqrt[D]{N}} \qquad 3.1$$

Which can be rearranged as the following:

$$N = \frac{1}{r^D} \qquad 3.2$$

When approaching a fractal from a different direction, given a self-similar object with *N* parts scaled by a ratio *r*, its fractal dimension or similarity dimension is given by:

$$D = \frac{\log(N)}{\log(\frac{1}{r})} \qquad 3.3$$

Fractals don't have whole-number dimensions due to their complex nature – they exist in the fractal dimension. To understand fractals requires a grasp of complex numbers, as the fractals will always have multiple connected (but separate) components; examine the following:

$$F(x) = x + yi \qquad 3.4$$

The imaginary component may never compromise the real component, but with extensive multiplication, the two will change with each other and repeat as often as is defined. Fractals generally have three different mathematical components: side length L, arrangement repetition factor (angle), and size ratio. For a 2D fractal, those are the only three factors needed.

Examining the Sierpinski Triangle is an excellent way to demonstrate the mathematical concepts comprising fractals. Designed in Italy by Sierpinski, the fractal forms a geometric pattern by connecting the midpoints of the sides of triangles, creating more as in a very regular pattern. The triangle utilizes the Lindenmayer system, or a type of string rewriting system on which rules are used to operate on a string that uses certain letters of the alphabet and is especially useful for generating successive iterations of some fractal types. Fractals are generated using a recurrence equation that is the discrete analog of a differential equation and takes a form much like the following:

$$f(n) - f(n-1) = g(n) \qquad 3.5$$

Probably the most well-known recurrence equation is the Fibonacci sequence for $n \geq 3$ and $F_1 = F_2 = 1$:

$$F_n = F_{n-2} + F_{n-1} \qquad 3.6$$

The Sierpinski sieve has its own equation. Let N_n be the count of black triangles after iteration *n*, and L_n the length of a side of a triangle. Lastly, A_n can be the fractional area left black after the n^{th} iteration, and angles are 60 degrees.

$$N_n = 3^n$$

$$L_n = (\tfrac{1}{2})^n = 2^{-n}$$

$$A_n = L_n^2 N_n = \left(\tfrac{3}{4}\right)^n \qquad 3.7$$

The capacity dimension has a compact metric space of *X* and is a real number *d*, such that the minimum number of open sets of a certain diameter can be proportionally quantified. The capacity dimension defines a fractal; specifically, objects that have a capacity dimension different from their Lebesgue covering dimension. The capacity dimension takes the following form:

$$d_{capacity} \equiv \lim_{\epsilon \to 0^+} \frac{\ln N}{\ln \frac{1}{\epsilon}} \qquad 3.8$$

Specifically in regards to the Sierpinski sieve, the capacity dimension equation demonstrated in Eq. 3.8 works as such to yield the fractal density:

$$d_{cap} = -\lim_{n \to \infty} \frac{lnN_n}{lnL_n}$$

$$= [\text{base}(2)]\log 3$$

$$= \frac{\ln 3}{\ln 2} = 1.58496 \ldots$$

The hierarchical nature of bones comes into play as the fractal structure and hereditariness of bones is examined. Each layer of bone will have its own strength and elastic modulus which combines into a larger system to be considered for bone strength, but must be scaled appropriately to account for size of each hierarchical component. Deseri created a comprehensive viscoelastic model to demonstrate this concept [34-37] that provides the basis for future work in composite fractal models that accurately represent material properties as a result of composition as well as arrangement.

4. MATERIALS AND METHODS

The image being analyzed was a micro-CT scan of the distal end of the radius. The scan was taken by Dr. Thomas Hangartner in November of 2014 using a SANCO Medical micro-CT scanner (model 10). The KVp amount was 70, with the exposure time at 381 seconds, with a total exposure of 43 μAs. More information regarding the size, sample rate, and resolution can be found the table below.

STACK PARAMETER	DATA
Width	20.938 mm (1102)
Height	26.619 mm (1401)
Depth	3.1161 mm (163)
Size	480MB
Resolution	52.6316 pixels per mm
Voxel size	0.019x0.019x0.0191 mm^3
Bits per pixel	16
Number of Images	163
Slice Thickness	0.019 mm

Table 2. The data from the micro-CT scans is shown in this table. Of primary importance is the resolution, which was optimized to minimize the blurring effect.

Due to the extremely small size of the trabeculae, micro-CT scans will not always accurately represent the size of each plate and rod appropriately due to the blurring at the edges of each object. When a threshold is applied to the micro-CT scan, this blurring affects the grayscale values along the sides of the trabeculae, forcing the thresholding to cut further into the sides of the trabeculae, yielding an inaccurate interpretation of their width and length. The images used in this study were pre-processed by Hangartner and his research associates to

minimize the effects of blurring. The image was not binary, but was strictly black and white through all 163 images, with each trabecular edge being as accurate in size as current methods allow.

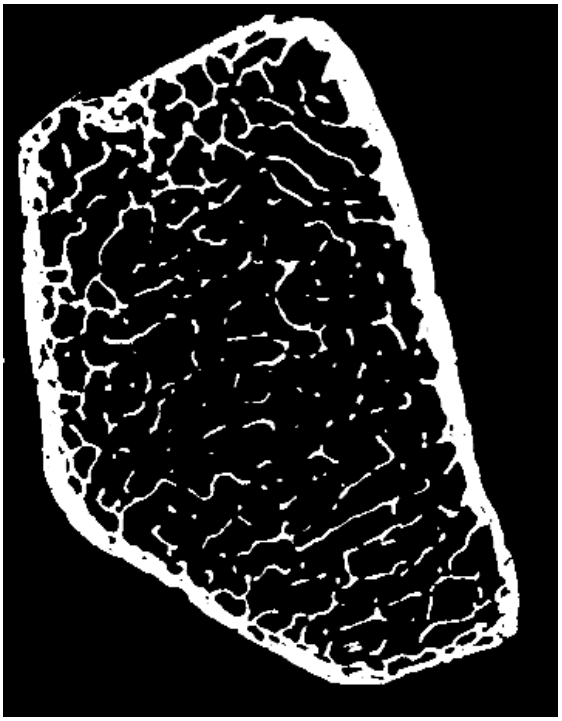

Figure 7. A sample slice of one of the micro-CT images. It was from these images that the physical measurements of plate and rod count and size, among other things, were taken.

The intentions of taking the following measurements were to not only compare the fractal density (FD) accuracy and variation based on accumulation method, but also to see which factors correlated best with the fractal density measurements by examining the R^2 values based on the line of best fit for the fractal density data. Following these correlation evaluations, the factors and the FD values were analyzed for significance using F-statistic test in JMP. Based on the significance of each factor, the interaction effects of each factor were eliminated to create a reduced model, which was then used to create a regression model to calculate FD based on the most statistically significant factors. The Young's Modulus values per image were calculated

from the bone volume fraction (BVF), and again, were compared to each of the factors for correlation and significance to create a regression model for Young's Modulus prediction. The regression models considered interactions of the different measured parameters, but the most ideal models are those which place primary value on single-factor effects.

Measurements were taken using ImageJ image processing software and Mimics (by Materialise). Each image was examined to yield values for the following average values per image: Total trabecular count, plate count, rod count, trabecular size (mm), percent area of trabecular bone, and average spatial angle between trabeculae. Following these measurements, the Young's Modulus was calculated, and based on the composite equations that will be discussed in the following paragraphs, the mineralization of the trabeculae in this image was able to be calculated into the amount of collagen and the amount of hydroxyapatite present, allowing for a more thorough understanding of the bone strength capabilities of the subject.

4.1 MEASURING FRACTAL DENSITY

Images of bone are typically separated into light and dark sections that indicate the locations of the bone segments. These areas are typically called the foreground and background, respectively, and it can be considered a curve in which the fractal dimension is able to be measured. There are several methods that are available to examine the fractal dimension of the segmented images; the one used in this experiment was the box counting method.

The Box Counting Method is the most commonly used when examining bone for density problems and gives the most accurate representation of the fractal dimension for bone. The linear fractal images are calculated exactly, through an absolute generation process. In the example of

Koch boxes, there are seven new segments generated at each step, each segment three times smaller than the last one; the first generation contains 7 segments at 1/3 size, and the second step creates 49 more segments at 1/9 size. The fractal dimension can be calculated exactly in this instance because it is a linear fractal image. However, in natural materials, the fractal dimension is non-linear and contains random elements that do not allow the exact calculation of the fractal dimension, and so it must be estimated. The box counting method is the most commonly used way to approximate the fractal dimension. Using this method, the average number of cubic boxes with a fixed side length (*r*) is designated as *N(r)*, and should represent the number of boxes necessary to completely cover the image which is a surface R^3 in space. The probability that once box of size *r* is centered on an arbitrary point on the surface and contains *m* points of the set is estimated as $P(m,r)$:

$$\forall r, \sum_{m=1}^{Np} P(m,r) = 1 \qquad 4.1$$

In which *Np* is the number of possible points in the cube. From here, the average total number of boxes needed to cover the surface is estimated as:

$$N(r) = \sum_{m=1}^{Np} N(m,r) = \sum_{m=1}^{Np} \frac{P(m,r)}{m} \qquad 4.2$$

This equation estimates, by the least squares method, the slope of the line created *(log(r) – log (N(r)))*, and gives the estimate of fractal dimension. After the application of the threshold and after the image is filtered, the set is probabilistically analyzed to find a box with side length *r* that contains a range of pixels between 0 and m. Following, a box (with dimension *r*) is centered

for any pixel *s*. Then the number *m* of pixels that belong to the specific box is counted, and therefore increments the probability *P(m,r)* by 1, and the process is repeated for every value of *r* until r_{max}. The total number is then summed. Finally, *N(r)* is calculated for each grid, and to calculate the fractal dimension *D*, the slope of the curve is used after finding the log-log plot of the sums.

In summary, the fractal density (*FD*) is the slope of the logarithmic regression line for how the detail (*N*) changes with scale (ε):

$$DF = \frac{\ln(N)}{\ln(\varepsilon)} \qquad 4.3$$

In this experiment, the fractal density was calculated using the FracLac plugin for ImageJ. Three variables were changed with each measurement; the number of grid positions, the scaling method, and whether or not the image was rotated while taking measurements. The number of grid positions indicates where the box count begins. If the grid position is set to 0, there is no origin position, and therefore, no box counting will occur (yielding no fractal density). For a grid position of 1, the box counting begins in the top left corner. Any value greater than one allows the box counting to go through multiple iterations with a varied start position of the sampling grid. This eliminates variation of the fractal density values as a result of grid orientation. Typically, the grid origin position is between 4 and 12 to balance the increased accuracy with sampling rate. There is minimal variation in fractal density with a grid orientation greater than 12. For this test, grid positions were varied between 4 and 12. While the grid always starts in the top left corner, the iterations following (in this case, 4 iterations or 12 iterations) have a randomly generated placement. However, the randomly generated set of numbers to determine where the grid placement begins stays consistent through the box scaling to maintain integrity throughout the fractal density measurements.

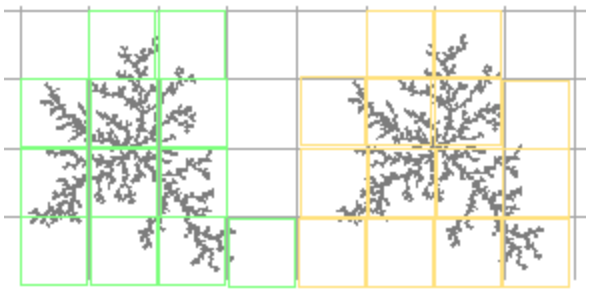

Figure 8. This figure shows the discrepancy in box count between different grid positions. For a box count iteration involving one pixel size, the grid orientation on the left uses only 12 boxes to cover the object of interest. The grid orientation on the right uses 14 boxes.

PARAMETER	High Level (+)	Low Level (-)
Grid Orientation	12	4

Table 3. The grid orientation for each FD variation was set at either 12, which was considered the "high" level and includes 12 iterations of grid placement, or 4, which was considered the "low" level, and uses only 4 iterations of grid placement.

The scaling method variation defines the difference in the size of boxes used in each iteration of the box count for a single test. Because the scaling rule (defined as (ε) above) was not known before testing, arbitrary sizes are defined based on the type of numerical series chosen in the FracLac program. The first used in this experiment was the "Default Sampling Sizes" series, where box sizes range from a minimum number of pixels to a maximum percentage of the image, both of which are defined by the user. Using the Default Sampling Sizes, the minimum number of pixels for a box was defined as 0, and the maximum percentage of the image covered by a single box was 45%. The second scaling method used was the "Power Series", in which the box sizes increase exponentially based on a base and exponent chosen by the user. The base chosen was 2, and the exponent was also 2, resulting in the first three box sizes as the following:

$$2^2 = 4; \quad 2^{(2+2)} = 16; \quad 2^{(2+2+2)} = 64$$

PARAMETER	High Level (+)	Low Level (-)
Scaling Method	Power Series	Default Sampling Series

Table 4. The scaling method for each FD variation utilized the Power Series, which was considered the "high" level and utilized exponential growth of boxes, or the Default Sampling Series, which was considered the "low" level, and allows for a maximum percentage area of 45% to be covered by one box through all iterations.

The final factor of variation in the fractal density measurements was the rotation of the image. Much like the grid orientation, rotation of the image affects how the boxes of various size lie across the entire picture, in turn affecting the total number of boxes that contain pixels of various color (which are considered "detailed" and count as part of the total box measurement for that box size). The rotation of this image changed between 0 degrees rotation and 36 degrees rotation, to line up with the strongest axis of repetition of the trabecular bone.

PARAMETER	High Level (+)	Low Level (-)
Rotation (degrees)	36	0

Table 5. The rotation for each FD variation was based on the initial orientation of the scans, which is the "low" level at 0 degrees of rotation, and the "high" level, which is 36 degrees of rotation, which aligns the strongest lines of repetition in the radius vertically. By lining the repetition vertically, the boxes are more likely to count a higher number of black pixels, perhaps increasing the fractal density.

The factor variation combinations are in the table below:

Pattern	Grid Orientation	Scaling Method	Rotation	FD Reference Number
+−−	1	-1	-1	FD1
+−+	1	-1	1	FD2
++−	1	1	-1	FD3
+++	1	1	1	FD4
−−−	-1	-1	-1	FD5
−−+	-1	-1	1	FD6
−+−	-1	1	-1	FD7
−++	-1	1	1	FD8

Table 6. All possible combinations of the three factors discussed above (grid orientation, scaling method, and rotation) yield a fractal density in the results section. They are demonstrated in this table and labeled FD1 – FD8 based on the order of testing.

4.2 COMPOSITE STRENGTH CALCULATIONS

Following these data collections, the total Young's Modulus was created for comparison to the various other factors to see which had the greatest effect on the FD measurement. The following simple equation is a derivation of the upper limit for the elastic modulus as defined by the Reuss model (with influence from the Hooke model) and was used to calculate Young's Modulus in this experiment:

$$E_P V_P + E_R V_R = E_T \qquad 4.1$$

Where E_P is the standard Young's Modulus for plates, E_R is the Young's Modulus for rods, V_P and V_R are the volume percentage of plates and rods (from the total cancellous bone quantity), respectively, and E_T is the total resulting Young's Modulus for the cancellous bone. This equation is for the upper limit of the Young's Modulus. The lower limit was not calculated in this experiment for the sake of simplicity and limited scope, but can be defined by equations developed by Voight, which apply to transverse loading of a segment instead of axial loading.

However, tissue material properties in the equation above are reflected in bulk; if the tissue mineralization is taken into account, the compressive Young's Modulus and ultimate stress can be related to the bone volume fraction in the following manner [30]:

$$E\ (GPa) = 84(\frac{BV}{TV})^{2.58}\alpha^{2.74} \qquad 4.2$$

$$\sigma_U(MPa) = 794(\frac{BV}{TV})^{1.92}\alpha^{2.79} \qquad 4.3$$

The $\frac{BV}{TV}$ component is bone volume over total volume, and α is representative of the degree of mineralization of the tissue, considering the total inorganic mass (or amount of HA present) in the cancellous bone. These are regression equations, and in both, there is a larger exponential value placed on the inorganic component, indicating that the degree of mineralization is more important than the bone volume fraction. In this experiment, these regression equations serve as a comparison point for the regression equations developed by the measured factors in the first section. Given the bone volume fractions gathered from the micro-CT image, the degree of mineralization was able to be calculated to examine what level of HA would yield an appropriate Young's Modulus and ultimate stress value (since the amount of HA could not actually be measured in the sample) based on the trabecular size, area, and thickness. The relationship between mineralization and trabecular size is demonstrated below.

Bone, on a micro level, must be examined as a composite to properly evaluate all materials complementing each other to reinforce the strength demonstrated by the overall structure. Fratzl and Weinkamer used a two-dimensional model to explore the possibility of combining the stiffness and toughness of the bone composite materials. The following terms are defined:

$\varepsilon^M, \varepsilon^P, \varepsilon^C$ Tensile strain in the matrix, particles, and composite

$\sigma^M, \sigma^P, \sigma^C$ Tensile stress in the matrix, particles, and composite

E^M, E^P, E^C Young's modulus in the matrix, particles, and composite

τ^M, η^M, G^M Shear stress, shear strain, and shear modulus in the matrix

L, D, d Length, thickness, and spacing of the particles

Φ Volume fraction = D/(D+d)

ρ Aspect ratio of particles = L/D

δ Increase in particle spacing in loading direction

L^* Length of loaded particles

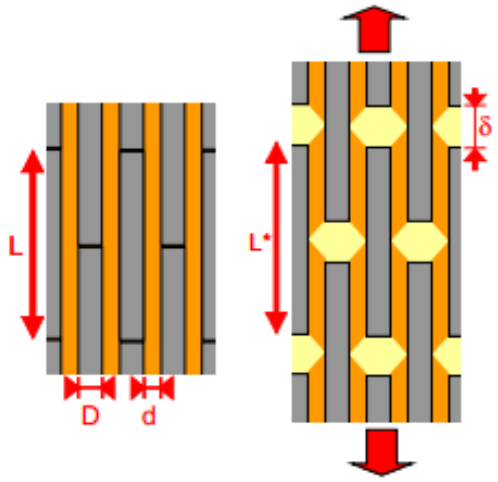

Figure 9. A representation of the yellow, hexagonal HA particles as they sit in-between the collagen fibrils. The grey columns are the collagen, and the orange between them represents the space occupied by the matrix. Lengths are defined and used in Eq. 4.4 through Eq. 4.14 below.

In this model, long, thin stiff objects (the fibrils) of length L, thickness D, and lateral thickness d are stuck together by a matrix. The model can easily be manipulated into a three-dimensional context by examining multiple layers of each 'glued' layer. In Eq. 1, the stress in the composite can be seen as being distributed between both the matrix and the individual particles since the particles lie parallel with stripes of the matrix. The model is as follows:

$$\sigma^C = (1 - \Phi)\sigma^M + \frac{F}{(2D+2d)} \qquad 4.4$$

The factor 2 in the second term stems from the fact that a load-bearing particle only occurs every 2(D+d). After calculating mean stress, mean strain must also be calculated, but the difficulty lies in the inconsistency of the loading along the particle due to the matrix's distribution of the shear forces. Linear approximation of the stress is the simplest; in that case, the stress is F/D in the center and zero at either end. Average stress in the particle is seen in Eq. 4.5, and the increase in particle spacing can be seen in Eq. 4.6:

$$\sigma^P = \frac{F}{2D} \qquad 4.5$$

$$\delta = L(\varepsilon^C - \varepsilon^P) = 2d\eta^M \qquad 4.6$$

Since half of the force has to be provided to the particle from each side, examining the shear stress more closely yield Eq. 4.7:

$$\tau^M = \frac{F}{2} * \frac{L}{2} \qquad 4.7$$

Combining all of the expressions yields:

$$\sigma^C = (1 - \Phi)\sigma^M + \Phi\sigma^P \qquad 4.8$$

$$\varepsilon^C = \frac{2}{\rho} * \frac{1-\Phi}{\Phi}\eta^M + \varepsilon^P \qquad 4.9$$

$$\tau^M = \frac{2}{\rho}\sigma^P \qquad 4.10$$

$$\varepsilon^M = \varepsilon^C \qquad 4.11$$

All of these relationships are simply geometric in relationship to FIGURE X above, and to keep the simplistic mindset for small deformation, we can assume all materials can be generalized using Hooke's Law, in which $\sigma^C = E^C\varepsilon^C$ (using the same equation for the matrix and the particle) and $\tau^M = \eta^M G^M$. The modulus can then be equated to []:

$$E^C = (1 - \Phi)E^M + \frac{\Phi E^P}{k} \qquad 4.12$$

$$\varepsilon^C = k\varepsilon^P \qquad 4.13$$

Where $k = 1 + \frac{4}{\rho^2}\frac{1-\Phi}{\Phi}\frac{E^P}{G^M}$.

The Young's Modulus of the particles would typically be expected to be larger than the shear modulus of the glue-like sheet, but if this were the case, *k* would in turn become very large and govern the already low stiffness of the matrix. However, if a large aspect ratio is given to the particles, the low stiffness is compensated. By this reasoning, the stiffness of the composite is to the same order of magnitude as the particles themselves simply through geometric arrangement, even though the volume fraction of the glue-layer is not incredibly small. As a result the actual

values obtained from these equations, when inserting mechanical property values for collagen, are quite close to that of compact bone. However, this also means that the strain is going to be shared similarly between the whole composite and the particles themselves, so if the particles are brittle, the composite too will be brittle. Strength of the particles limits the performance of the composite with optimal geometric design.

The size of the particles can affect the overall strength beyond their intrinsic material strength. If small enough particles are used, the strength is not limited by defects, and it has been demonstrated [32] that glued composites are much more tolerant to defects if particles are smaller than a critical length:

$$h^* \approx \frac{\pi \gamma E^P}{\sigma_{th}^2} \qquad 4.14$$

Where γ is the surface energy of the particle material and σ_{th} is theoretical strength. If a particle is smaller than h^*, it cannot have flaws that are so significant to affect overall strength. Mineral particles have been estimated at h^* = 30 nm [33].

Examining these mathematical relationships on a larger 2D scale is more complicated in that the fibril array type (plate, rod) and inter-trabecular angle must be accounted for. Each branch of the fibril arrays complicates the mathematical representation of the cancellous bone as a whole. To simplify, the system can be cut down to the load distribution between two fibril arrays at a certain angle using the composite equations Eq. 4.8 through Eq. 4.11, but doubling to account for the two arrays and adding in an angular geometric component to account for load distribution. While impossible to exactly predict all trabecular growth, and also while it is further complicated by stress lines resonating through the structures, a fairly accurate picture of the overall

cancellous bone strength can be painted by taking the mathematical expressions and exponentially manipulating them on varying scales and to a certain quantity. The easiest and most accurate way to do so is through fractal analysis and fractal expression.

5. RESULTS

Post-processing microCT data in ImageJ yielded the total trabecular counts per image, the number of plates, the number of rods, the percent area occupied by the bone, the total number of objects throughout the image stack and the associated areas of each object, and the average angular orientation between trabeculae. The fractal density was estimated using 8 different testing methods and FracLac plugin settings outlined in **Table 6**. Based on the average accepted Young's Modulus values for plates and rods, the total Young's Modulus of the trabecular bone was estimated based on the volume fraction observed in each image. The measured data was compared to the FD and Young's Modulus values to identify which parameters had a significant effect on these values.

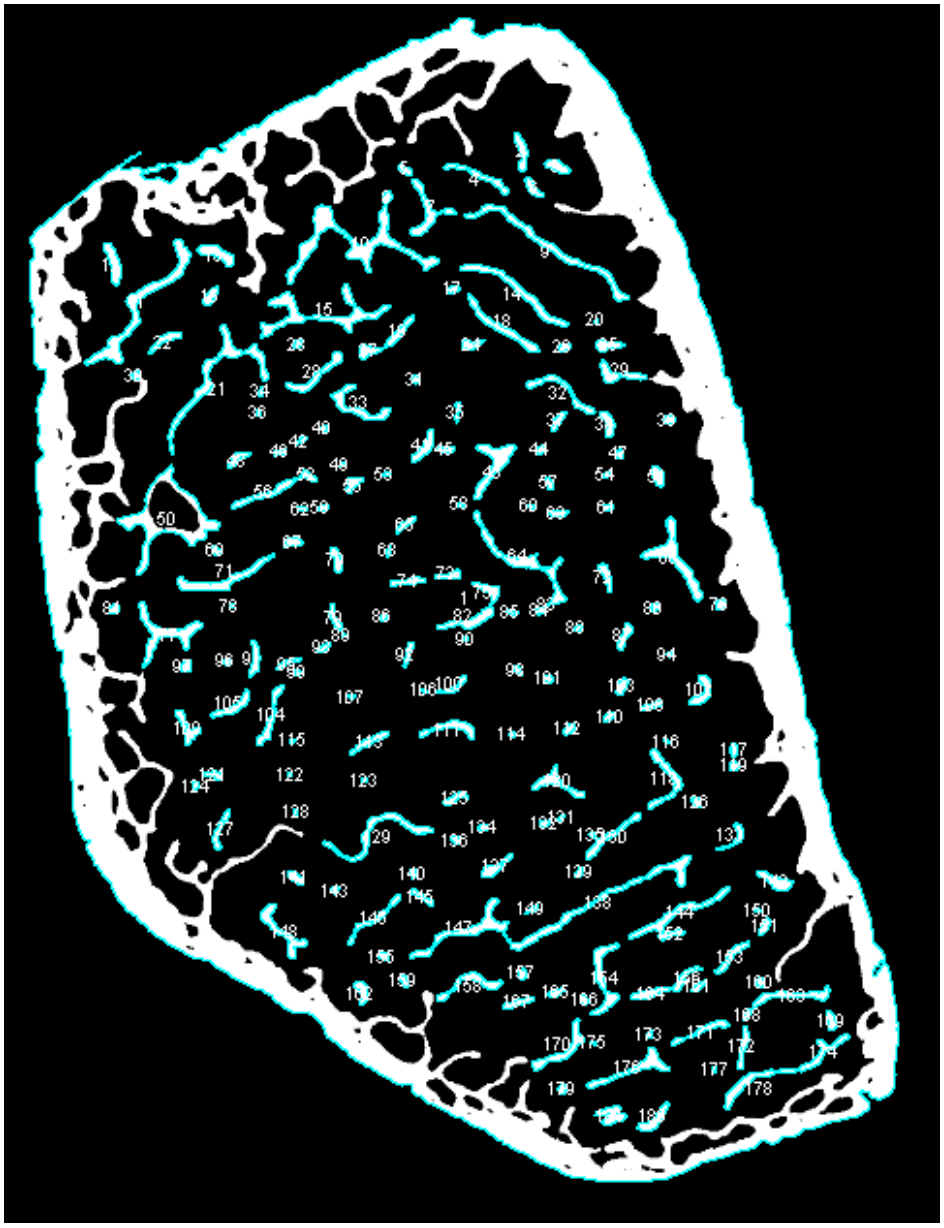

Figure 10. Each object identified is outlined in blue and given a number. Each enclosed blue line had a number, area, and size (distance between furthest pixels) associated with it. Objects were counted per image and in total amongst all 163 images.

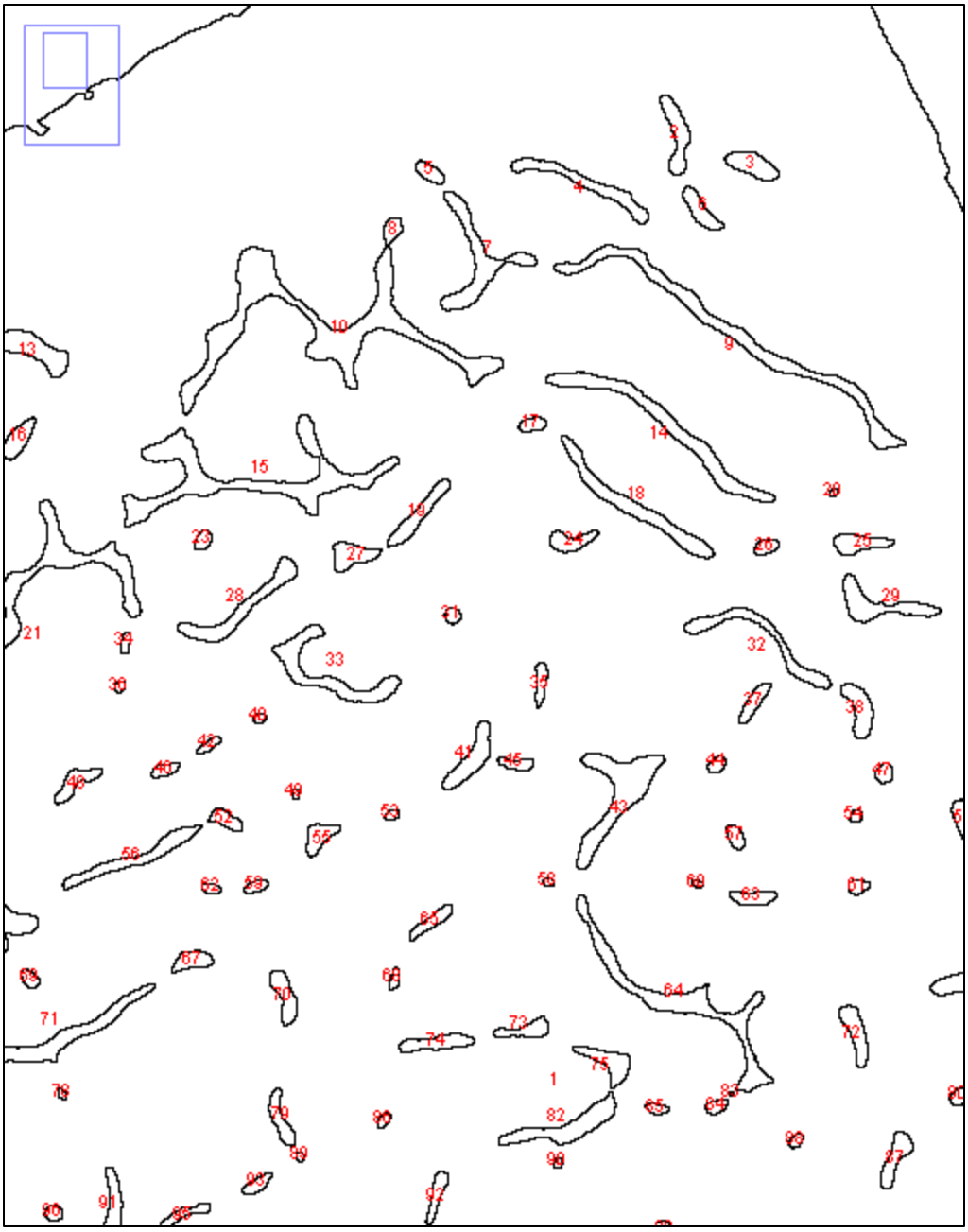

Figure 11. A close-up view of the outlines of the trabeculae. Small numbers can be seen over each outline, indicating the trabecular object number.

Aggregate Parameter	Mean	Std Dev	Min	Max	Variance	Std Error
FD1	1.630	0.007	1.614	1.652	0.000	0.001
FD2	1.634	0.014	1.611	1.669	0.000	0.001
FD3	1.581	0.005	1.567	1.592	0.000	0.000
FD4	1.568	0.007	1.558	1.594	0.000	0.001
FD5	1.661	0.009	1.644	1.684	0.000	0.001
FD6	1.667	0.014	1.647	1.703	0.000	0.001
FD7	1.596	0.006	1.578	1.604	0.000	0.000
FD8	1.579	0.009	1.562	1.607	0.000	0.001

Table 7. The differences in mean can be seen between all FD variations. The variation with the lowest standard deviation is FD3, closely followed by FD7, indicating that these two variations should be examined more carefully.

The mean in both **Table 7** and **Table 8** is defined as the sum of each measured value over the total number of values, which, given that there are 163 images, would be 163. Variance was calculated as the squared difference of each value from the mean in each category, and the standard deviation was defined as the square root of the variance. The *Std Error* column refers to standard error of the mean, which is calculated by dividing the mean by the square root of the number of samples (which is 163).

The next section presents scatter plots of each fractal density (FD1 – FD8) against each of the measured parameters listed in **Table 7** above (with the exception of Et; the r^2 values for FD1 – FD8 against Et can be found in section 6. Because the fractal density increased with the image slice number, just as most of the measured parameters did, the linear fit can easily be confused as a function of image slice. In fact, the scatter plots directly show the measured parameter against the fractal density, generally in a positive linear manner.

5.1 FD1 COMPARISONS

Fractal density with grid orientation of 12, Default Scaling Series, and no rotation.

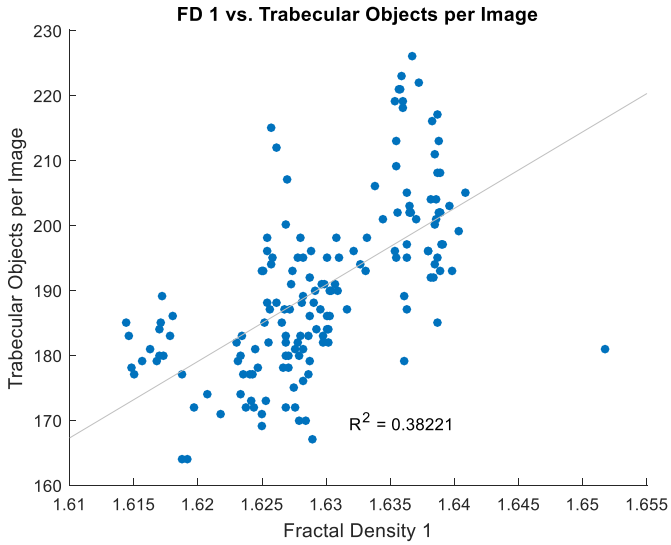

Figure 12. The number of trabecular objects per image has a weak correlation with the values obtained for FD1.

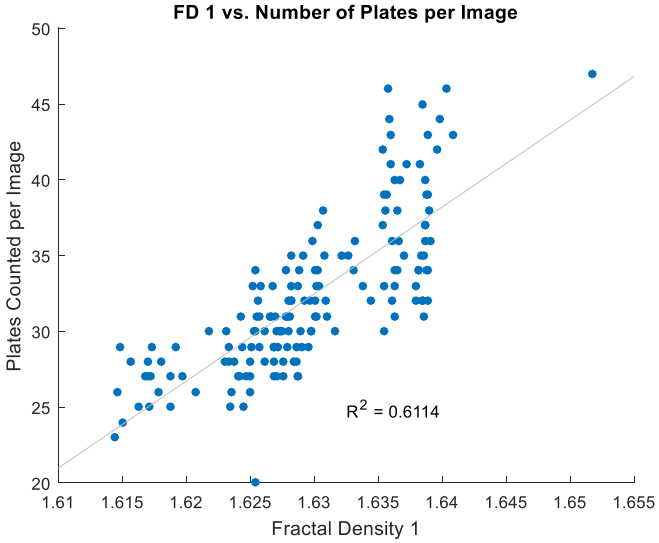

Figure 13., The number of plates observed per image had a noticeable, though mild, correlation with FD1 $R^2 = 0.6114$.

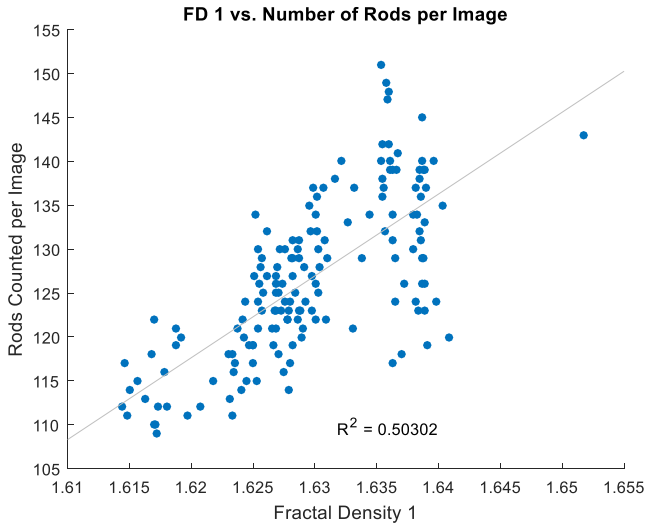

Figure 14. FD1 showed some correlation with the number of rods counted per image, although the R^2 value shows a weaker correlation than FD1 with the number of plates.

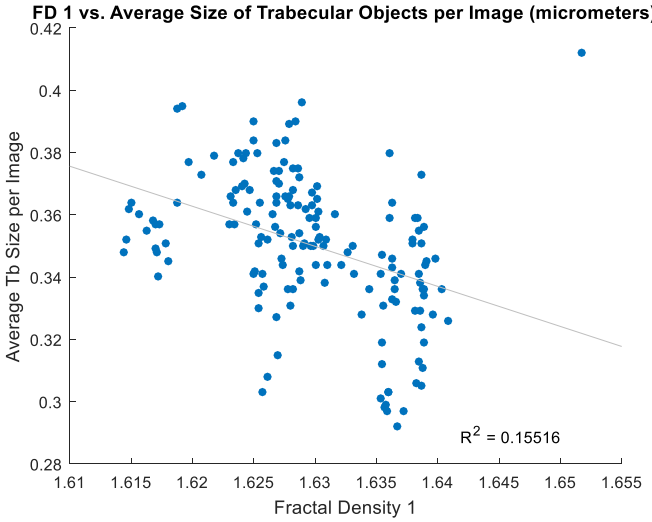

Figure 15. The average size of trabecular objects in a given image appears to have a very weak correlation with FD1 with $R^2 = 0.11516$.

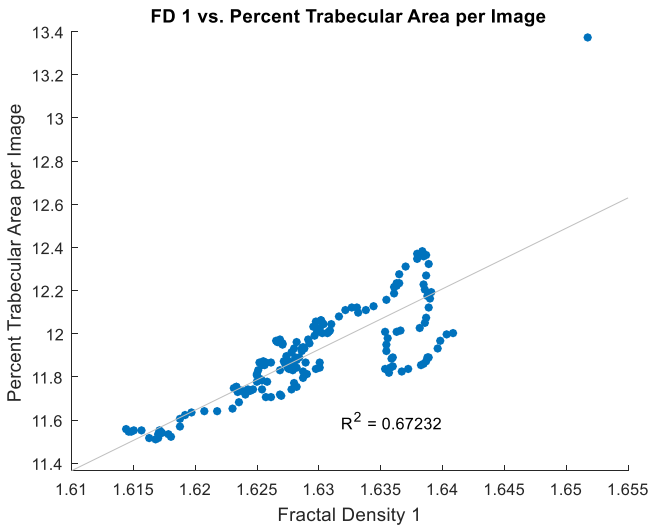

Figure 16. The percent of trabecular area covered per image has the greatest linear correlation with FD1 out of any individual factor with $R^2 = 0.6723$.

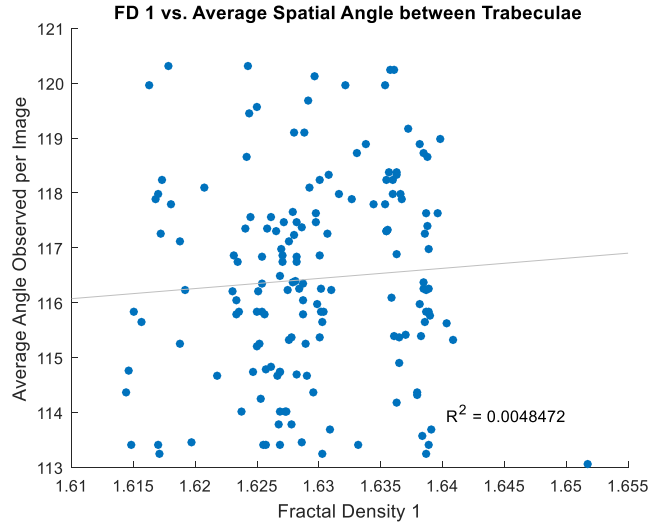

Figure 17. FD1 has the weakest correlation with the average angular offset, showing almost no correlation at all.

5.2 FD2 COMPARISONS

Fractal density measured grid orientation of 12, Default Scaling Series, and 36° rotation.

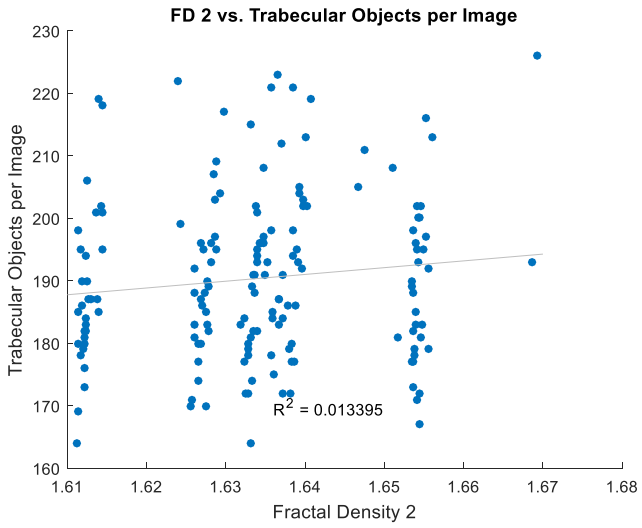

Figure 18. The $R^2 = 0.0134$ value indicates there was very little correlation between the total number of trabecular objects identified and FD2.

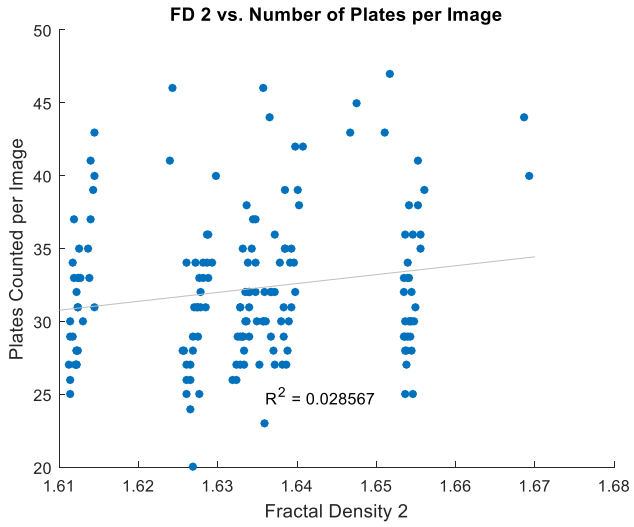

Figure 19. Again, FD2 showed a weak correlation with the number of plates observed per image with $R^2 = 0.0286$.

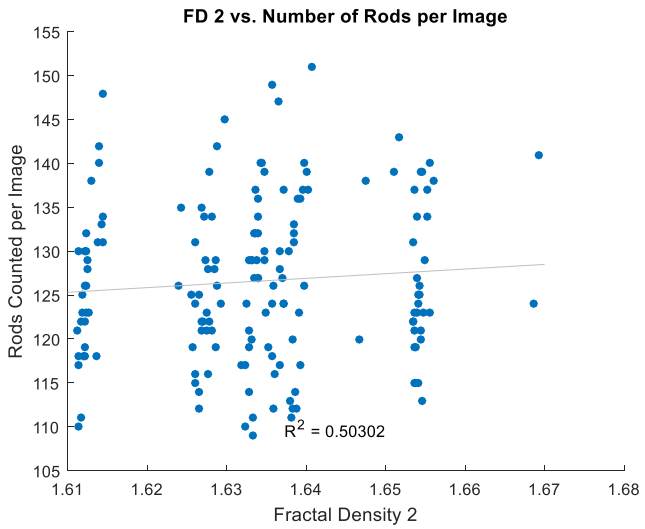

Figure 20. In contrast to the number of plates, FD2 showed its highest correlation value with the number of rods counted per image, though $R^2 = 0.503$ is not a strong correlation.

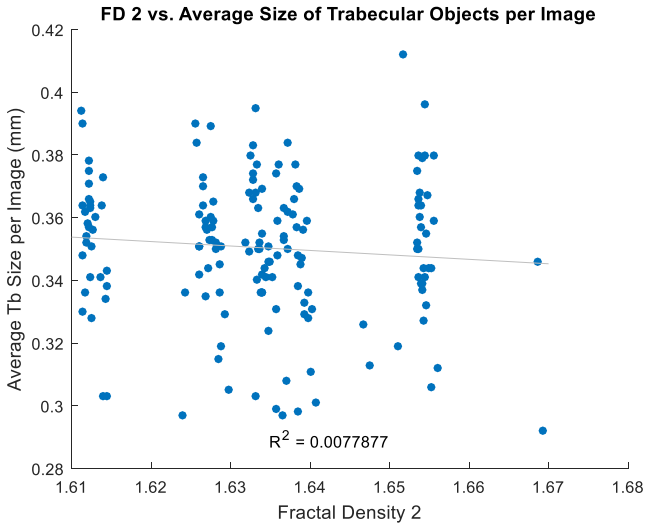

Figure 21. FD2 showed almost no correlation with average trabecular size with a correlation value of 0.0078.

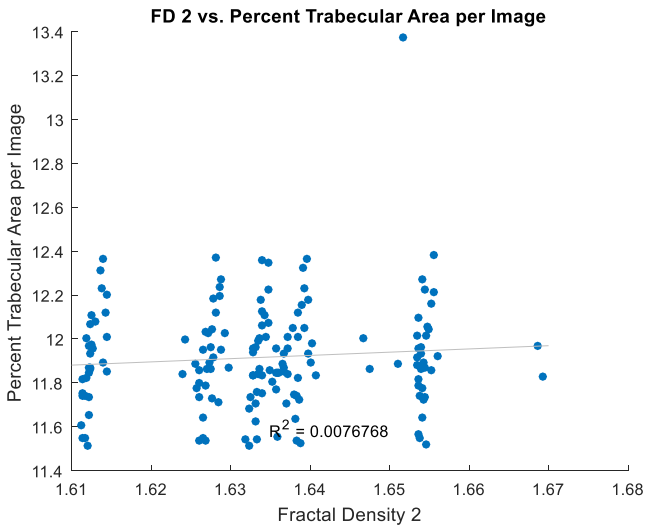

Figure 22. The percentage of area occupied by trabeculae in the image has an extremely low R^2 value of 0.0077 with FD2.

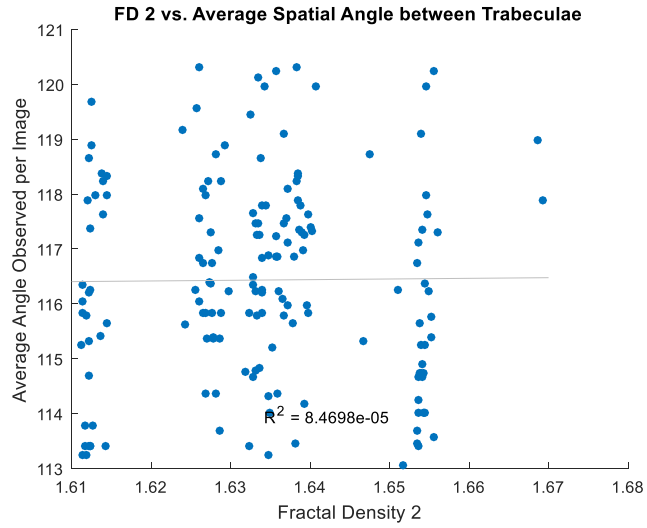

Figure 23. FD2 shows no correlation with the average angular spacing between trabeculae, despite previous research showing that angular spacing is important in determining FD; this comparison is examined more thoroughly as a probability-based interaction.

5.3 FD3 COMPARISONS

Fractal density measured grid orientation of 12, Power Series, and no rotation.

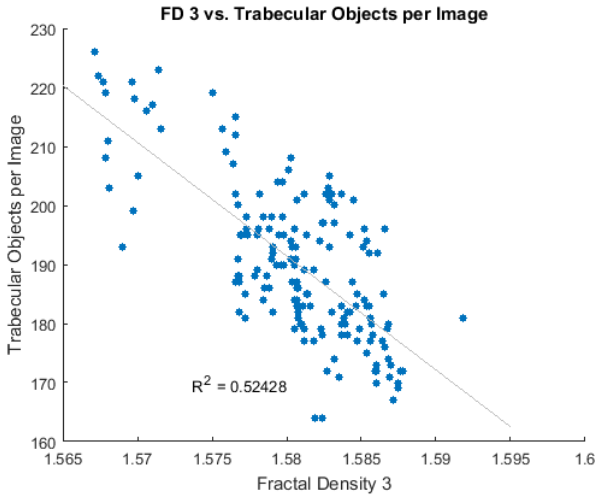

Figure 24. FD3 showed a low correlation with the spatial angle between trabeculae. $R^2 = 0.0548$.

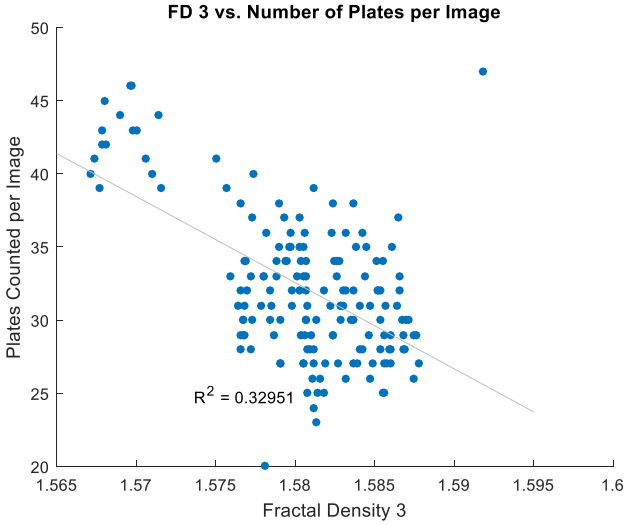

Figure 25. The number of plates per image showed a lower correlation with FD3 with $R^2 = 0.3295$.

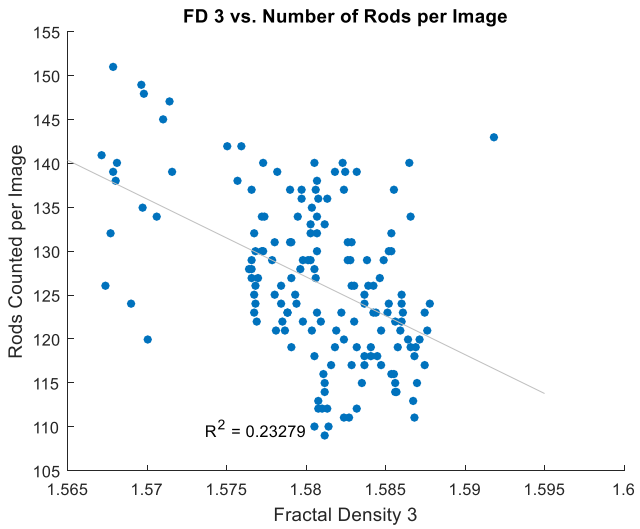

Figure 26. The number of rods showed a lower correlation value with FD3 than the number of plates per image did with a correlation value of 0.2328.

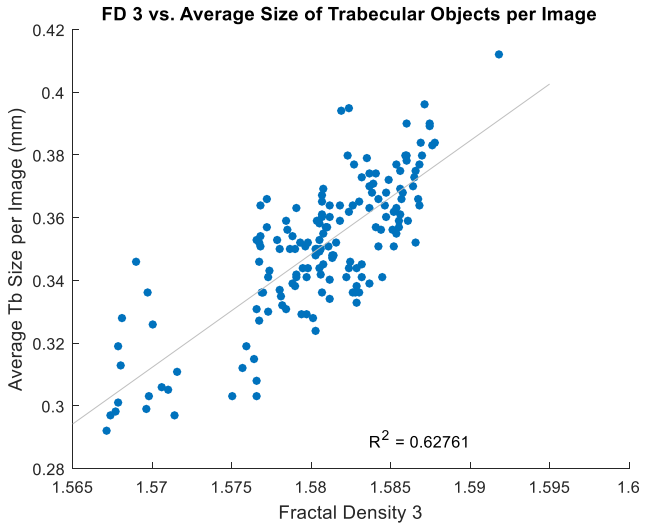

Figure 27. The average number of trabecular objects observed per image showed $R^2 = 0.5243$, which implies a medium amount of correlation with FD3.

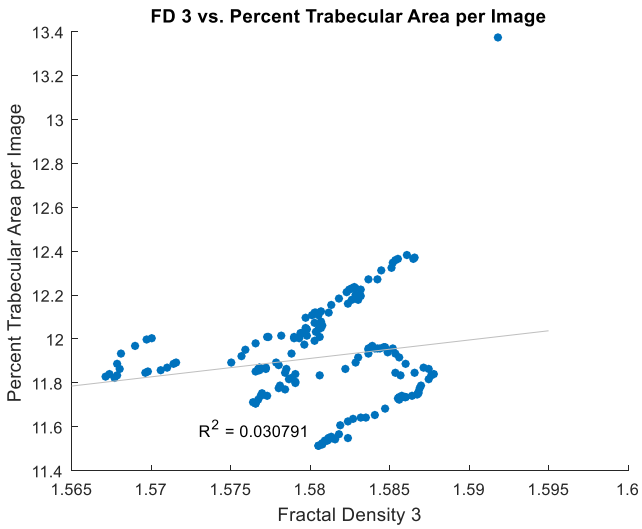

Figure 28. FD3 showed a very low correlation with the percent area with a correlation of 0.0308.

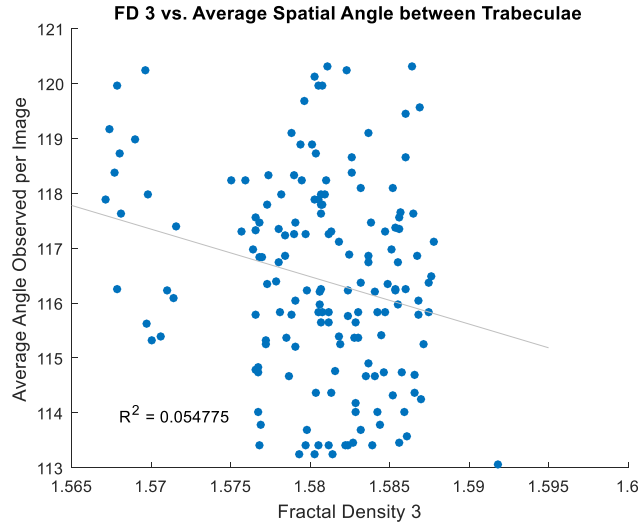

Figure 29. FD3 showed a low correlation with the spatial angle between trabeculae. $R^2 = 0.0548$.

5.4 FD4 COMPARISONS

Fractal density measured grid orientation of 12, Power Series, and 36° rotation.

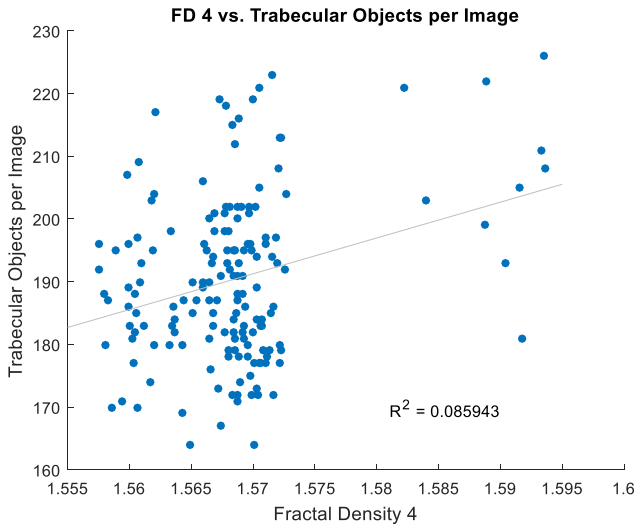

Figure 30. Trabecular objects per image has a very low correlation with FD4 with a correlation value 0.0859.

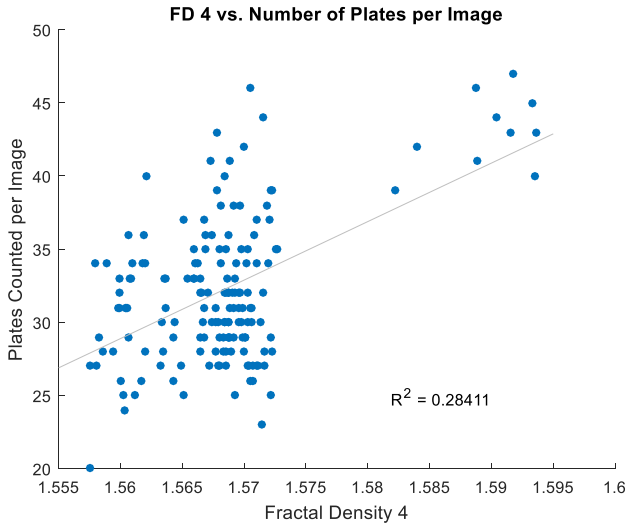

Figure 31. The correlation equation of $R^2 = 0.2841$ shows a fairly weak correlation between the number of plates observed per image and FD4.

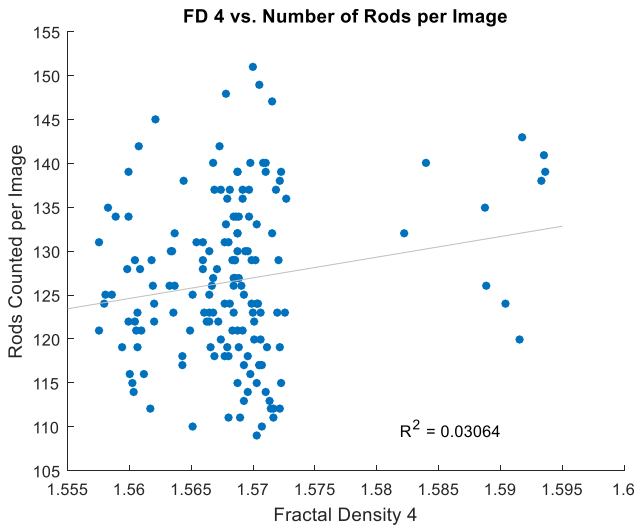

Figure 32. The correlation of number of rods observed with FD4 is much lower than that of plates with $R^2 = 0.0306$.

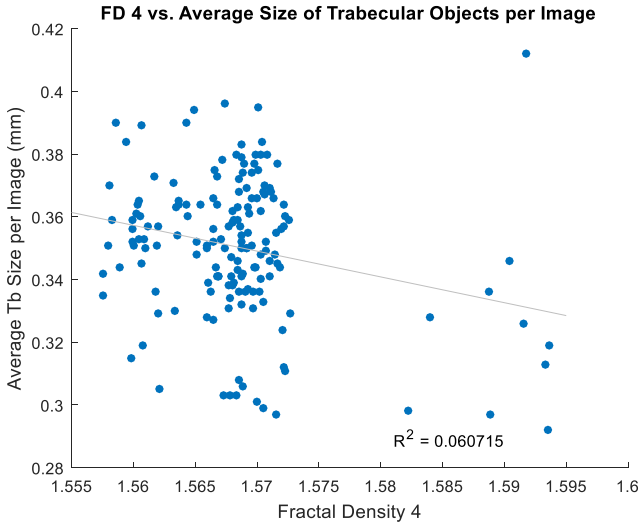

Figure 33. FD4 demonstrates a very weak ($R^2 = 0.0607$) correlation with average trabecular size per image.

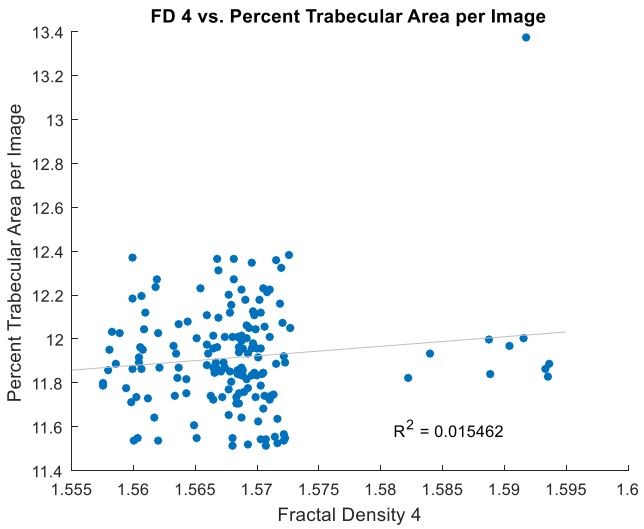

Figure 34. The percent of trabecular area per image also shows a very weak correlation with FD4 (R^2 = 0.0155).

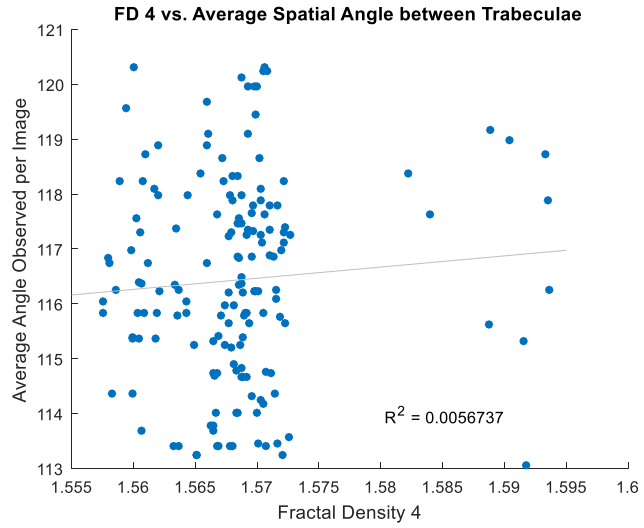

Figure 35. Like all other comparisons with FD4, the average spatial distance between trabeculae has a very weak (the weakest overall) correlation with FD4 with R^2 = 0.0057.

5.5 FD5 COMPARISONS

Fractal density measured grid orientation of 4, Default Scaling Series, and no rotation.

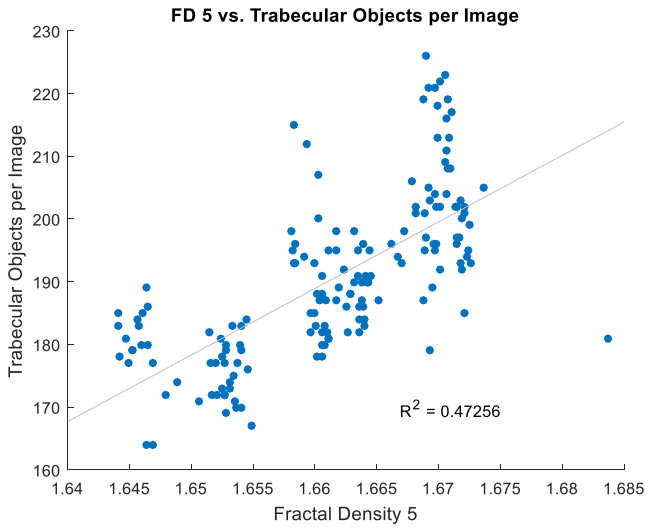

Figure 36. FD5 has a mild-to-low correlation with the number of trabecular objects per image with $R^2 = 0.4726$.

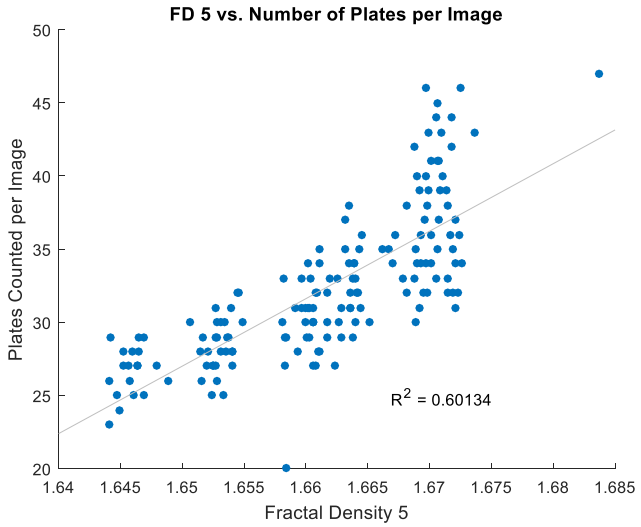

Figure 37. The number of plates per image has a somewhat strong correlation with FD5 with a correlation of 0.6013.

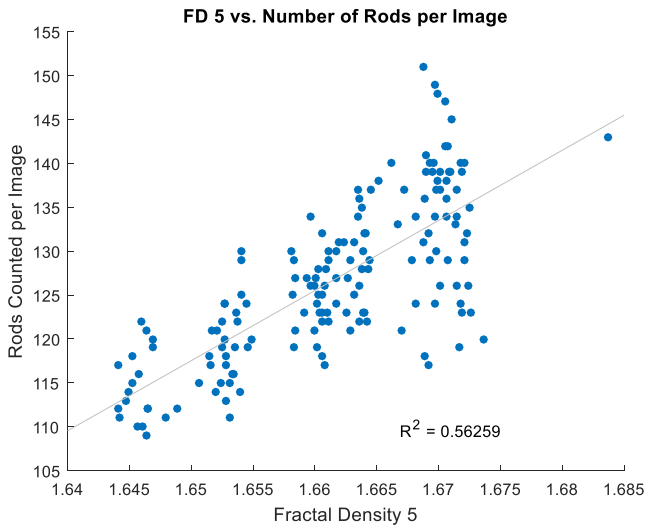

Figure 38. The rod count per image also has a medium amount of correlation ($R^2 = 0.5626$) to FD5.

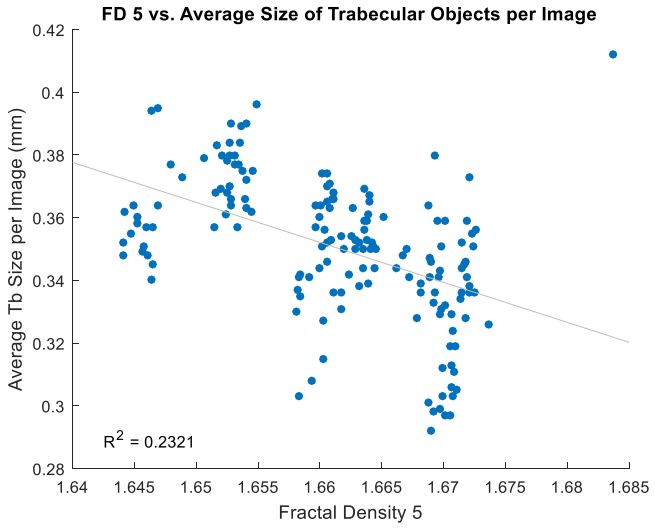

Figure 39. FD5 does not have a particularly strong correlation with the number of trabecular objects per image ($R^2 = 0.2321$).

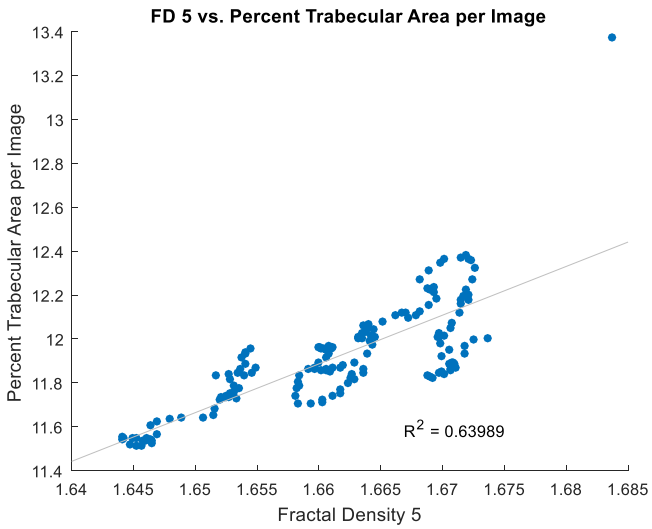

Figure 40. The highest correlation for FD5 was found with the percentage of area occupied by trabeculae with $R^2 = 0.6399$.

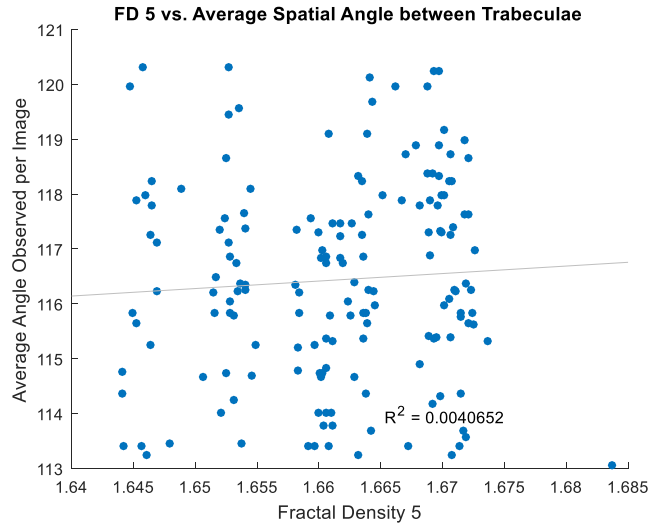

Figure 41. The lowest correlation with FD5 was with the average spatial angle observed between trabeculae with $R^2 = 0.0041$.

5.6 FD6 COMPARISONS

Fractal density measured grid orientation of 4, Default Scaling Series, and 36° rotation.

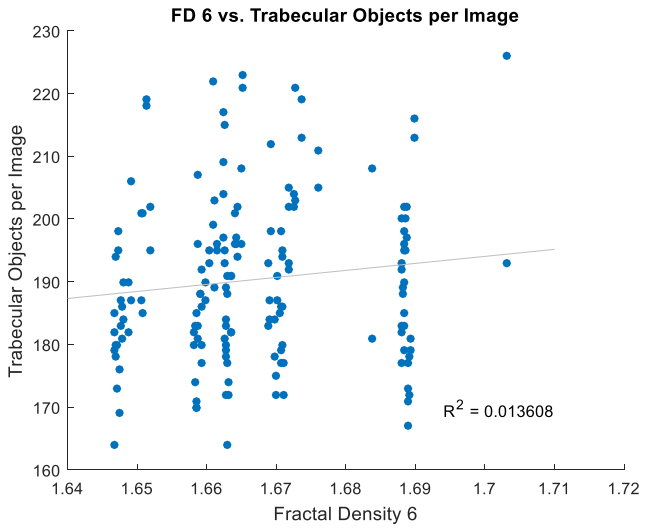

Figure 42. FD6 has a very low correlation with the number of trabecular objects per image with $R^2 = 0.0136$.

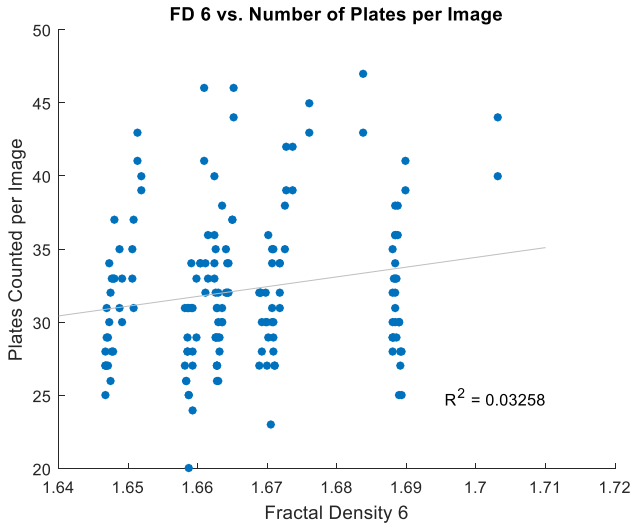

Figure 43. The correlation between FD6 and the plate count was the highest for the FD6 variation at $R^2 = 0.0326$, but still extremely low correlation value overall.

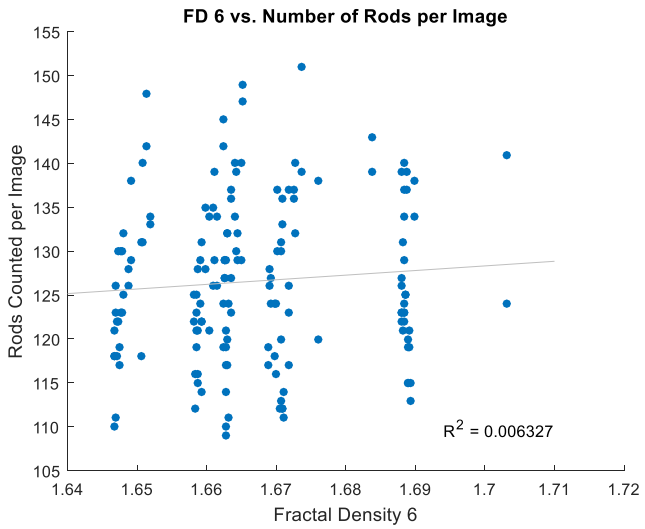

Figure 44. The second lowest correlation value with FD6 is shown above with the number of rods per image (R^2 = 0.0063).

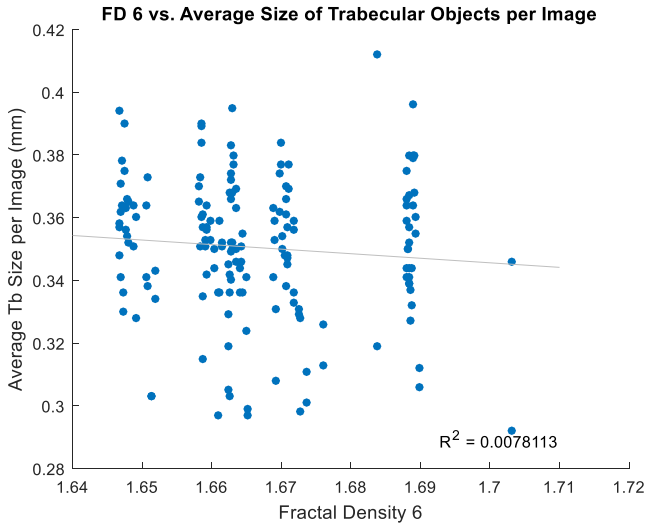

Figure 45. The average size of trabecular objects showed almost no correlation with FD6 values (R^2 = 0.0078).

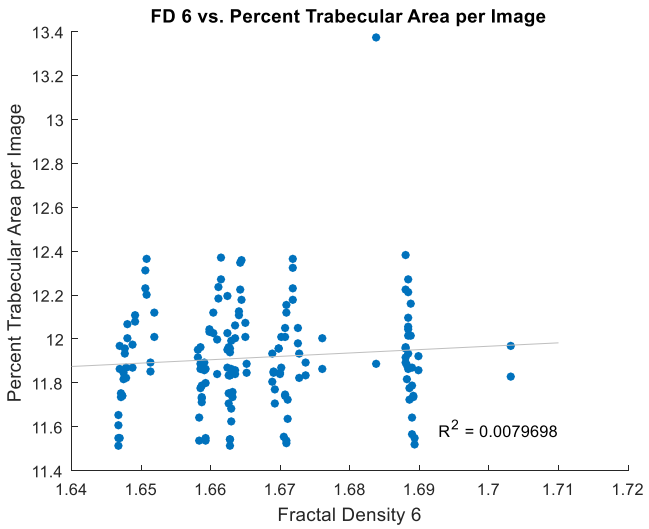

Figure 46. Once again, the FD6 values showed almost no correlation with the percentage of area occupied by trabeculae with $R^2 = 0.008$.

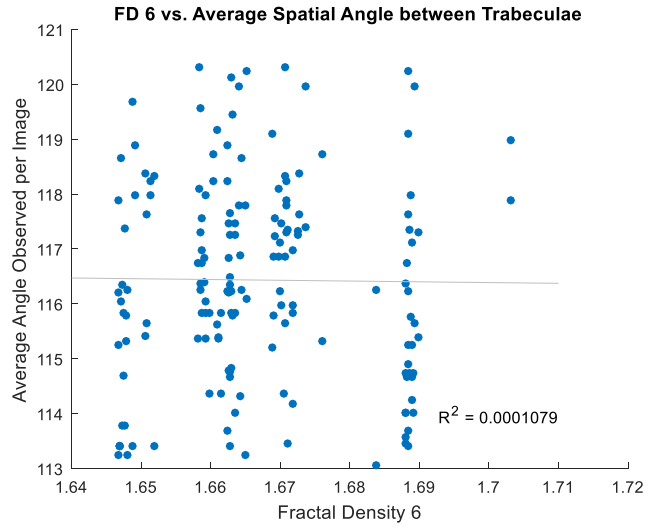

Figure 47. The lowest correlation ($R^2 = 0.0001$) was between FD6 and the spatial angular arrangement between trabeculae.

5.7 FD7 COMPARISONS

Fractal density measured grid orientation of 4, Power Series, and no rotation.

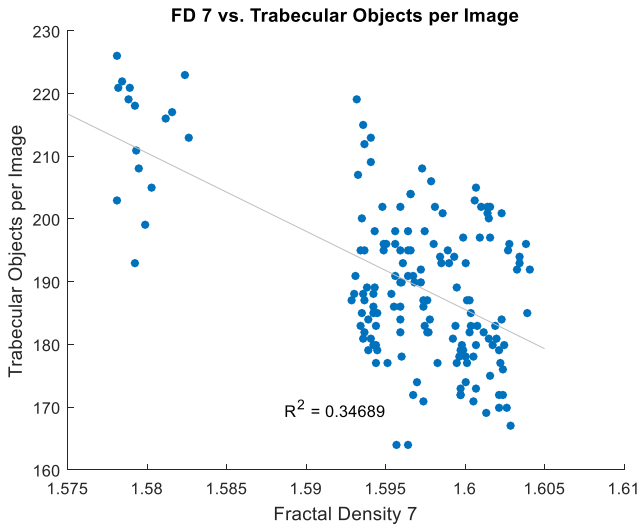

Figure 48. The correlation between FD7 and the average trabecular object count was somewhat low at $R^2 = 0.3469$.

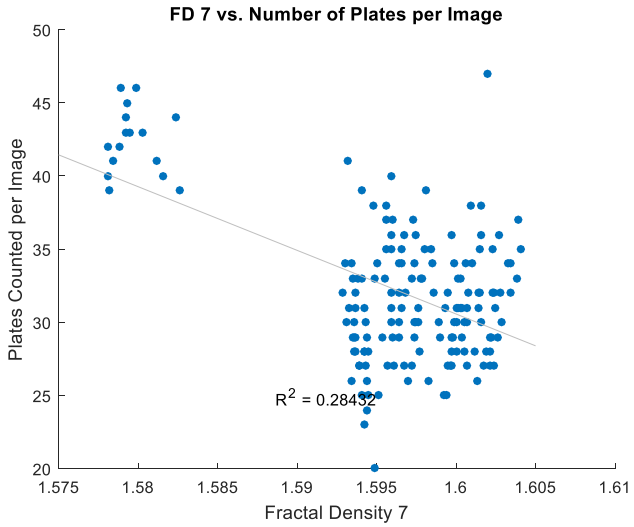

Figure 49. The correlation between FD7 and the number of plates observed per image also had a low correlation value of $R^2 = 0.2843$.

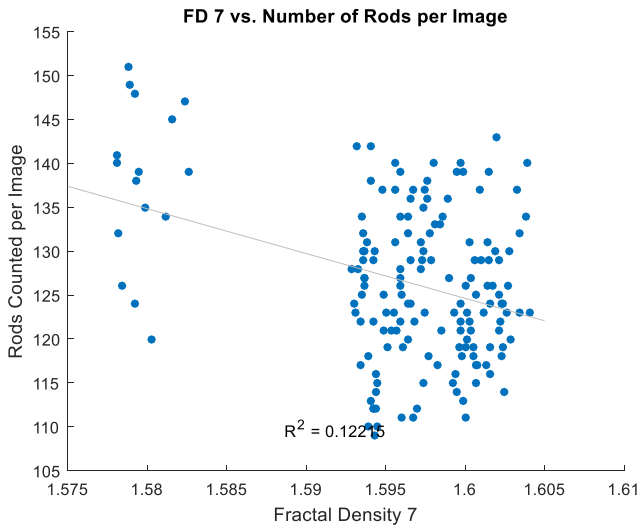

Figure 50. The correlation between the rod count and FD7 ($R^2 = 0.1221$) was even lower than the correlation between plate count and FD7.

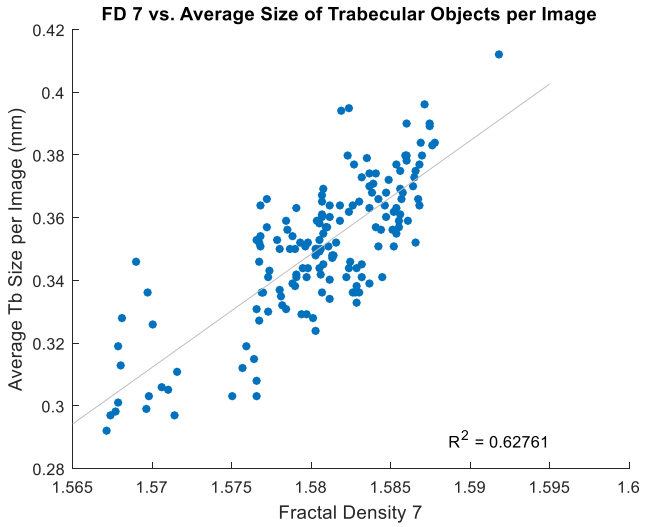

Figure 51. The correlation value was highest ($R^2 = 0.6276$) between the average size of trabeculae per image and FD7.

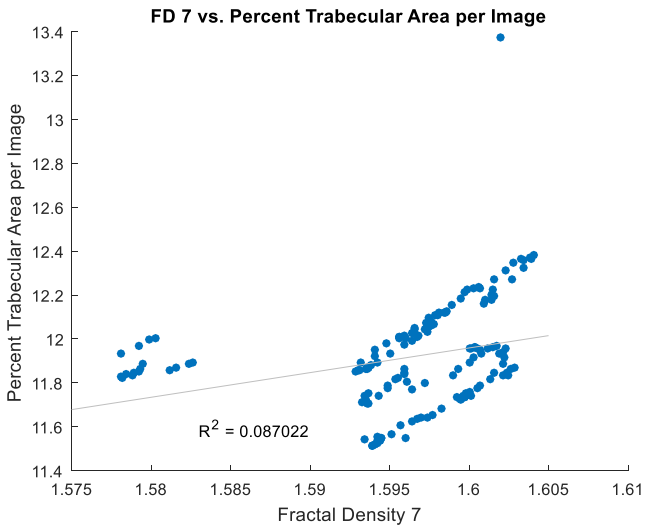

Figure 52. A low correlation was observed between the percent area occupied by trabeculae and FD7 with $R^2 = 0.087$.

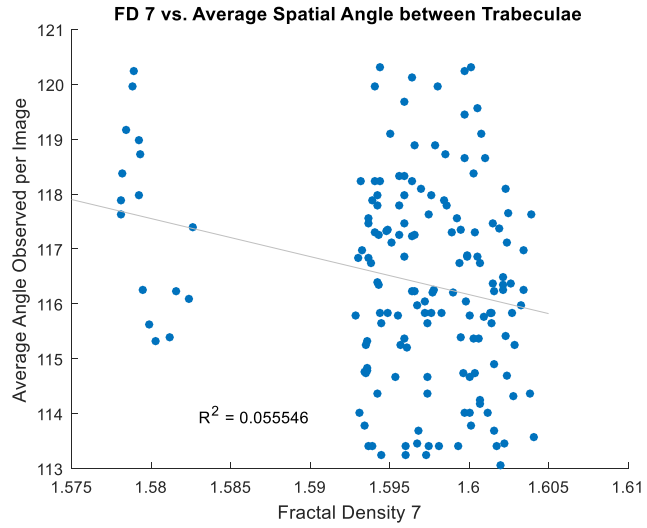

Figure 53. The lowest correlation for FD7 ($R^2 = 0.0555$) was observed with the average spatial angle.

5.8 FD8 COMPARISONS

Fractal density measured grid orientation of 4, Power Series, and 36° rotation.

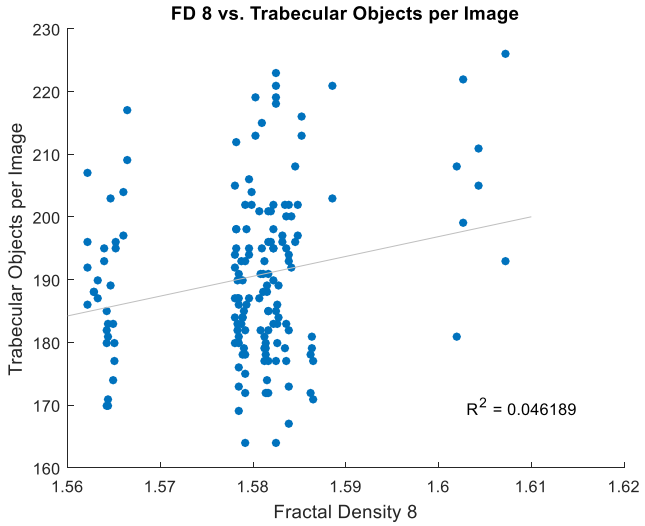

Figure 54. There is a very low correlation between FD8 and the trabecular object count (R^2 = 0.0462).

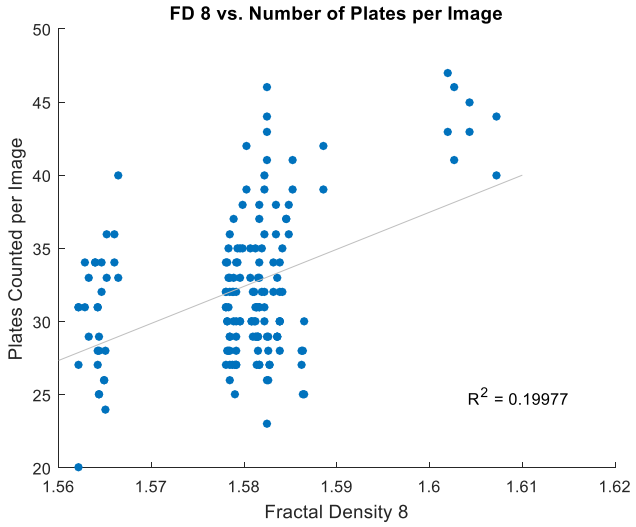

Figure 55. The increase in plate count does not appear to increase at the same interval as FD8 measurements do(R^2 = 0.1998).

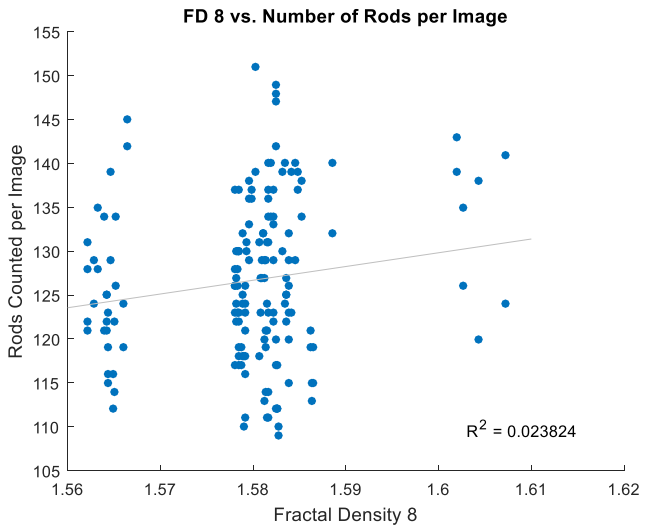

Figure 56. A low correlation is seen between the number of rods in an image and FD8 with R^2 = 0.0238.

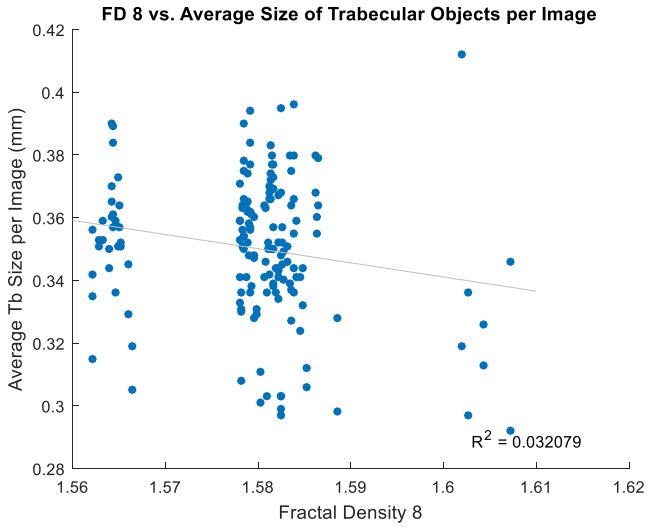

Figure 57. FD8 values only demonstrate a very low correlation with the average size of trabeculae in a given image (R^2 = 0.0321).

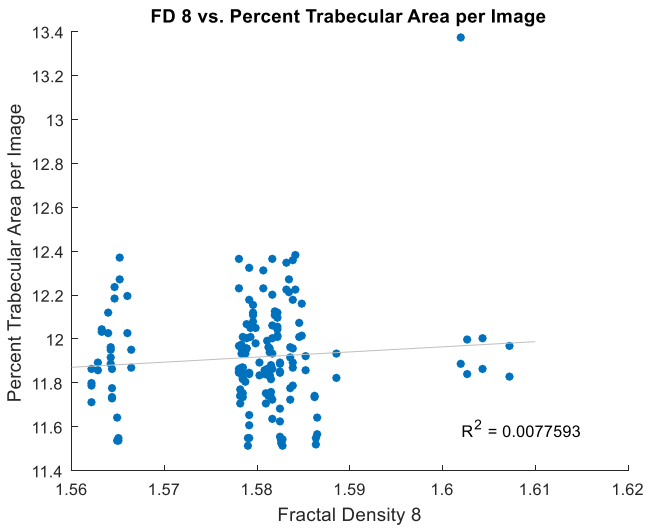

Figure 58. The percentage of area occupied by trabeculae has no correlation with FD8 values (R^2 = 0.0078).

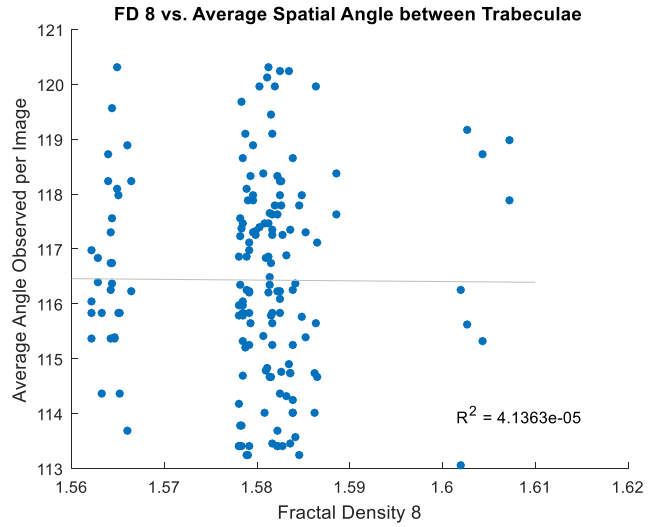

Figure 59. The values of FD8 do not appear to have any correlation with the spatial angle between trabeculae (R^2 = 4.14E-5)

5.9 TWO-DIMENSIONAL FRACTAL MODELS

The following models utilized the average measurements for angular arrangement, inter-trabecular angles, perceived iteration numbers, and sizes of the segments (plates and rods), found in **Table 8**, to create a visual representation of how the trabeculae may grow *in vivo*. The

Young's Modulus was calculated in **Table 8** using Eq. 4.1 from the previous section, which defined the volume fractions of the plates and rods as the plate or rod count divided by total trabecular object count. The Young's Modulus for plates is defined as 6.3, and for the rods as 9.3 GPa, respectively.

Measured Parameter	Mean	Std Dev	Min	Max	Variance	Std Error
Tb. Object Count	190.337	13.212	164	226	174.558	1.035
Plate Count	32.233	5.089	20	47	25.896	0.399
Rod Count	126.779	9.119	109	151	83.148	0.714
Avg. Tb. Size	0.350	0.023	0.292	0.412	0.001	0.002
% Area	11.916	0.238	11.513	13.373	0.056	0.019
Tb. Angular Offset	116.433	1.834	113.053	120.312	3.362	0.144
Et	8.694	0.057	8.509	8.874	0.003	0.004

Table 8. Summary of physically measured parameters gathered from each image. The abbreviation Tb. stands for "Trabecular", and Et for the overall Young's Modulus of the sample based on the bone volume fraction. All of the measurements fall within normal ranges for trabecular bone with the exception of the plate, rod, and total trabecular count; standardized data for these measurements could not be found for the human radius.

FRACTAL BOUNDARY CONDITIONS	
ITERATIONS	5
ANGLE	115
CONSTANT	X
AXIOM	X
RULE 1	X = C0F – [C2[X]+C3X]+C1F[C3+FX]+X
RULE 2	F=FF

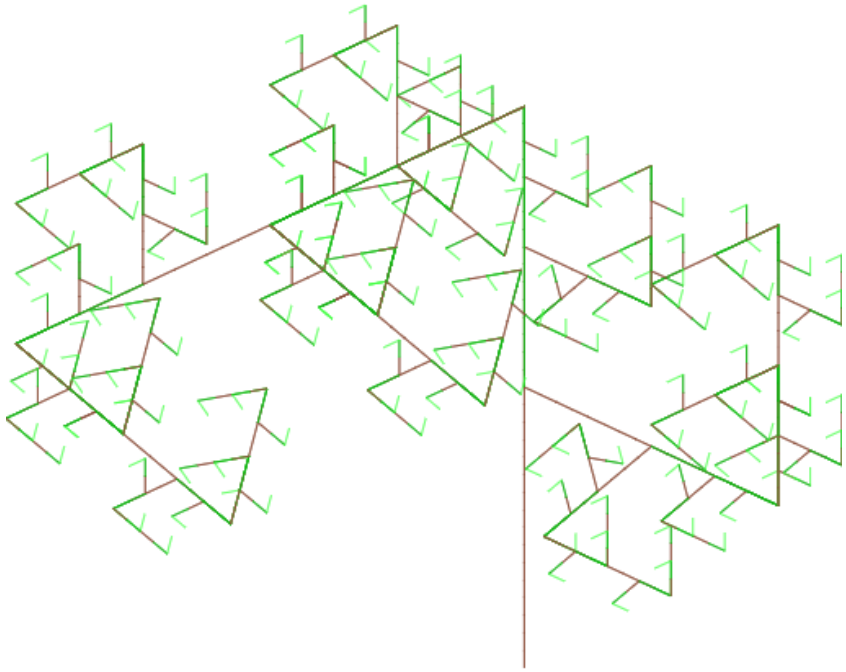

Figure 60. This model uses the average spatial angle found between trabeculae, but the excessive branching in 2D seems overwhelming and does not bear a strong resemblance to cancellous bone structure. If each iteration occurred at a different depth, one can imagine how the structure would begin to resemble that of cancellous bone

FRACTAL BOUNDARY CONDITIONS	
ITERATIONS	3
ANGLE	120
CONSTANT	N/A
AXIOM	F
RULE 1	F = C0F – [C1-F+F+F]+{C2+F-F-F]
RULE 2	N/A

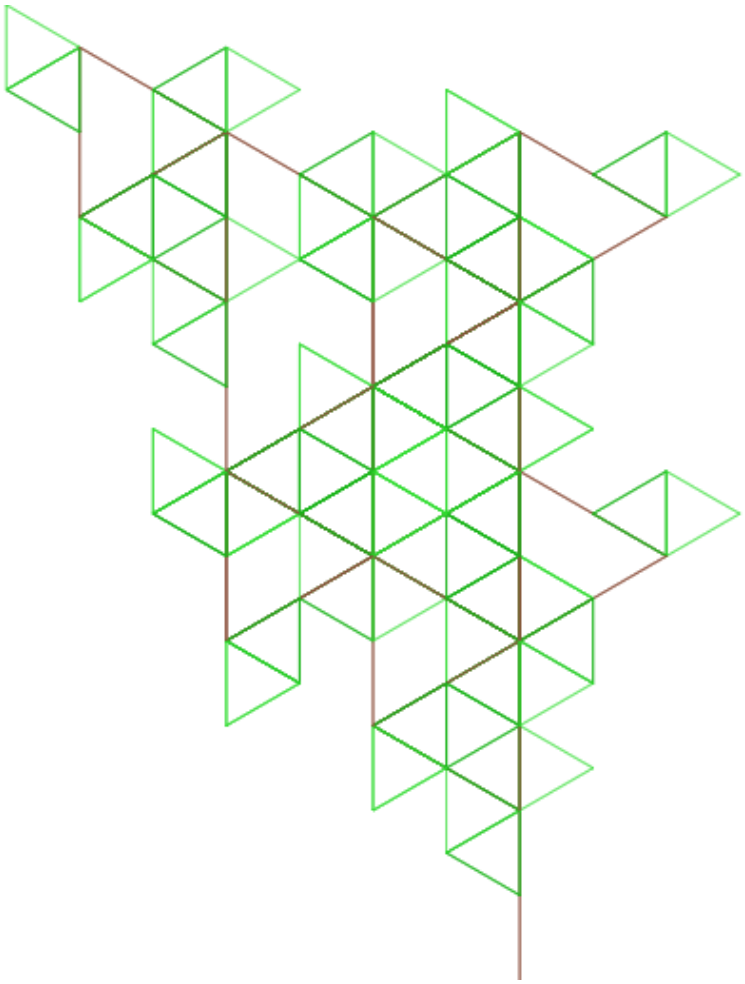

Figure 61. This fractal model shows fewer iterations than the first and uses a slightly larger spatial angle of 120 degrees. This model's iterations once again are better suited for 3D purposes, as only one iteration would occur per image slice if this were a micro-CT scan. The spatial angles prevent the complexity from changing dramatically from iteration to iteration, which is an accurate representation of the fractal properties of bone; fractal density is used more to define arrangement and overall complexity instead of scale and complexity on a scalar level.

FRACTAL BOUNDARY CONDITIONS	
ITERATIONS	2
ANGLE	120
CONSTANT	N/A
AXIOM	F
RULE 1	F = C0F – [C1-F+F+F]+{C2+F-F-F]
RULE 2	N/A

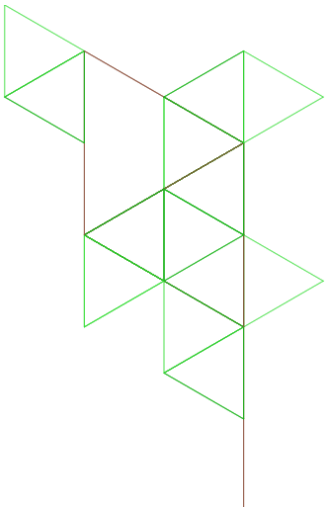

Figure 62. This model uses one less iteration than the one before it (with 2 iterations instead of 3). This model makes it easier to see the progression between the iterations and the density of the iterations because there is more space. The fractals observed in the image used in this experiment demonstrated similar triangular patterns from level to level.

6. DISCUSSION

The results for the comparisons between FD1 through FD8 and the measured parameters were analyzed for significance using JMP statistical analysis software. For every FD variation, the predictive model was found by comparing all measured factors as single-factor effects in addition to examining two-factor and three-factor effect combinations to see how the interactions of these parameters affected the regression model being developed. In the next couple sections, the predictive models that were created using JMP are examined in terms of overall effectiveness and accuracy.

Each of the measured factors was compared with FD and E_t to determine which of the factors had the best correlation. Factors that had R^2 values of 0.70 or higher were considered to be highly correlated and were of primary importance in the factor interaction effects calculated in JMP. However, any factor with R^2 values over 0.5 was considered mildly correlated. Factors that had a high correlation to FD or E_t could potentially be the limiting factor in bone strength and bone arrangement. Initial graphical representation of each of the factors linearly compared with FD or the Young's Modulus show that few had a high correlation value with FD and E_t. The fractal dimensions that appeared to have the most correlation with all factors were FD1 and FD5, each of which had correlation values higher than $R^2 = 0.5$ for plate count, rod count, and the percent area of bone. The best linear fit for FD values was the x-y fit of the percent area of bone with FD1 ($R^2 = 0.6723$), closely followed by x-y fit of the percent area of bone with FD5 ($R^2 = 0.6399$) and average trabecular size with FD3 ($R^2 = 0.6276$). The variations FD1 and FD5 both use the Default Scaling Series with no rotation, the only difference being that FD1 uses a grid

orientation of 12 and FD3 uses a grid orientation of 4. It appeared that FD3 had two factor relationships that indicated correlation (Tb. object count and average Tb. Size), and although the correlated factors are different than those seen between FD1 and FD5, FD3 is similar in variation terms in that it also had no rotation (with grid orientation 12 and utilizing the Power Series). All FD variations had the lowest correlation with trabecular angular offset; the highest correlation value was $R^2 = 0.0555$ with FD7. The Young's Modulus had an overall somewhat low correlation with all FD variations. The lowest correlation was between Et and FD2 ($R^2 = 0.0228$), and the highest was between Et and FD1 ($R^2 = 0.3685$). However, the R^2 value only gives information on the nature of the relationship between variables. To determine the statistical significance based on probability of a scenario and develop a regression model to more appropriately predict the FD and Et values based on the statistics measured in this experiment, F-test applied. The F-statistic was measured for the factorial design but only to the third degree for each FD to avoid severe distortion of interaction effects due to over-complexity.

The factors were compared to FD variations using the "Fit Model" tool in JMP. Each of the factors (Tb. Object Count, Tb. Angular Offset, Avg. Tb. Size, Percent Area, Plate Count, and Rod Count) were compared to examine interactions with each other, up to 3 factors per interaction. The models each went through 4 reductions (maximum) to only include factor effects in the model that were either single-factors or had a significant p-value of $p < 0.05$. FD4 shows a regression model, as all of the coefficients apply only to the single factors, without any interactions at all. The plate count and rod count appear to be the most prominent factors, as they appear both as single factor effects and as interaction effects with a significant influence on the regression model direction (all $p<0.001$). The average trabecular size seemed to have the least effect on the regression model for each FD type; with the exception of FD4, only appeared twice

in FD2 and once in FD1, as opposed to all of the other factors which appeared at least once in every other model. The initial reduction of F5 did not initially show any significant effects from any interactions, indicating that this regression model is likely to be less accurate than the others.

6.1 FD1 REGRESSION MODEL

The following regression model was developed for FD1, which included test variations defined as a grid orientation of 12, the use of the Default Scaling System with box sizes up to 45% of the image, and no rotation:

$$1.0762 + (0.0015 * Tb.Object\ Count) + (0.7491 * Avg.Tb.Size) + (0.0004 * Plate\ Count)$$
$$+ [(Tb.Object\ Count - 190.3374) * (Plate\ Count - 32.2331)$$
$$* (Rod\ Count - 126.7791) * -0.000012]$$
$$+ [(Avg.Tb.Size - 0.03504) * (Plate\ Count - 32.2331) * (Rod\ Count - 126.7791)$$
$$* -0.0072] + [(\%\ Area - 11.9161) * (Plate\ Count - 32.2331)$$
$$* (Rod\ Count - 126.7791) * 0.0002]$$

The FD1 interaction-based regression model shows that single-factor effects have the largest impact on the fractal density prediction as a whole, with all but one factor having a significance of $p < 0.0001$ and the largest coefficient of 0.749 being placed with the average trabecular size. A more visual representation of effects ranked by significance can be found in the Normal Plot for FD1 in the Appendix **Figure A10**. Other interactions are placed with much lower coefficients, indicating smaller effects (the next largest in absolute value is -0.007 on the interaction of average trabecular size, plate count, and rod count). FD1 used a grid origin position of 12, with the default scaling system and no rotation. The consistency allowed the relationship between factors and their effects to remain linear, as evidenced by the residual plot in the Appendix **Figure A11**. The residual plot is a random distribution of data points, but two

linear trends can begin to be form going from top to bottom in the residual plot. A log-log transform on the average trabecular size may be appropriate for models going forward. However, FD1 did have the highest correlation to the calculated Young's Modulus, indicating that it may be the best fit for predictive models governing overall bone strength and flexibility based on composition.

6.2 FD2 REGRESSION MODEL

The following regression model was developed for FD2, which included test variations defined as a grid orientation of 12, the use of the Default Scaling System with box sizes up to 45% of the image, and 36 degree rotation:

$$
\begin{aligned}
1.6337 &+ [(Tb.Object\ Count - 190.3374) * (Tb.Angular\ Offset - 116.4334) \\
&* (Plate\ Count - 32.2331) * -0.0004] \\
&+ [(Tb.Object\ Count - 190.3374) * (Tb.Angular\ Offset - 116.4334) \\
&* (Rod\ Count - 126.7991) * -0.0003] \\
&+ [(Tb.Object\ Count - 190.3374) * (Avg.Tb.Size - 0.3504) \\
&* (Plate\ Count - 32.2331) * -0.2614] \\
&+ [(Tb.Object\ Count - 190.3374) * (Avg.Tb.Size - 0.3504) \\
&* (Rod\ Count - 126.7991) * 0.1909] \\
&+ [(Tb.Object\ Count - 190.3374) * (\%\ Area - 11.9161) \\
&* (Plate\ Count - 32.2331) * 0.0067] \\
&+ [(Tb.Object\ Count - 190.3374) * (\%\ Area - 11.9161) * (Rod\ Count - 126.7991 \\
&* 0.0067]
\end{aligned}
$$

In comparison to FD1, the regression model for FD2 contained no single factor effects as none of them were significant ($p < 0.05$) during model reduction. The most significant

interactions had a p-value of less than 0.0001; the lowest was for the interaction of the trabecular object count, angular offset, and rod count at $p < 0.0004$. In general, the most significant effects are expected to remain in the single factors, so it is unusual to see all the significant effects in this model are 3-factor interactions. The least significant interaction was the angular offset, percent area, and plate count combined to yield $p < 0.0093$. The abnormality of the data continues through the residual plot, where three groupings of data points are observed. The only difference between FD1 and FD2 is that FD2 used a 36 degree rotation of the image while compiling the fractal density data. It is plausible that, even though more data was collected for better averages, the variation within the data set also increased. A data transformation for further analysis is strongly recommended for FD2 based on the Appendix **Figure A15** of the residual plot.

6.3 FD3 REGRESSION MODEL

The following regression model was developed for FD3, which included test variations defined as a grid orientation of 12, the use of the Power Scaling Series, and no rotation:

$$1.3768 + (0.2727 * Avg.Tb.Size) + (0.0061 * \%Area) + (-0.0005 * Plate\ Count) + (-0.0001 * Rod\ Count) + [(Tb.Object\ Count - 190.3374) * (\%Area - 11.9161) * (0.0003)] + (0.0003 * Tb.Object\ Count)$$

The FD3 regression model, similar to FD1 and in contrast to FD2, had its highest levels of significance placed onto the single-factor effects, with only one two-factor effect in the regression model. The most significant effect was plate count as the only factor that had $p <$

0.001, but due to scaling, the highest coefficient was placed with the single-factor average trabecular size. The two-factor effect ($p < 0.0021$) containing the percentage of area occupied by trabeculae and the trabecular object count per image, oddly enough, was composed of the two single-factor effects that were the least significant when standing alone (percent area yielded $p < 0.0155$, whereas trabecular object count was hardly significant at all with $p < 0.0655$). The residual plot for FD3, which can be found in the Appendix **Figure A19**, appeared to be the best out of all of the residual plots for FD1 – FD8 due to the fact that its data points appeared to not only have the best random distribution with few sections evidencing any clumping, but it also appeared to have the most symmetry across the horizontal axis.

6.4 FD4 REGRESSION MODEL

The following regression model was developed for FD4, which included test variations defined as a grid orientation of 12, the use of the Power Scaling Series, and 36 degree rotation:

$$1.4438 + (0.0008 * Tb.Object\ Count) + (0.4327 * Avg.Tb.Size) + (-0.0147 * \%\ Area) + (0.0010 * Plate\ Count) * (-0.0002 * Rod\ Count)$$

The regression model for FD4 was unusual in that it was one of only two regression models to include exclusively single-factor effects, the most significant of which was the plate count per image, as was seen in both FD1 and FD3, confirmed as a relevant statistic by Parfitt [38] with total bone volume to help determine the age of a subject, or vice versa. The regression models developed by Parfitt, though widely well-received, were accepted for publication in 1982, more recent methods should likely go through the plate measurement process again due to the increased imaging capabilities available today. The residual plot for FD4 does seem to have

some outliers that drift toward the top right of the plot. Although the effects line up cohesively with those seen in FD1, the residual plot for FD4 (which can be found in the Appendix **Figure A23**) has enough data point clumping and asymmetry that a transform on the data set may be helpful for future analysis.

6.5 FD5 REGRESSION MODEL

The following regression model was developed for FD5, which included test variations defined as a grid orientation of 4, the use of the Default Scaling Series, and no rotation:

$$1.3608 + (0.232 * \%Area) + [(Tb.Object\ Count - 190.3374) * (\%\ Area - 11.9161) * -0.0006] + [(Avg.Tb.Size - 0.3504) * (\%\ Area - 11.9161) * -0.0239]$$

The combination for analysis used in FD5 was one of the few that yielded a regression model with all factors having significant levels of $p < 0.0001$. The regression equation for FD5 utilized two single-factor effects, one two-factor effect, and one three-factor effect. The percent area was utilized in all levels: single, two-factor, and three-factor, indicating that it had the greatest effect on the regression model for fractal density. The normal plot confirms that the percent area has the largest effect which is found in the Appendix **Figure A26** with the residual plot showing some abnormalities in the data set in **Figure A27**. A study completed by Giesen has shown that the percentage of area covered by trabecular components, also called the bone volume fraction, has a direct relationship to the Young's Modulus [37] in the regression calculations, FD5 did show some correlation with the calculated Young's Modulus (R^2 = 0.3685).

6.6 FD6 REGRESSION MODEL

FD6 utilized the default scaling series with a grid origin of 4 and a 36 degree rotation during analysis.

$$1.6667 + [(Tb.Object\ Count - 190.3374) * (Tb.Angular\ Offset - 116.4334) * (Plate\ Count - 32.2331) * -0.0004]$$
$$+ [(Tb.Object\ Count - 190.3374) * (Tb.Angular\ Offset - 116.4334) * (Rod\ Count - 126.7991) * -0.0003]$$
$$+ [(Tb.Angular\ Offset - 116.4334) * (Avg.Tb.Size - 0.3504) * (Plate\ Count - 32.2331) * -0.2432]$$
$$+ [(Tb.Angular\ Offset - 116.4334) * (Avg.Tb.Size - 0.3504) * (Rod\ Count - 126.7991) * 0.1897]$$
$$+ [(Tb.Angular\ Offset - 116.4334) * (\%Area - 11.9161) * (Plate\ Count - 32.2331) * 0.0061]$$
$$+ [(Tb.Angular\ Offset - 116.4334) * (\%Area - 11.9161) * (Rod\ Count - 126.7791) * -0.0047]$$

The results were very similar to FD2 in that no single-factor effects were used in the regression model, since none of them appeared to be significant, although the normal plot in **Figure A30** and the residual plot in **Figure A31** show abnormalities in data distribution. The common FD variation between FD5 and FD2 was the use of the Default Scaling Series and 36 degree rotation; the grid orientation was different between them. Usually the single-factor effects are considered the most likely to have significant effects on the model. All of the significant interactions were three-factor interactions, and the most significant was only $p < 0.0003$, which is quite small, but not the ideal $p < 0.0001$. The most significant effect was the interaction of angular offset, average trabecular size, and the rod count. Each of the significant effects included

the spatial angular offset and the addition of either the plate count or the rod count, which confirms and aligns with Parfitt, who discovered that the mean trabecular plate thickness had a direct linear correlation with total bone volume [38]. Additionally, Giesen [37] determined that the spatial angular offset had the largest effect on bone mineral density in prediction equations, which can also be directly related to fractal density in terms of arrangement.

6.7 FD7 REGRESSION MODEL

The following regression model was developed for FD7, which included test variations defined as a grid orientation of 4, the use of the Power Scaling Series, and no rotation:

$$1.3835 + (0.0220 * \%Area) + (-0.0010 * Plate\ Count) + (-0.0001 * Rod\ Count) + [(Avg\ Tb.Size - 0.3504) * (\%Area - 11.9161) * (Rod\ Count - 126.7991) * -0.0064]$$

The regression model for FD7 is simple and direct. It contains three single factor effects, the percent area, plate count, and rod count, and one three-factor effect that contains each of the single-factor effects. The progression of each of the single factor effects into the amplified significance of the three-factor effect indicates that this regression model is good for fractal density, and the effects (percent area, or BVF, and plate and rod counts) are ones that have been confirmed as significant by Giesen and Profitt. However, the residual plot for FD7 seen in the Appendix **Figure A35** is very similar to that seen in FD3 (**Figure A19**) and FD5 (**Figure A27**), with a spread out but defined concentration of data points toward the center line and a smaller grouping of points toward one corner of the regression plot. As was suggested for FD3 and FD5 data, a transformation to ensure a normal distribution would likely be useful in solidifying the regression model for FD7.

6.8 FD8 REGRESSION MODEL

The following regression model was developed for FD8, which included test variations defined as a grid orientation of 4, the use of the Power Scaling Series, and 36 degree rotation:

$$1.6700 + (-0.0107 * \%Area) + (0.0011 * Plate\ Count)$$
$$+ [(Tb.Angular\ Offset - 116.4334) * (Plate\ Count - 32.2331)$$
$$* (Rod\ Count - 126.7791) * -0.00001]$$

FD8 is very similar to FD7 in that it has all the same effects with the exception of the single-factor plate count, which is included in FD7 and excluded in FD8. The regression model for FD8 is based off of a grid orientation of 4, the power series, and includes the 36 degree rotation; it only differs from FD7 in that FD7 does not include rotation. However, the residuals for FD8 seen in the Appendix **Figure A39**, show three distinct linear clusters. Because fractal density is log based, a log transformation of data is recommended. Alternatively, because the power series was being used, an exponential transformation of the data would also be useful.

6.9 REGRESSION EQUATION FOR FRACTAL DENSITY

Significant effects from all regression models were combined to develop a generic prediction model for the fractal density. The single- and two-factor effects from each model were accounted to determine which parameter appeared most frequently, and four were selected as most significant to include in the generic regression model. The generic regression model serves as a method by which any one of these factors can be calculated using the fractal density measurement parameters for a given FD. Using the measured parameters one can use this model to find fractal density also. The coefficients for each of the four factors were examined from

each regression model and then averaged to determine the following coefficients seen in the equation. The model is linear, although other fits (such as polynomial or logarithmic) may be used if needed, the majority of the measured parameters exhibited a linear fit. For the sake of consistency and ability for comparison, all of the parameters were linearized. All parameters that showed interactions $p < 0.05$ included in this regression model.

FD = Fractal Density
A = Percent Area
B = Average Trabecular Size
C = Plate Count
D = Rod Count

$$FD = 1.3698 + 0.0230 * A + [(-0.0748) * B]$$
$$+ [(-0.0116) * (B - 0.3504) * (D - 32.2331)] + 0.0003 * C$$
$$+ [0.0004 * (B - 0.3509) * (C - 32.2331) * (D - 126.583)] + [(-0.005623)$$
$$* (B - 0.3509) * (A - 11.9161) * (C - 32.2331)]$$

Summary of R^2 Values and FD Regression Models per Factors

	FD1	FD2	FD3	FD4	FD5	FD6	FD7	FD8
Tb. Object Count	0.3822	0.0134	**0.5243**	0.0859	0.4726	0.0136	0.3469	0.0462
Plate Count	**0.6114**	0.0286	0.3295	0.2841	**0.6013**	0.0326	0.2843	0.1998
Rod Count	**0.503**	**0.503**	0.2328	0.0306	**0.5626**	0.0063	0.1221	0.0238
Avg. Tb. Size	0.1552	0.0078	**0.6276**	0.0607	0.2321	0.0078	**0.6276**	0.0321
% Area	**0.6723**	0.0077	0.0308	0.0155	**0.6399**	0.008	0.087	0.0078
Tb. Angular Offset	0.0048	8.47E-05	0.0548	0.0057	0.0041	1.08E-04	0.0555	4.14E-05
Et	***0.3685***	*0.0288*	*0.1951*	*0.3257*	*0.3336*	*0.0347*	***0.3685***	*0.228*

Table 9. This table is a summary of the R^2 values for all FD variations with the measured parameters from the micro-CT images. The highlighted boxes show medium-to-high correlation values. Correlation values are highest with FD1 and FD5 across all the same micro-CT measurements; FD1 and FD5 both used the default power series and did not use rotation during FD measurements. The greatest number of medium-to-high correlations was seen with rod count.

The values seen in **Table 9** demonstrate the correlation values of each fractal density test with the measured parameters. Based on the correlation values, the best of which are highlighted in yellow, and the average fractal density values calculated for FD1 – FD8 and displayed in

Table 8, it can be seen that the grid position did not have a significant effect on the FD outcome. The "high" grid positions included FD5 – FD8, whereas the "low" included FD1 – FD4, and not only was the distribution between them normal, but the distribution also appeared to be consistent. If the FD values are split according to high and low values based on the scaling series used, more obvious discrepancies are seen, especially in the mean FD value. The FD tests that utilized the Default Sampling Series had a higher average FD value than those using the Power Series, and even more so, had a higher number of correlations with the measured parameters, indicating that the Default Sampling Series could be more accurate than the Power Series. This is due to the fact that the Default Sampling Series sizes boxes based on a maximum percentage of the image being covered by a single box, whereas the Power Series has a much smaller range of box sizes, therefore, using a lower amount for sampling. Finally, when the FD values are split according to rotation, the greatest discrepancy can be seen. Only one of the FD sets that utilized a 36 degree rotation showed any correlations with the measured parameters, and the FD tests that utilized the 36 degree rotation had the highest amount of variation between the means. These results are likely because the 36 degree rotation was chosen to line the image up horizontally along the axis of the highest repetition in the plates; by doing so, the boxes could fit across the image more cleanly, allowing the differences in scaling systems to become very obvious and forcing the means further apart. The lack of correlation with the measured parameters is likely due to the consistency of the measurement within each FD set. There would be little variation or change in each respective FD measurement per image for each FD variation because the axis was aligned for a cleaner box count. Based on these results, it would be recommended that the highest grid orientation value should be used in further testing, along with the Default Sampling Series and no rotation.

7. CONCLUSION

Monitoring and predicting the strength of bone based on its growth can be a very useful tool in the future of medicine. Particularly in patients that are subject to osteoporosis from either age or stress shielding from implants, the modeling of bone opens up many new possibilities for innovation in treatments. Patients having same hierarchical bone structure may have different fractal dimensions. However, with proper scanning of the bone using either micro-CT or high-resolution 3T MRI, the microstructure can be modeled and fractal dimension calculated.

The fractal dimension has direct mathematical correlations to both the Young's Modulus and strength of the bone, both of which can be made more accurate by taking into consideration the composite nature of the bone mathematically. In this research it was shown that the mean Young's modulus of cancellous bone using FD methods was 8.7 GPa compared to global value used in the literature of 10.4 GPa.

Although the area of fractal dimensions and their relationship to plate and rod strength and arrangement has a good basis using law of mixture in calculating composite properties, there are a few parameters that limit and have the greatest impact on fractal density. The variables are angular arrangement in the x, y, and z planes of each scan, the ratio of lengths between the plates and rods, the total percentage the trabeculae occupy, the number of plates versus the number of rods, the spacing of the plates and rods from the distal-to-proximal, medial-to-lateral, or from the cortical shell to the center of the bone, among others.

Many of these questions may be answered using software tools to take a few simple measurements. ImageJ is one such program that allows the user to quickly and easily convert and

image to binary then take measurements. The micro-CT scans used in this study were pre-thresholded for the most accurate depiction of the plates and rods, considering that when taking a CT scan, blurring around the edges due to quality of resolution can yield up to 30% error in determining the actual size of the trabeculae.

The fractal density has a very direct correlation to bone strength that bone mineral density cannot account for due to the hierarchical nature of bone. The layers of bone are too complex and too individual in a composite sense to treat their mechanical characteristics as a global material behavior. Further evaluation of each individual layer as outlined in this research should be considered in order to creating a comprehensive computational model for strength prediction.

REFERENCES

[1] Weiner S, Wagner HD. The material bone: structure–mechanical function relations. Ann Rev Mat Sci 1998;28:271–98.

[2] Fratzl P, Weinkamer R. Nature's hierarchical materials. Progr Mat Sci 2007;52:1263–334.

[3] Rho JY, Kuhn-Spearing L, Zioupos P. Mechanical properties and the hierarchical structure of bone. Med Eng Phys 1998;20:92–102.

[4] Havers C. Osteologia Nova. London: Samuel Smith; 1691. [6] Munro A. The Anatomy of the human bones, nerves, and lacteal sac and duct. G. Hamilton & J. Balfour; 1763.

[5] Gebhardt FSMW. Über funktionell wichtige Anordnungweisen der feineren und großeren Bauelemente des Wirbeltierknoches. II Spezieller Teil. 1. Der Bau der haversschen Lamellensysteme und seine funktionelle Bedeutung. Roux Arch 1905;20:187–334.

[6] Weidenreich F. Das Knochengewebe. In: Mollendorf WV, editor. Handbuch der mikroskopischen Anatomie des Menschen. Berlin: Springer; 1930. p. 391–520.

[7] Martin RB, Burr DB. Structure, function and adaptation of compact bone. New York: Raven Press; 1989.

[8] Hatchett C. Experiments and observations on shell and bone. Philos. Trans. 1799;XVIII:315–34.

[9] Humphry GM. A treatise on the human skeleton. London: MacMillan & Company; 1858.

[10] de Jong WF. La substance minerale dans les os. Recl Trav Chim Pays-Bas Belg 1926;45:445–8.

[11] McConnell D. The crystal chemistry of carbonate apatites and their relationship to the composition of calcified tissues. J Dent Res 1952;31:53–63.

[12] Schmidt WJ. Uber die Kristallorientierung im Zahnschmelz. Naturwissenschaften 1936;24:361.

[13] Stuhler R. Uber den Feinbau des Knochens. Fortscht Geb Rontgenstrahlen 1937;57:231–64

[14] Robey PG. Biochemistry of bone. In: Riggs BL, Melton LJ, editors. Osteoporosis: etiology, diagnosis and management. Philadelphia: Lippincott-Raven Publishers; 1995. p. 41–66.

[15] Mehta SS. Analysis of the mechanical properties of bone material using nondestructive ultrasound reflectometry. PhD Dissertation, The University of Texas Southwestern Medical Center at Dallas, 1995.

[16] Weiner S, Traub W. Bone structure: from angstroms to microns. FASEB 1992;6:879–85.

[17] Landis WJ. The strength of a calcified tissue depends in part on the molecular structure and organization of its constituent mineral crystals in their organic matrix. Bone 1995;16:533–44.

[18] Reilly DT, Burstein AH, Frankel VH. The elastic modulus of bone. J Biomech 1974;7:271–5.

[19] Choi K, Kuhn JL, Ciarelli MJ, Goldstein SA. The elastic moduli of human subchondral trabecular, and cortical bone tissue and the size-dependency of cortical bone modulus. J Biomech 1990;23:1103–13.

[20] Rho JY, Tsui TY, Pharr GM. Elastic properties of human cortical and trabecular lamellar bone measured by nanoindentation. Biomaterials 1997;18:1325–30.

[21] Bundy KJ. Composite material models for bone. In: Cowin SC, editor. Bone mechanics. Boca Raton, Florida: CRC Press, 1989:197–210.

[22] Kaye BH. Discovering texture fractals. In A random Walk through Fractal Dimensions, Kaye BH (ed.). VCH: Weinheim, 1989; 20–25.

[23] Cross SS, Rogers S, Silcocks PB, et al. Trabecular bone does not have a fractal signature on light microscopic examination. J Pathol 1993; 170: 311–313.

[24] Parkinson IH, Fazzalari NL. Methodological priciples for fractal analysis of trabecular bone. J Microsc 2000; 198: 134–142.

[25] Buckland-Wright JC, Lynch JA, Macfarlane DG. Fractal signature analysis measures cancellous bone organisation in macroradiographs of patients with knee osteoarthritis. Ann Rheum Dis 1996; 55: 749–755.

[26] Cross SS. The application of fractal geometric analysis to microscopic images. Micron 1994; 25: 101–113.

[27] Losa GA, Nonnenmacher TF. Self-similarity and fractal irregularity in pathologic tissues. Mod Pathol 1996; 9: 174–182.

[28] Mandelbrot BB. The Fractal Geometry of Nature. W. H. Freeman: New York, 1982.

[29] Heymann JAW, Hayles M, Gestmann I, Giannuzzi L, Lich B, Subramaniam S. Site-specific 3D imaging of cells and tissues with a dual beam microscope. J Struct Biol 2006;155:63–73.

[30] Reznikov N, Shahar R, Weiner S. Three-dimensional structure of human lamellar bone: the presence of two different materials and new insights into the hierarchical organization. Bone 2014;59:93–104.

[31] Reznikov N, Almany-Magal R, Shahar R, Weiner S. Three-dimensional imaging of collagen fibril organization in rat circumferential lamellar bone using a dual beam electron microscope reveals ordered and disordered sub-lamellar structures. Bone 2013;52:676–83.

[32] Reznikov N, Shahar R, Weiner S. Bone hierarchical structure in three dimensions. Acta Biomater 2014;10(9):3815–26.

[33] Hayat AM. Principles and techniques of electron microscopy: biological applications. 4th ed. Cambridge University Press; 2000.

[34] Chissoe WF, Vezey EL, Skvarla JJ. The use of osmium-thiocarbohydrazide for structural stabilization and enhancement of secondary electron images in scanning electron microscopy of pollen. Grana 1995;34:317–24.

[35] Leser V, Drobne D, Pipan Z, Milani M, Tatti F. Comparison of different preparation methods of biological samples for FIB milling and SEM investigation. J Microsc 2009;233(2):309–19.

[36] Rinnerthaler S, Roschger P, Jakob HF, Nader A, Klaushofer K, Fratzl P. Scanning small angle X-ray scattering analysis of human bone sections. Calcif Tissue Int 1999;64(5): 422–9.

[37] Giesen, E. B. W., et al. Mechanical properties of cancellous bone in the human mandibular condyle are anisotropic. *Journal of biomechanics* 34.6 (2001): 799-803.

[38] Parfitt, A. M., et al. Relationships between surface, volume, and thickness of iliac trabecular bone in aging and in osteoporosis. Implications for the microanatomic and cellular mechanisms of bone loss. *Journal of clinical investigation* 72.4 (1983): 1396.

APPENDIX

PLOTS FOR FD1

```
%Grid position: 12
%Default Scaling Series
%No Rotation

close all
clc
```

FD1 vs. TbObjectCount

```
figure
x1 = FD1;
y1 = TbObjectCount;
sz=25;
scatter(x1,y1,sz,'o','filled')
title('FD 1 vs. Trabecular Objects per Image')
xlabel('Fractal Density 1')
ylabel('Trabecular Objects per Image')

mdl = fitlm(x1,y1)
lsline
mdl.Rsquared.Ordinary

rsq = ['R^2 = ',num2str(mdl.Rsquared.Ordinary)];
text(1.64,170,rsq,'HorizontalAlignment','right')

hold on
```

```
mdl =


Linear regression model:
    y ~ 1 + x1

Estimated Coefficients:
                   Estimate      SE      tStat       pValue
                   ________    ______    ______    __________

    (Intercept)    -1729.8      192.4    -8.991    6.4047e-16
    x1              1178.3     118.06    9.9804    1.4623e-18

Number of observations: 163, Error degrees of freedom: 161
Root Mean Squared Error: 10.4
R-squared: 0.382,  Adjusted R-Squared 0.378
F-statistic vs. constant model: 99.6, p-value = 1.46e-18

ans =
```

```
0.3822
```

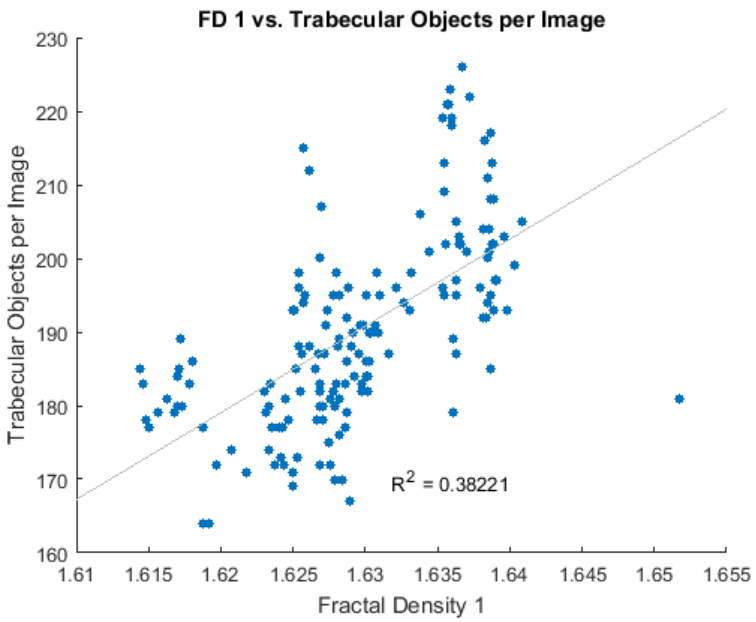

FD1 vs. Plates

```
figure
x2 = FD1;
y2 = Plates;
sz=25;
scatter(x2,y2,sz,'o','filled')
title('FD 1 vs. Number of Plates per Image')
xlabel('Fractal Density 1')
ylabel('Plates Counted per Image')

mdl = fitlm(x2,y2)
lsline
mdl.Rsquared.Ordinary

rsq = ['R^2 = ',num2str(mdl.Rsquared.Ordinary)];
text(1.64,25,rsq,'HorizontalAlignment','right')

hold on
```

```
mdl =


Linear regression model:
    y ~ 1 + x1

Estimated Coefficients:
                   Estimate       SE       tStat       pValue
```

```
                   ________    _______    ________    __________

    (Intercept)    -903.15      58.772    -15.367     2.2038e-33
    x1                 574      36.065     15.916     7.2159e-35


Number of observations: 163, Error degrees of freedom: 161
Root Mean Squared Error: 3.18
R-squared: 0.611,  Adjusted R-Squared 0.609
F-statistic vs. constant model: 253, p-value = 7.22e-35

ans =

    0.6114
```

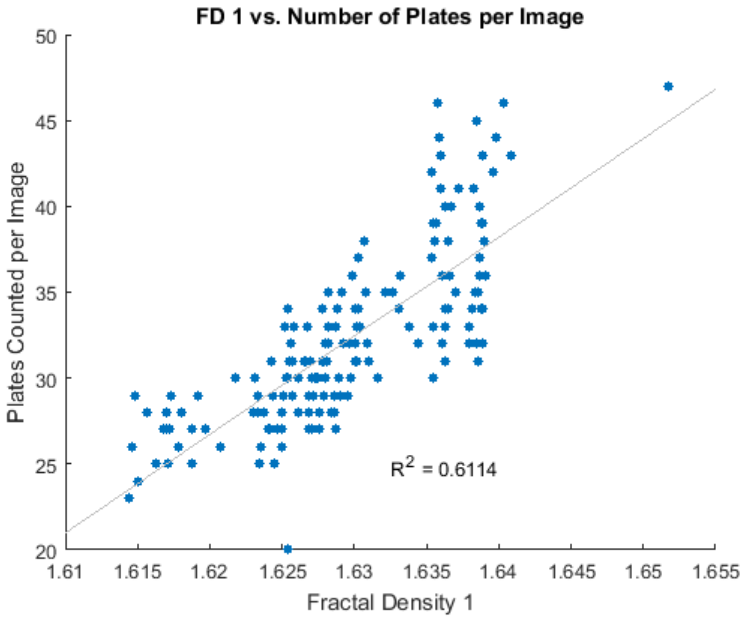

FD1 vs. Rods

```
figure
x3 = FD1;
y3 = Rods;
sz=25;
scatter(x3,y3,sz,'o','filled')
title('FD 1 vs. Number of Rods per Image')
xlabel('Fractal Density 1')
ylabel('Rods Counted per Image')

mdl = fitlm(x3,y3)
lsline
mdl.Rsquared.Ordinary

rsq = ['R^2 = ',num2str(mdl.Rsquared.Ordinary)];
text(1.64,110,rsq,'HorizontalAlignment','right')
```

```
hold on
```

```
mdl =


Linear regression model:
    y ~ 1 + x1

Estimated Coefficients:
                   Estimate      SE       tStat       pValue
                   ________    _______    _______    __________

    (Intercept)    -1392.6     119.01    -11.702    2.8004e-23
    x1              932.23     73.028     12.765    3.1624e-26


Number of observations: 163, Error degrees of freedom: 161
Root Mean Squared Error: 6.44
R-squared: 0.503,  Adjusted R-Squared 0.5
F-statistic vs. constant model: 163, p-value = 3.16e-26

ans =

    0.5030
```

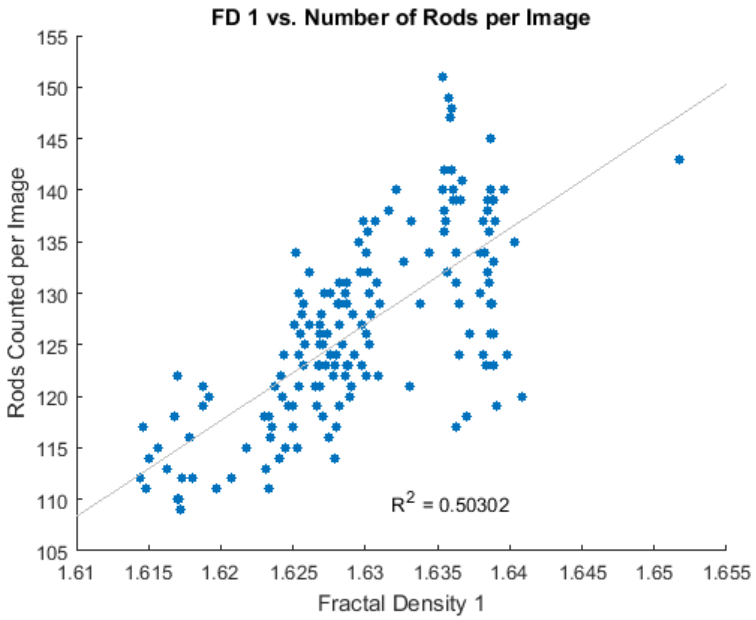

FD1 vs. Avg Tb Size

```
figure
x4 = FD1;
y4 = AverageSize;
```

```
sz=25;
scatter(x4,y4,sz,'o','filled')
title('FD 1 vs. Average Size of Trabecular Objects per Image')
xlabel('Fractal Density 1')
ylabel('Average Tb Size per Image (mm)')

mdl = fitlm(x4,y4)
lsline
mdl.Rsquared.Ordinary

rsq = ['R^2 = ',num2str(mdl.Rsquared.Ordinary)];
text(1.65,0.29,rsq,'HorizontalAlignment','right')

hold on
```

```
mdl =


Linear regression model:
    y ~ 1 + x1

Estimated Coefficients:
                   Estimate      SE        tStat       pValue
                   ________    _______    _______    __________

    (Intercept)     2.4469     0.38556     6.3464    2.1441e-09
    x1             -1.2865     0.23659    -5.4376    1.9699e-07


Number of observations: 163, Error degrees of freedom: 161
Root Mean Squared Error: 0.0209
R-squared: 0.155,  Adjusted R-Squared 0.15
F-statistic vs. constant model: 29.6, p-value = 1.97e-07

ans =

    0.1552
```

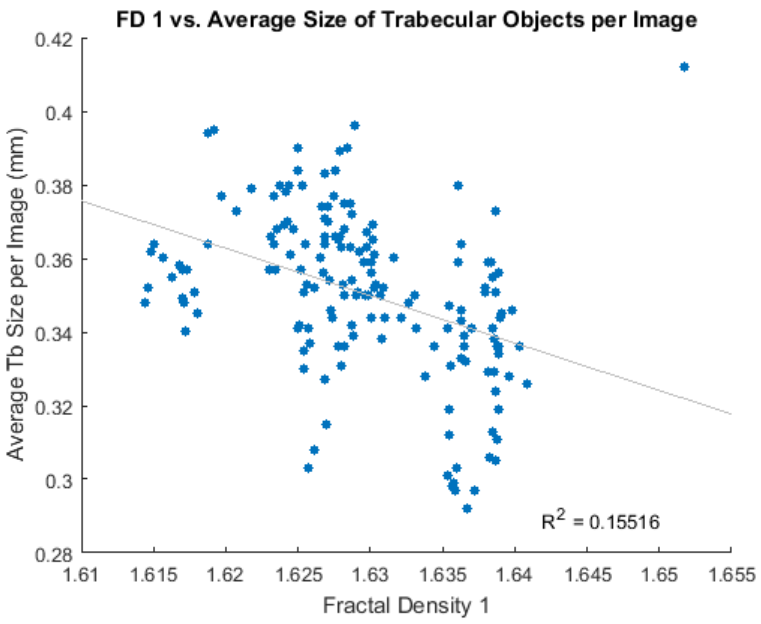

FD1 vs. % Tb Area

```
figure
x5 = FD1;
y5 = Area;
sz=25;
scatter(x5,y5,sz,'o','filled')
title('FD 1 vs. Percent Trabecular Area per Image')
xlabel('Fractal Density 1')
ylabel('Percent Trabecular Area per Image')

mdl = fitlm(x5,y5)
lsline
mdl.Rsquared.Ordinary

rsq = ['R^2 = ',num2str(mdl.Rsquared.Ordinary)];
text(1.64,11.6,rsq,'HorizontalAlignment','right')

hold on
```

```
mdl =


Linear regression model:
    y ~ 1 + x1

Estimated Coefficients:
                   Estimate      SE       tStat       pValue
                   ________    ______    ________    __________

    (Intercept)    -33.865     2.5189    -13.444     4.1686e-28
    x1              28.094     1.5457     18.175      7.525e-41
```

```
Number of observations: 163, Error degrees of freedom: 161
Root Mean Squared Error: 0.136
R-squared: 0.672,  Adjusted R-Squared 0.67
F-statistic vs. constant model: 330, p-value = 7.52e-41

ans =

    0.6723
```

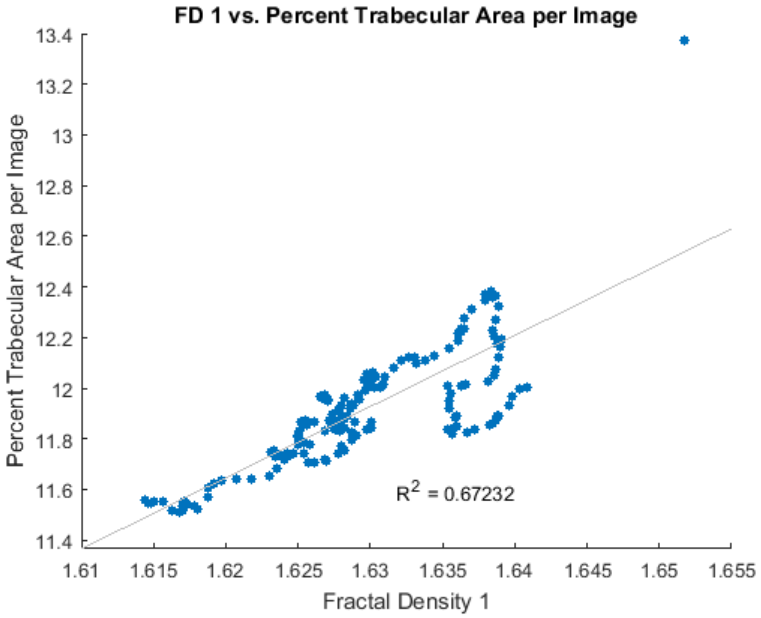

FD1 vs. Avg Spatial Anglular Offset in 2D

```
figure
x6 = FD1;
y6 = AvgAngle;
sz=25;
scatter(x6,y6,sz,'o','filled')
title('FD 1 vs. Average Spatial Angle between Trabeculae')
xlabel('Fractal Density 1')
ylabel('Average Angle Observed per Image (degrees)')

mdl = fitlm(x6,y6)
lsline
mdl.Rsquared.Ordinary

rsq = ['R^2 = ',num2str(mdl.Rsquared.Ordinary)];
text(1.65,114,rsq,'HorizontalAlignment','right')

hold on
```

```
mdl =


Linear regression model:
    y ~ 1 + x1

Estimated Coefficients:
                   Estimate      SE       tStat      pValue
                   ________    ______    _______    ________

    (Intercept)    86.422       33.89     2.5501    0.011703
    x1             18.416      20.796    0.88555     0.37718


Number of observations: 163, Error degrees of freedom: 161
Root Mean Squared Error: 1.83
R-squared: 0.00485,  Adjusted R-Squared -0.00133
F-statistic vs. constant model: 0.784, p-value = 0.377

ans =

    0.0048
```

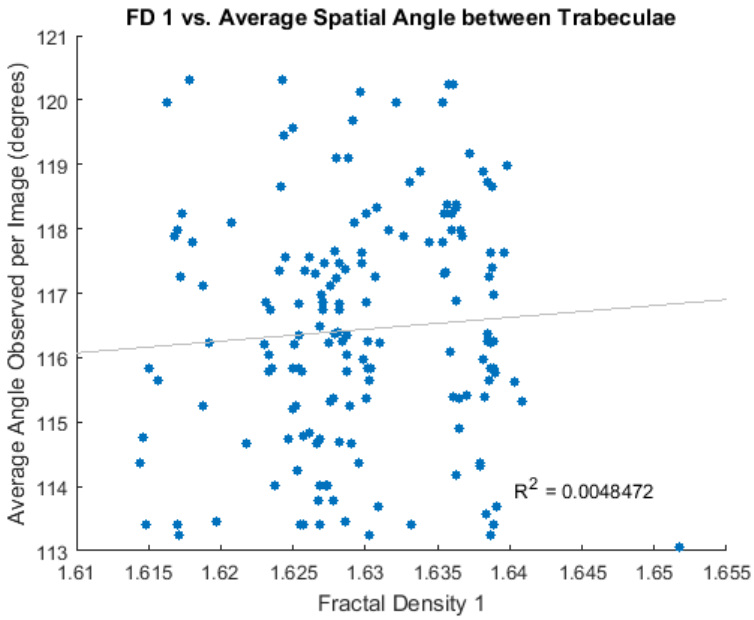

A1. All of the plots for FD1 were generated using the MATLAB code above.

PLOTS FOR FD2

```
%Grid position: 12
%Default Scaling Series
%36 Degrees Rotation
```

```
close all
clc
```

FD2 vs. TbObjectCount

```
figure
b1 = FD2;
y1 = TbObjectCount;
sz=25;
scatter(b1,y1,sz,'o','filled')
title('FD 2 vs. Trabecular Objects per Image')
xlabel('Fractal Density 2')
ylabel('Trabecular Objects per Image')

mdl = fitlm(b1,y1)
lsline
mdl.Rsquared.Ordinary

rsq = ['R^2 = ',num2str(mdl.Rsquared.Ordinary)];
text(1.65,170,rsq,'HorizontalAlignment','right')

hold on
```

```
mdl =


Linear regression model:
    y ~ 1 + x1

Estimated Coefficients:
                   Estimate      SE      tStat     pValue
                   ________    _______    ______    _______

    (Intercept)    13.204      119.81    0.1102    0.91239
    x1             108.41      73.329    1.4785    0.14124


Number of observations: 163, Error degrees of freedom: 161
Root Mean Squared Error: 13.2
R-squared: 0.0134,  Adjusted R-Squared 0.00727
F-statistic vs. constant model: 2.19, p-value = 0.141

ans =

    0.0134
```

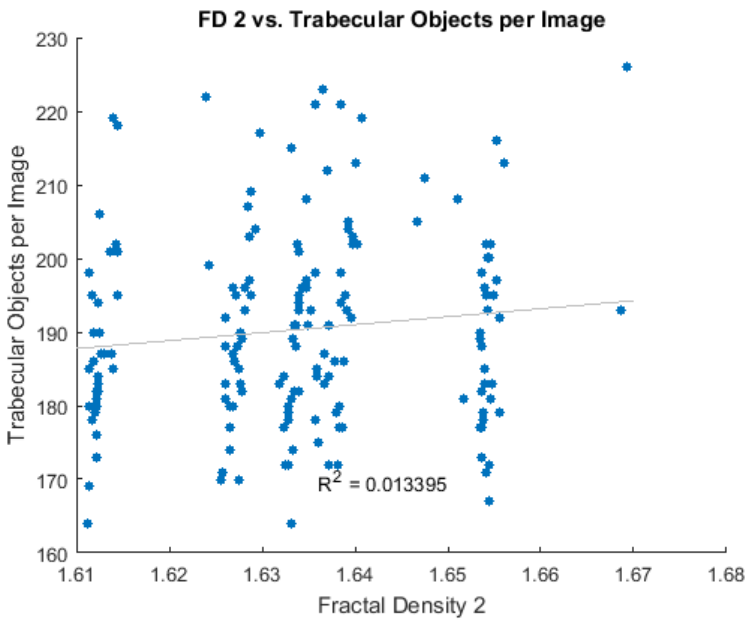

FD2 vs. Plates

```
figure
b2 = FD2;
y2 = Plates;
sz=25;
scatter(b2,y2,sz,'o','filled')
title('FD 2 vs. Number of Plates per Image')
xlabel('Fractal Density 2')
ylabel('Plates Counted per Image')

mdl = fitlm(b2,y2)
lsline
mdl.Rsquared.Ordinary

rsq = ['R^2 = ',num2str(mdl.Rsquared.Ordinary)];
text(1.65,25,rsq,'HorizontalAlignment','right')

hold on
```

```
mdl =


Linear regression model:
    y ~ 1 + x1

Estimated Coefficients:
                   Estimate      SE       tStat      pValue
                   ________    ______    _______    _______

    (Intercept)    -67.402     45.792    -1.4719      0.143
    x1              60.981     28.026     2.1759    0.03102
```

```
Number of observations: 163, Error degrees of freedom: 161
Root Mean Squared Error: 5.03
R-squared: 0.0286,  Adjusted R-Squared 0.0225
F-statistic vs. constant model: 4.73, p-value = 0.031

ans =

    0.0286
```

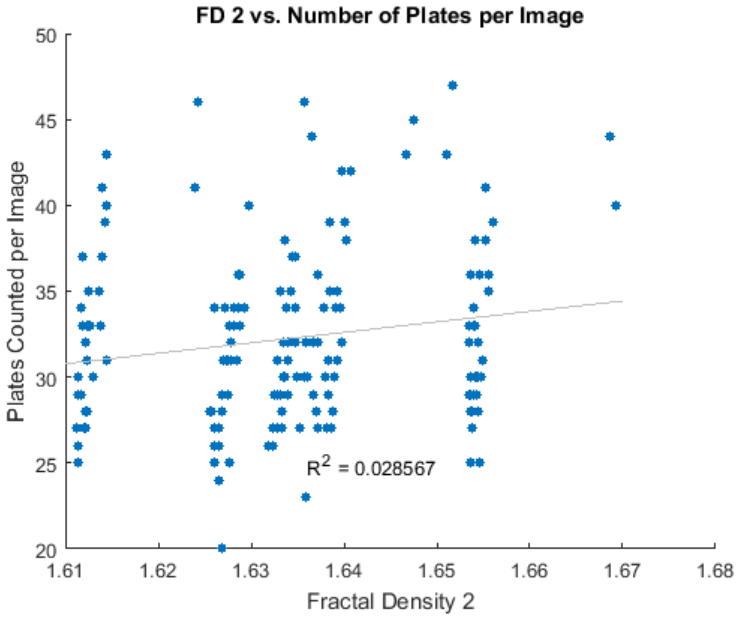

FD2 vs. Rods

```
figure
b3 = FD2;
y3 = Rods;
sz=25;
scatter(b3,y3,sz,'o','filled')
title('FD 2 vs. Number of Rods per Image')
xlabel('Fractal Density 2')
ylabel('Rods Counted per Image')

mdl = fitlm(x3,y3)
lsline
mdl.Rsquared.Ordinary

rsq = ['R^2 = ',num2str(mdl.Rsquared.Ordinary)];
text(1.65,110,rsq,'HorizontalAlignment','right')

hold on
```

```
mdl =


Linear regression model:
    y ~ 1 + x1

Estimated Coefficients:
                   Estimate      SE       tStat       pValue
                   ________    ______    _______    __________

    (Intercept)    -1392.6     119.01    -11.702    2.8004e-23
    x1              932.23     73.028     12.765    3.1624e-26


Number of observations: 163, Error degrees of freedom: 161
Root Mean Squared Error: 6.44
R-squared: 0.503,  Adjusted R-Squared 0.5
F-statistic vs. constant model: 163, p-value = 3.16e-26

ans =

    0.5030
```

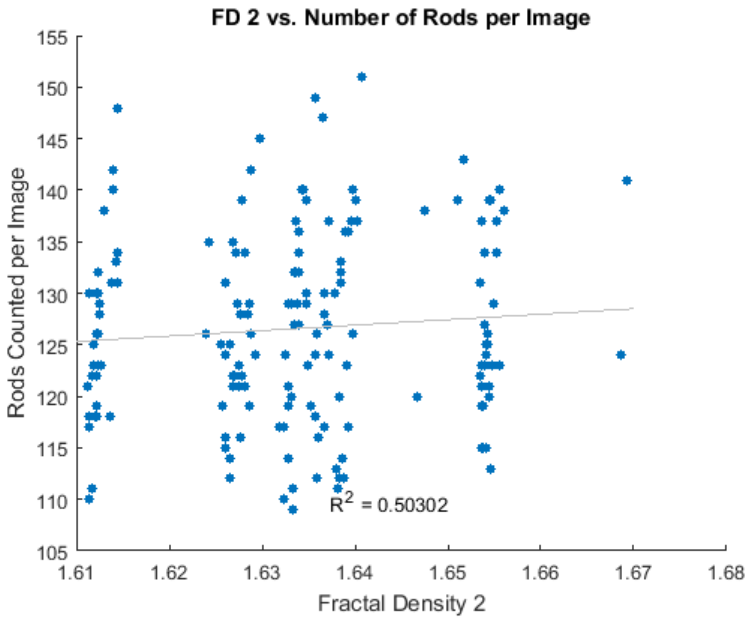

FD2 vs. Avg Tb Size

```
figure
b4 = FD2;
y4 = AverageSize;
sz=25;
scatter(b4,y4,sz,'o','filled')
title('FD 2 vs. Average Size of Trabecular Objects per Image')
```

```
xlabel('Fractal Density 2')
ylabel('Average Tb Size per Image (mm)')

mdl = fitlm(b4,y4)
lsline
mdl.Rsquared.Ordinary

rsq = ['R^2 = ',num2str(mdl.Rsquared.Ordinary)];
text(1.65,0.29,rsq,'HorizontalAlignment','right')

hold on
```

```
mdl =


Linear regression model:
    y ~ 1 + x1

Estimated Coefficients:
                   Estimate      SE        tStat      pValue
                   ________    _______    _______    _________

    (Intercept)     0.58184     0.2059     2.8258    0.0053136
    x1             -0.14166    0.12602    -1.1241      0.26263


Number of observations: 163, Error degrees of freedom: 161
Root Mean Squared Error: 0.0226
R-squared: 0.00779,  Adjusted R-Squared 0.00162
F-statistic vs. constant model: 1.26, p-value = 0.263

ans =

    0.0078
```

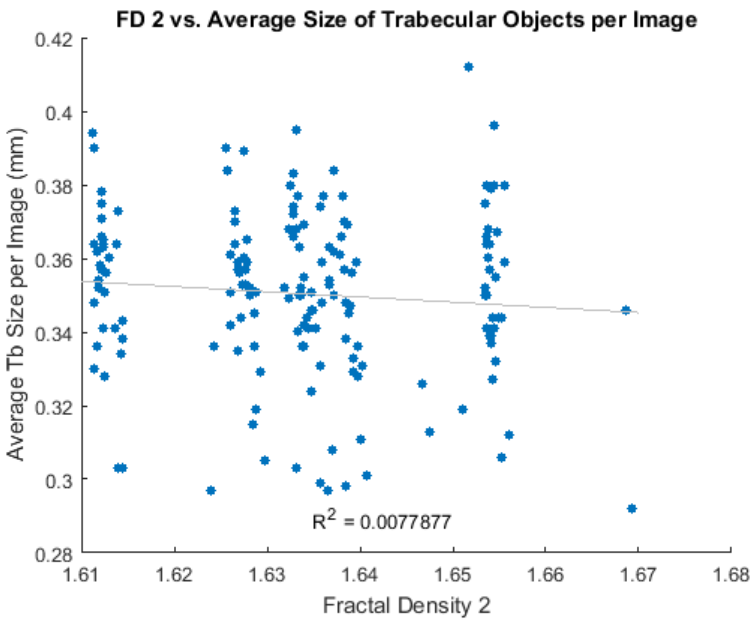

FD2 vs. % Tb Area

```
figure
b5 = FD2;
y5 = Area;
sz=25;
scatter(b5,y5,sz,'o','filled')
title('FD 2 vs. Percent Trabecular Area per Image')
xlabel('Fractal Density 2')
ylabel('Percent Trabecular Area per Image')

mdl = fitlm(b5,y5)
lsline
mdl.Rsquared.Ordinary

rsq = ['R^2 = ',num2str(mdl.Rsquared.Ordinary)];
text(1.65,11.6,rsq,'HorizontalAlignment','right')

hold on
```

```
mdl =


Linear regression model:
    y ~ 1 + x1

Estimated Coefficients:
                   Estimate      SE      tStat       pValue
                   ________    ______    ______    __________

    (Intercept)    9.5055      2.1601    4.4004    1.9589e-05
    x1             1.4754       1.322     1.116       0.26607
```

```
Number of observations: 163, Error degrees of freedom: 161
Root Mean Squared Error: 0.237
R-squared: 0.00768,  Adjusted R-Squared 0.00151
F-statistic vs. constant model: 1.25, p-value = 0.266

ans =

    0.0077
```

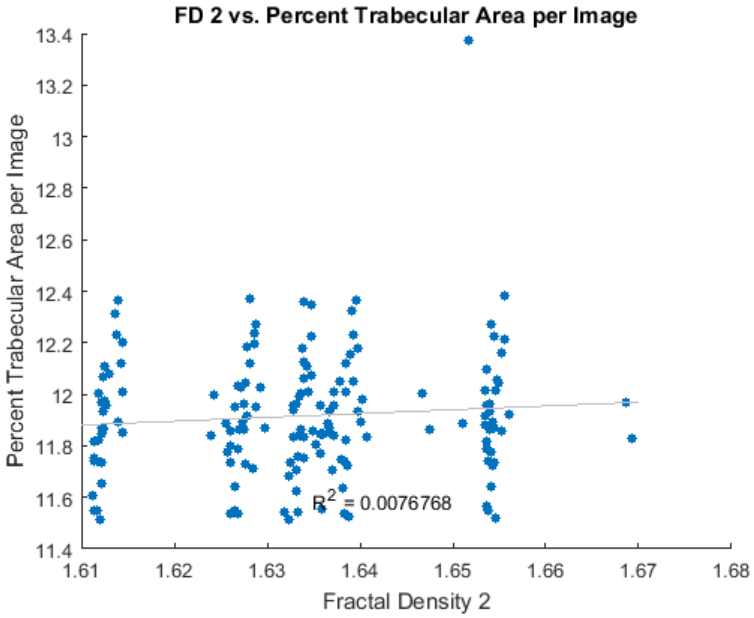

FD2 vs. Avg Spatial Anglular Offset in 2D

```
figure
b6 = FD2;
y6 = AvgAngle;
sz=25;
scatter(b6,y6,sz,'o','filled')
title('FD 2 vs. Average Spatial Angle between Trabeculae')
xlabel('Fractal Density 2')
ylabel('Average Angle Observed per Image')

mdl = fitlm(b6,y6)
lsline
mdl.Rsquared.Ordinary

rsq = ['R^2 = ',num2str(mdl.Rsquared.Ordinary)];
text(1.65,114,rsq,'HorizontalAlignment','right')

hold on
```

```
mdl =


Linear regression model:
    y ~ 1 + x1

Estimated Coefficients:
                   Estimate      SE       tStat       pValue
                   ________    ______    _______    __________

    (Intercept)    114.48      16.741     6.8384    1.5778e-10
    x1             1.1965      10.246    0.11678       0.90718


Number of observations: 163, Error degrees of freedom: 161
Root Mean Squared Error: 1.84
R-squared: 8.47e-05,  Adjusted R-Squared -0.00613
F-statistic vs. constant model: 0.0136, p-value = 0.907

ans =

   8.4698e-05
```

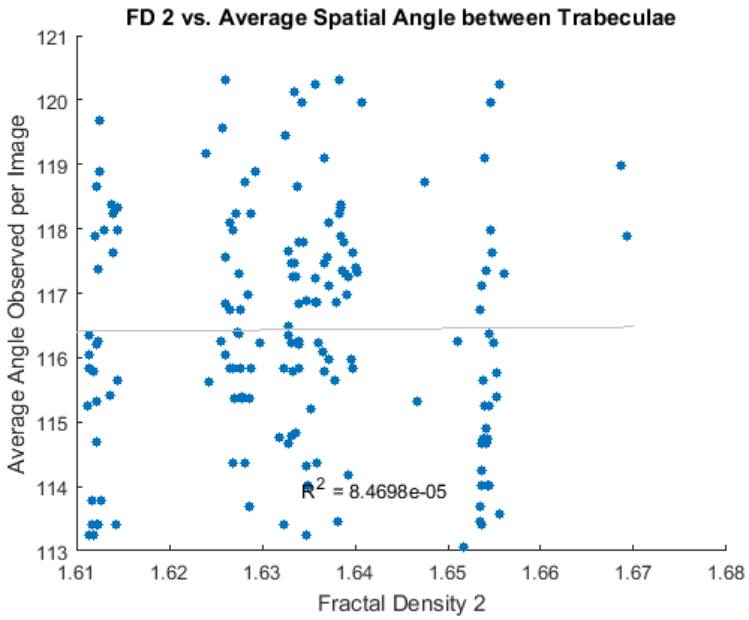

A2. All of the plots for FD2 were generated using the MATLAB code above.

PLOTS FOR FD3

```
%Grid position: 12
%Power Series
```

```
%No Rotation

close all
clc
```

FD3 vs. TbObjectCount

```
figure
c1 = FD3;
y1 = TbObjectCount;
sz=25;
scatter(c1,y1,sz,'o','filled')
title('FD 3 vs. Trabecular Objects per Image')
xlabel('Fractal Density 3')
ylabel('Trabecular Objects per Image')

mdl = fitlm(c1,y1)
lsline
mdl.Rsquared.Ordinary

rsq = ['R^2 = ',num2str(mdl.Rsquared.Ordinary)];
text(1.58,170,rsq,'HorizontalAlignment','right')

hold on
```

```
mdl =


Linear regression model:
    y ~ 1 + x1

Estimated Coefficients:
                   Estimate      SE       tStat       pValue
                   ________    ______    _______    __________

    (Intercept)     3236.8     228.71     14.153     4.624e-30
    x1             -1927.5      144.7    -13.321    9.1666e-28


Number of observations: 163, Error degrees of freedom: 161
Root Mean Squared Error: 9.14
R-squared: 0.524,  Adjusted R-Squared 0.521
F-statistic vs. constant model: 177, p-value = 9.17e-28

ans =

    0.5243
```

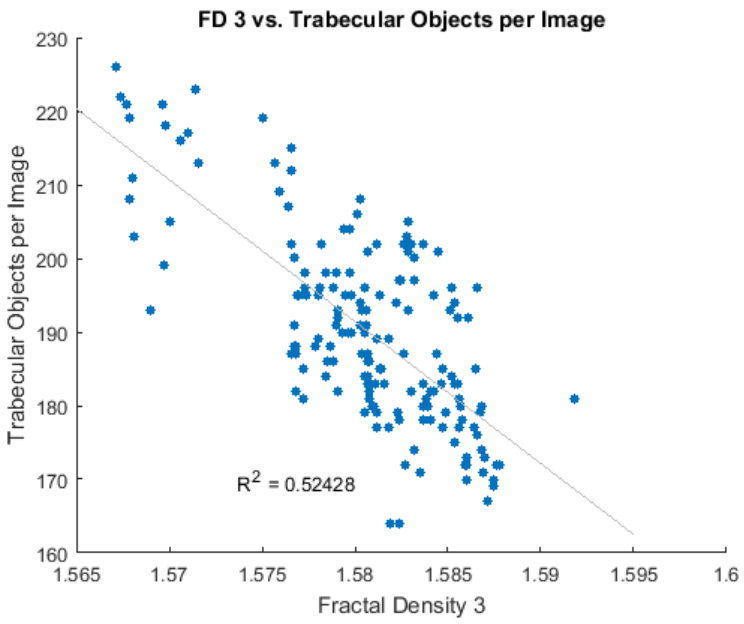

FD3 vs. Plates

```
figure
c2 = FD3;
y2 = Plates;
sz=25;
scatter(c2,y2,sz,'o','filled')
title('FD 3 vs. Number of Plates per Image')
xlabel('Fractal Density 3')
ylabel('Plates Counted per Image')

mdl = fitlm(c2,y2)
lsline
mdl.Rsquared.Ordinary

rsq = ['R^2 = ',num2str(mdl.Rsquared.Ordinary)];
text(1.58,25,rsq,'HorizontalAlignment','right')

hold on
```

```
mdl =


Linear regression model:
    y ~ 1 + x1

Estimated Coefficients:
                   Estimate      SE      tStat       pValue
                   ________    ______    ______    __________

    (Intercept)     962.47     104.58    9.2032    1.7629e-16
    x1             -588.55     66.166    -8.895    1.1441e-15
```

```
Number of observations: 163, Error degrees of freedom: 161
Root Mean Squared Error: 4.18
R-squared: 0.33,  Adjusted R-Squared 0.325
F-statistic vs. constant model: 79.1, p-value = 1.14e-15

ans =

    0.3295
```

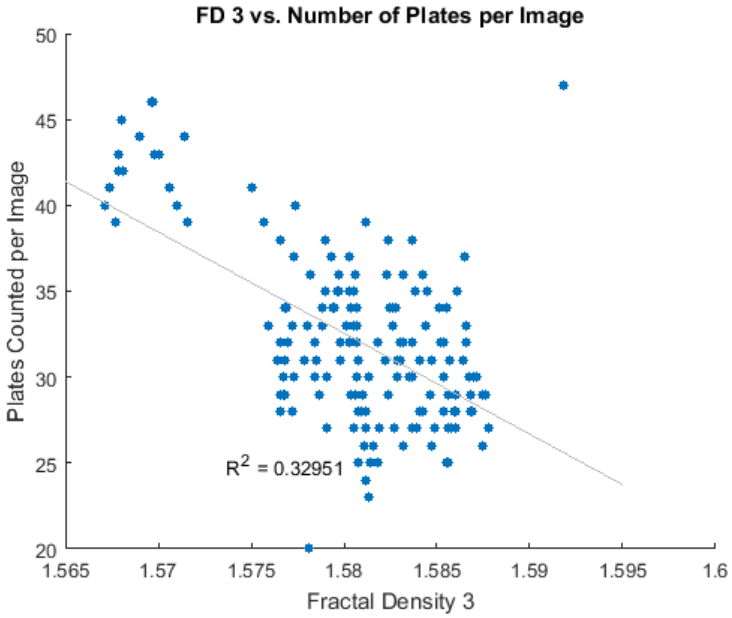

FD3 vs. Rods

```
figure
c3 = FD3;
y3 = Rods;
sz=25;
scatter(c3,y3,sz,'o','filled')
title('FD 3 vs. Number of Rods per Image')
xlabel('Fractal Density 3')
ylabel('Rods Counted per Image')

mdl = fitlm(c3,y3)
lsline
mdl.Rsquared.Ordinary

rsq = ['R^2 = ',num2str(mdl.Rsquared.Ordinary)];
text(1.58,110,rsq,'HorizontalAlignment','right')

hold on
```

```
mdl =


Linear regression model:
    y ~ 1 + x1

Estimated Coefficients:
                   Estimate      SE       tStat       pValue
                   ________    ______    _______    __________

    (Intercept)     1526.6      200.3     7.6214    2.0378e-12
    x1             -885.77     126.73    -6.9894    6.9407e-11


Number of observations: 163, Error degrees of freedom: 161
Root Mean Squared Error: 8.01
R-squared: 0.233,  Adjusted R-Squared 0.228
F-statistic vs. constant model: 48.9, p-value = 6.94e-11

ans =

    0.2328
```

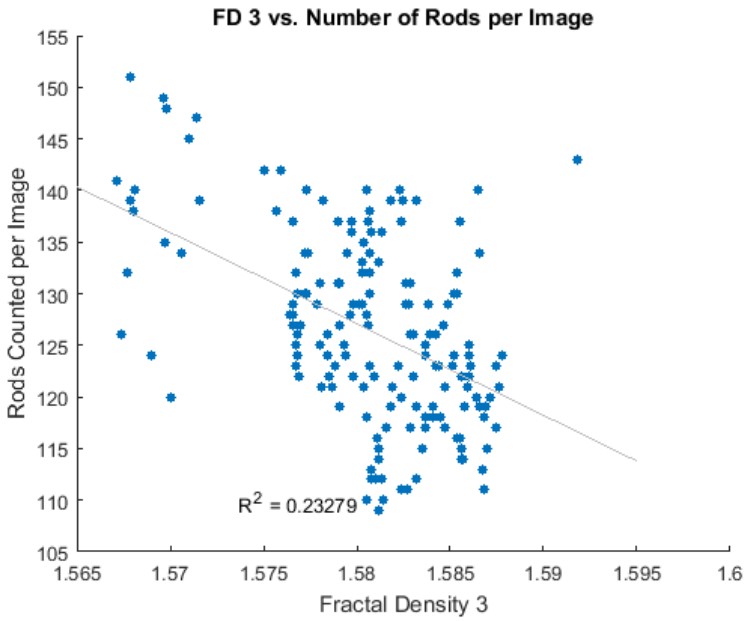

FD3 vs. Avg Tb Size

```
figure
c4 = FD3;
y4 = AverageSize;
sz=25;
scatter(c4,y4,sz,'o','filled')
title('FD 3 vs. Average Size of Trabecular Objects per Image')
```

```
xlabel('Fractal Density 3')
ylabel('Average Tb Size per Image (mm)')

mdl = fitlm(c4,y4)
lsline
mdl.Rsquared.Ordinary

rsq = ['R^2 = ',num2str(mdl.Rsquared.Ordinary)];
text(1.59,0.29,rsq,'HorizontalAlignment','right')

hold on
```

```
mdl =


Linear regression model:
    y ~ 1 + x1

Estimated Coefficients:
                   Estimate      SE        tStat       pValue
                   ________    _______    _______    __________

    (Intercept)    -5.3616     0.34676    -15.462    1.2175e-33
    x1              3.6139     0.21939     16.472    2.3064e-36


Number of observations: 163, Error degrees of freedom: 161
Root Mean Squared Error: 0.0139
R-squared: 0.628,  Adjusted R-Squared 0.625
F-statistic vs. constant model: 271, p-value = 2.31e-36

ans =

    0.6276
```

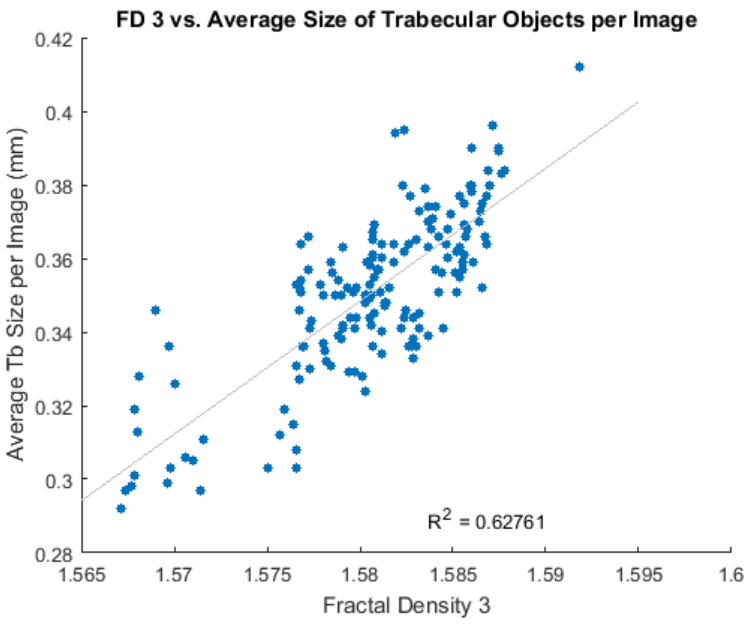

FD3 vs. % Tb Area

```
figure
c5 = FD3;
y5 = Area;
sz=25;
scatter(c5,y5,sz,'o','filled')
title('FD 3 vs. Percent Trabecular Area per Image')
xlabel('Fractal Density 3')
ylabel('Percent Trabecular Area per Image')

mdl = fitlm(c5,y5)
lsline
mdl.Rsquared.Ordinary

rsq = ['R^2 = ',num2str(mdl.Rsquared.Ordinary)];
text(1.58,11.6,rsq,'HorizontalAlignment','right')

hold on
```

```
mdl =


Linear regression model:
    y ~ 1 + x1

Estimated Coefficients:
                   Estimate      SE       tStat       pValue
                   ________    ______    ________    ________

    (Intercept)     -1.356      5.8685    -0.23107     0.81756
    x1              8.3971      3.7129      2.2616    0.025061
```

```
Number of observations: 163, Error degrees of freedom: 161
Root Mean Squared Error: 0.235
R-squared: 0.0308,  Adjusted R-Squared 0.0248
F-statistic vs. constant model: 5.11, p-value = 0.0251

ans =

    0.0308
```

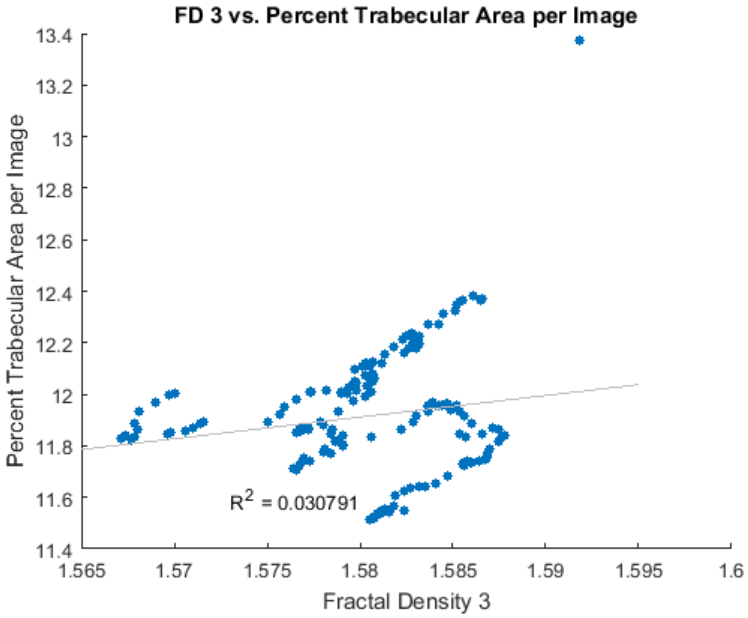

FD3 vs. Avg Spatial Anglular Offset in 2D

```
figure
c6 = FD3;
y6 = AvgAngle;
sz=25;
scatter(c6,y6,sz,'o','filled')
title('FD 3 vs. Average Spatial Angle between Trabeculae')
xlabel('Fractal Density 3')
ylabel('Average Angle Observed per Image')

mdl = fitlm(c6,y6)
lsline
mdl.Rsquared.Ordinary

rsq = ['R^2 = ',num2str(mdl.Rsquared.Ordinary)];
text(1.575,114,rsq,'HorizontalAlignment','right')

hold on
```

```
mdl =


Linear regression model:
    y ~ 1 + x1

Estimated Coefficients:
                   Estimate      SE       tStat       pValue
                   ________    ______    _______    __________

    (Intercept)      253.1     44.743     5.6567    6.8847e-08
    x1              -86.467    28.308    -3.0545     0.0026391


Number of observations: 163, Error degrees of freedom: 161
Root Mean Squared Error: 1.79
R-squared: 0.0548,  Adjusted R-Squared 0.0489
F-statistic vs. constant model: 9.33, p-value = 0.00264

ans =

    0.0548
```

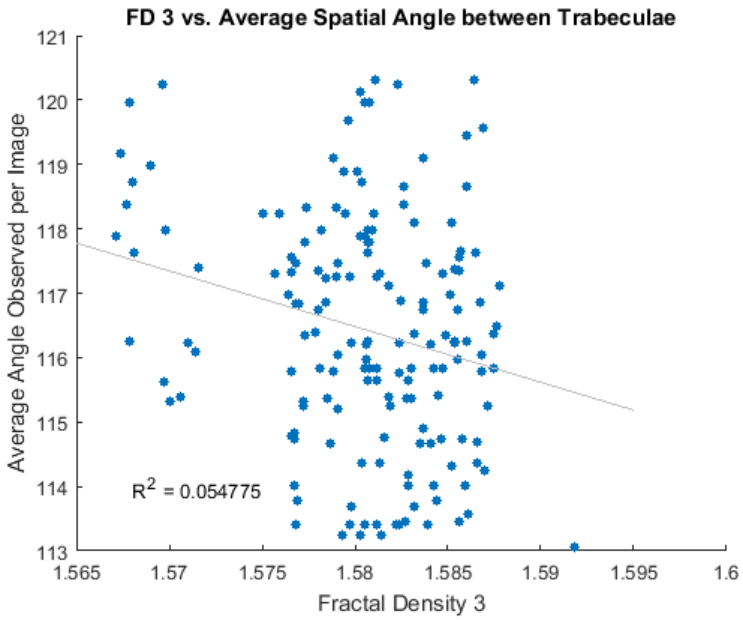

A3. All of the plots for FD3 were generated using the MATLAB code above.

PLOTS FOR FD4

```
%Grid position: 12
%Power Series
```

```
%36 Degree Rotation

close all
clc
```

FD4 vs. TbObjectCount

```
figure
d1 = FD4;
y1 = TbObjectCount;
sz=25;
scatter(d1,y1,sz,'o','filled')
title('FD 4 vs. Trabecular Objects per Image')
xlabel('Fractal Density 4')
ylabel('Trabecular Objects per Image')

mdl = fitlm(d1,y1)
lsline
mdl.Rsquared.Ordinary

rsq = ['R^2 = ',num2str(mdl.Rsquared.Ordinary)];
text(1.59,170,rsq,'HorizontalAlignment','right')

hold on
```

```
mdl =


Linear regression model:
    y ~ 1 + x1

Estimated Coefficients:
                   Estimate      SE       tStat       pValue
                   ________    ______    ________    __________

    (Intercept)    -704.96     230.11    -3.0635      0.0025648
    x1              570.85     146.72     3.8907    0.00014599


Number of observations: 163, Error degrees of freedom: 161
Root Mean Squared Error: 12.7
R-squared: 0.0859,  Adjusted R-Squared 0.0803
F-statistic vs. constant model: 15.1, p-value = 0.000146

ans =

    0.0859
```

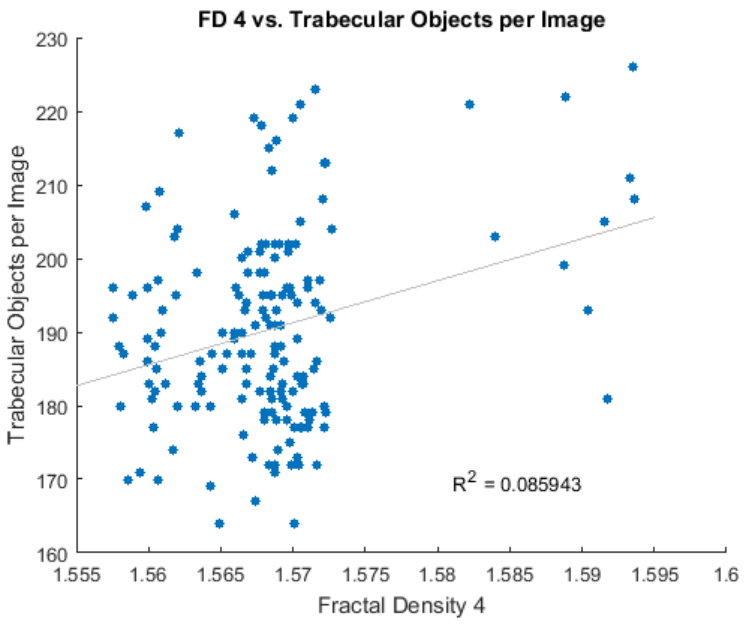

FD4 vs. Plates

```
figure
d2 = FD4;
y2 = Plates;
sz=25;
scatter(d2,y2,sz,'o','filled')
title('FD 4 vs. Number of Plates per Image')
xlabel('Fractal Density 4')
ylabel('Plates Counted per Image')

mdl = fitlm(d2,y2)
lsline
mdl.Rsquared.Ordinary

rsq = ['R^2 = ',num2str(mdl.Rsquared.Ordinary)];
text(1.59,25,rsq,'HorizontalAlignment','right')

hold on
```

```
mdl =


Linear regression model:
    y ~ 1 + x1

Estimated Coefficients:
                   Estimate      SE       tStat       pValue
                   ________    ______    _______    __________

    (Intercept)    -594.75     78.438    -7.5825    2.5424e-12
    x1              399.77     50.012     7.9935    2.3968e-13
```

```
Number of observations: 163, Error degrees of freedom: 161
Root Mean Squared Error: 4.32
R-squared: 0.284,  Adjusted R-Squared 0.28
F-statistic vs. constant model: 63.9, p-value = 2.4e-13

ans =

    0.2841
```

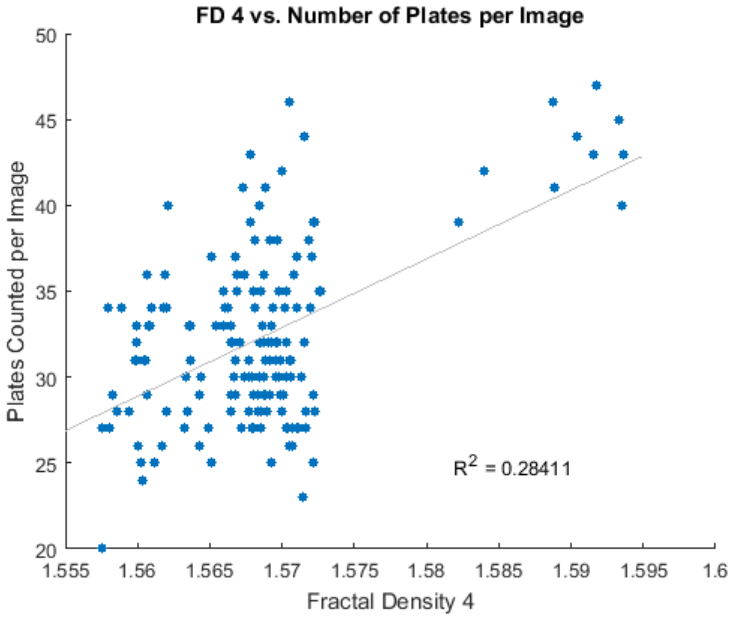

FD4 vs. Rods

```
figure
d3 = FD4;
y3 = Rods;
sz=25;
scatter(d3,y3,sz,'o','filled')
title('FD 4 vs. Number of Rods per Image')
xlabel('Fractal Density 4')
ylabel('Rods Counted per Image')

mdl = fitlm(d3,y3)
lsline
mdl.Rsquared.Ordinary

rsq = ['R^2 = ',num2str(mdl.Rsquared.Ordinary)];
text(1.59,110,rsq,'HorizontalAlignment','right')

hold on
```

```
mdl =


Linear regression model:
    y ~ 1 + x1

Estimated Coefficients:
                   Estimate      SE       tStat      pValue
                   ________    ______    _______    ________

    (Intercept)    -242.09     163.43    -1.4813     0.14048
    x1              235.06      104.2     2.2559    0.025425


Number of observations: 163, Error degrees of freedom: 161
Root Mean Squared Error: 9
R-squared: 0.0306,  Adjusted R-Squared 0.0246
F-statistic vs. constant model: 5.09, p-value = 0.0254

ans =

    0.0306
```

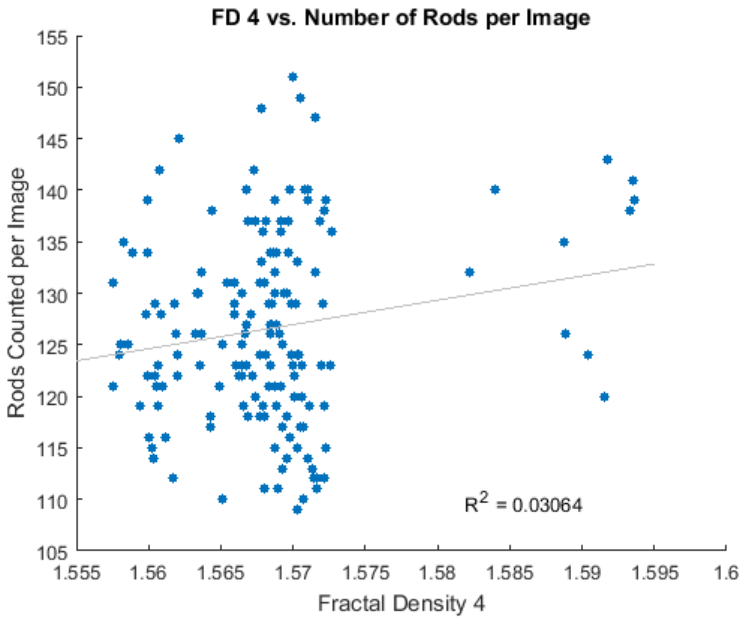

FD4 vs. Avg Tb Size

```
figure
d4 = FD4;
y4 = AverageSize;
sz=25;
scatter(d4,y4,sz,'o','filled')
title('FD 4 vs. Average Size of Trabecular Objects per Image')
```

```
xlabel('Fractal Density 4')
ylabel('Average Tb Size per Image (mm)')

mdl = fitlm(d4,y4)
lsline
mdl.Rsquared.Ordinary

rsq = ['R^2 = ',num2str(mdl.Rsquared.Ordinary)];
text(1.59,0.29,rsq,'HorizontalAlignment','right')

hold on
```

```
mdl =


Linear regression model:
    y ~ 1 + x1

Estimated Coefficients:
                   Estimate      SE       tStat       pValue
                   ________    _______    ______    __________

    (Intercept)      1.6399    0.39974    4.1025    6.4744e-05
    x1              -0.82222   0.25487    -3.226     0.0015207


Number of observations: 163, Error degrees of freedom: 161
Root Mean Squared Error: 0.022
R-squared: 0.0607,  Adjusted R-Squared 0.0549
F-statistic vs. constant model: 10.4, p-value = 0.00152

ans =

    0.0607
```

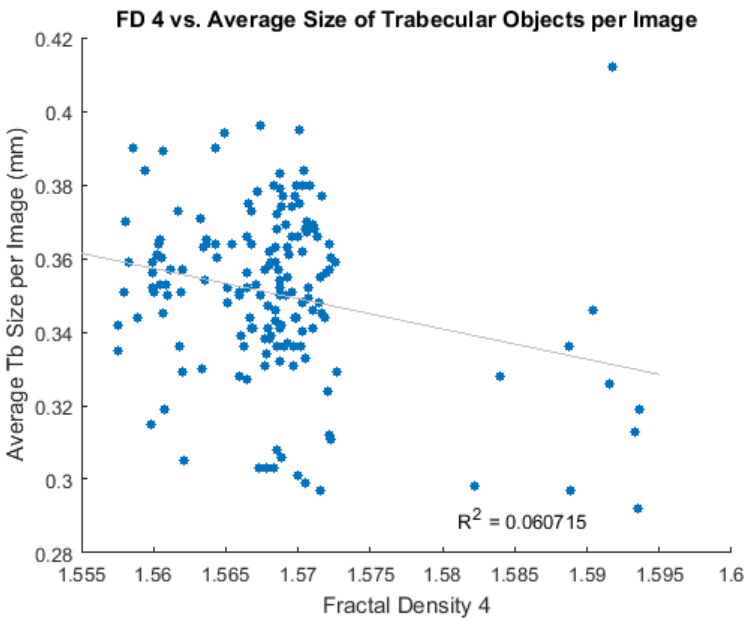

FD4 vs. % Tb Area

```
figure
d5 = FD4;
y5 = Area;
sz=25;
scatter(d5,y5,sz,'o','filled')
title('FD 4 vs. Percent Trabecular Area per Image')
xlabel('Fractal Density 4')
ylabel('Percent Trabecular Area per Image')

mdl = fitlm(d5,y5)
lsline
mdl.Rsquared.Ordinary

rsq = ['R^2 = ',num2str(mdl.Rsquared.Ordinary)];
text(1.59,11.6,rsq,'HorizontalAlignment','right')

hold on
```

```
mdl =


Linear regression model:
    y ~ 1 + x1

Estimated Coefficients:
                   Estimate      SE      tStat     pValue
                   ________    ______    ______    _______

    (Intercept)    5.0893      4.2933    1.1854    0.23759
    x1             4.3528      2.7374    1.5901    0.11377
```

```
Number of observations: 163, Error degrees of freedom: 161
Root Mean Squared Error: 0.236
R-squared: 0.0155,  Adjusted R-Squared 0.00935
F-statistic vs. constant model: 2.53, p-value = 0.114

ans =

    0.0155
```

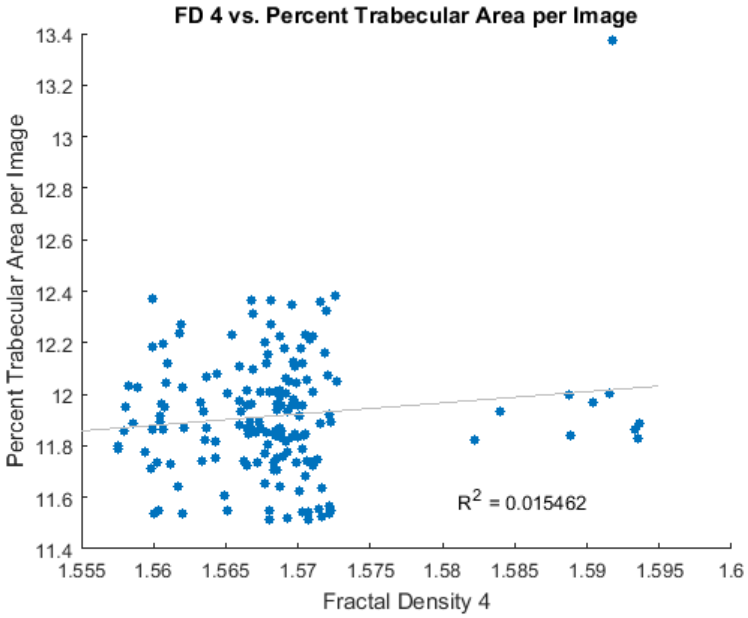

FD4 vs. Avg Spatial Anglular Offset in 2D

```
figure
d6 = FD4;
y6 = AvgAngle;
sz=25;
scatter(d6,y6,sz,'o','filled')
title('FD 4 vs. Average Spatial Angle between Trabeculae')
xlabel('Fractal Density 4')
ylabel('Average Angle Observed per Image')

mdl = fitlm(d6,y6)
lsline
mdl.Rsquared.Ordinary

rsq = ['R^2 = ',num2str(mdl.Rsquared.Ordinary)];
text(1.59,114,rsq,'HorizontalAlignment','right')

hold on
```

```
mdl =


Linear regression model:
    y ~ 1 + x1

Estimated Coefficients:
                   Estimate      SE       tStat      pValue
                   ________    _______    _______    _________

    (Intercept)    84.507       33.31       2.537    0.012131
    x1             20.356      21.238     0.95848     0.33926


Number of observations: 163, Error degrees of freedom: 161
Root Mean Squared Error: 1.83
R-squared: 0.00567,  Adjusted R-Squared -0.000502
F-statistic vs. constant model: 0.919, p-value = 0.339

ans =

    0.0057
```

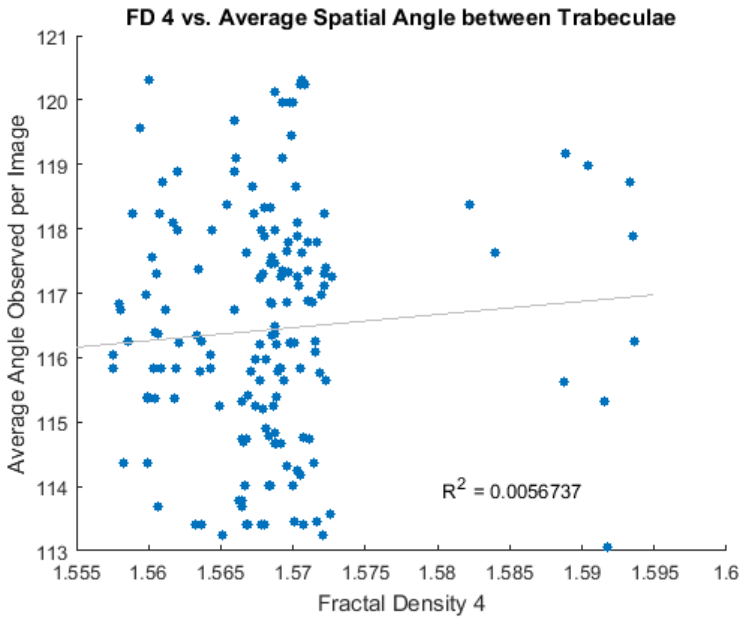

A4. All of the plots for FD4 were generated using the MATLAB code above.

PLOTS FOR FD5

```
%Grid position: 4
%Default Scaling Series
```

```
%No Rotation

close all
clc
```

FD5 vs. TbObjectCount

```
figure
e1 = FD5;
y1 = TbObjectCount;
sz=25;
scatter(e1,y1,sz,'o','filled')
title('FD 5 vs. Trabecular Objects per Image')
xlabel('Fractal Density 5')
ylabel('Trabecular Objects per Image')

mdl = fitlm(e1,y1)
lsline
mdl.Rsquared.Ordinary

rsq = ['R^2 = ',num2str(mdl.Rsquared.Ordinary)];
text(1.675,170,rsq,'HorizontalAlignment','right')

hold on
```

```
mdl =


Linear regression model:
    y ~ 1 + x1

Estimated Coefficients:
                   Estimate      SE       tStat       pValue
                   ________    ______    ________    __________

    (Intercept)    -1573.1     146.83    -10.714      1.472e-20
    x1              1061.4     88.377      12.01    3.9136e-24


Number of observations: 163, Error degrees of freedom: 161
Root Mean Squared Error: 9.63
R-squared: 0.473,  Adjusted R-Squared 0.469
F-statistic vs. constant model: 144, p-value = 3.91e-24

ans =

    0.4726
```

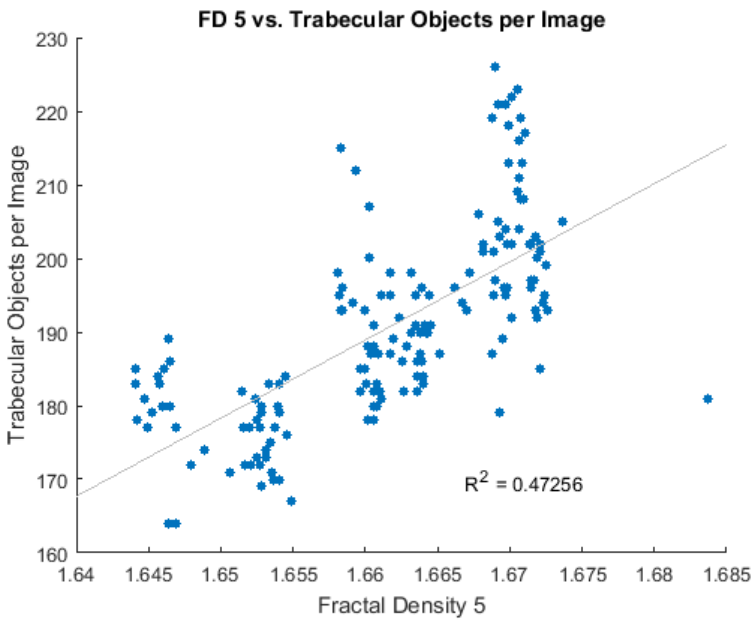

FD5 vs. Plates

```
figure
e2 = FD5;
y2 = Plates;
sz=25;
scatter(e2,y2,sz,'o','filled')
title('FD 5 vs. Number of Plates per Image')
xlabel('Fractal Density 5')
ylabel('Plates Counted per Image')

mdl = fitlm(e2,y2)
lsline
mdl.Rsquared.Ordinary

rsq = ['R^2 = ',num2str(mdl.Rsquared.Ordinary)];
text(1.675,25,rsq,'HorizontalAlignment','right')

hold on
```

```
mdl =


Linear regression model:
    y ~ 1 + x1

Estimated Coefficients:
                   Estimate      SE       tStat       pValue
                   ________    ______    _______    __________

    (Intercept)    -733.94     49.166    -14.928    3.4626e-32
    x1              461.18     29.594     15.584    5.6929e-34
```

```
Number of observations: 163, Error degrees of freedom: 161
Root Mean Squared Error: 3.22
R-squared: 0.601,  Adjusted R-Squared 0.599
F-statistic vs. constant model: 243, p-value = 5.69e-34

ans =

    0.6013
```

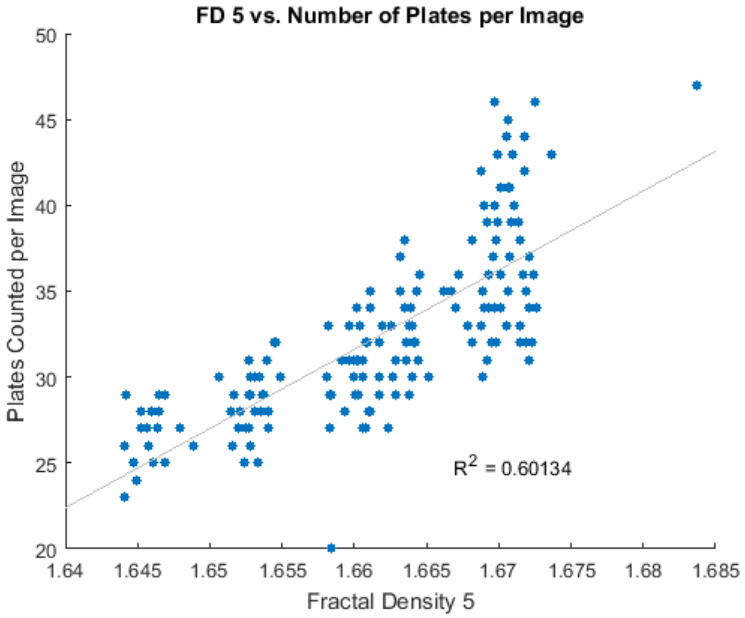

FD5 vs. Rods

```
figure
e3 = FD5;
y3 = Rods;
sz=25;
scatter(e3,y3,sz,'o','filled')
title('FD 5 vs. Number of Rods per Image')
xlabel('Fractal Density 5')
ylabel('Rods Counted per Image')

mdl = fitlm(e3,y3)
lsline
mdl.Rsquared.Ordinary

rsq = ['R^2 = ',num2str(mdl.Rsquared.Ordinary)];
text(1.675,110,rsq,'HorizontalAlignment','right')

hold on
```

```
mdl =


Linear regression model:
    y ~ 1 + x1

Estimated Coefficients:
                   Estimate      SE       tStat       pValue
                   ________    ______    _______    __________

    (Intercept)    -1200.3     92.212    -13.017    6.3456e-27
    x1              798.71     55.504      14.39    1.0294e-30


Number of observations: 163, Error degrees of freedom: 161
Root Mean Squared Error: 6.04
R-squared: 0.563,  Adjusted R-Squared 0.56
F-statistic vs. constant model: 207, p-value = 1.03e-30

ans =

    0.5626
```

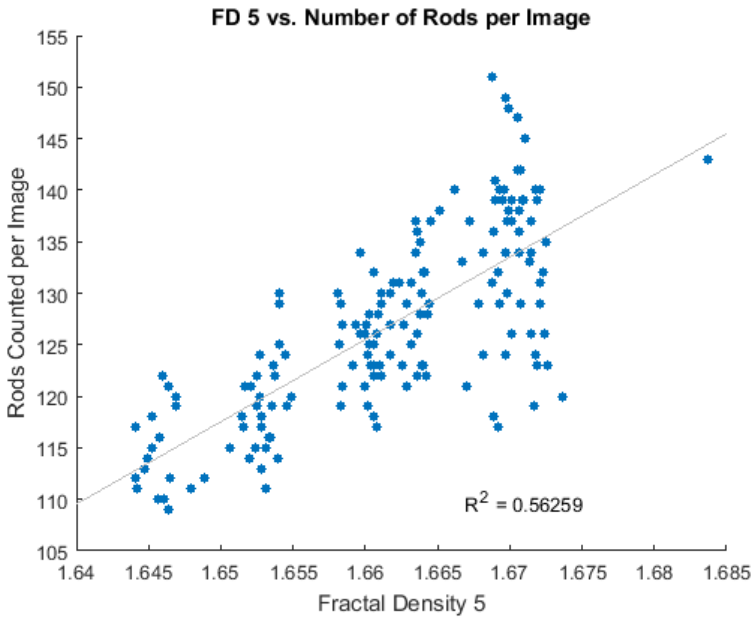

FD5 vs. Avg Tb Size

```
figure
e4 = FD5;
y4 = AverageSize;
sz=25;
scatter(e4,y4,sz,'o','filled')
title('FD 5 vs. Average Size of Trabecular Objects per Image')
```

```
xlabel('Fractal Density 5')
ylabel('Average Tb Size per Image (mm)')

mdl = fitlm(e4,y4)
lsline
mdl.Rsquared.Ordinary

rsq = ['R^2 = ',num2str(mdl.Rsquared.Ordinary)];
text(1.65,0.29,rsq,'HorizontalAlignment','right')

hold on
```

```
mdl =


Linear regression model:
    y ~ 1 + x1

Estimated Coefficients:
                   Estimate      SE        tStat       pValue
                   ________    _______    _______    __________

    (Intercept)     2.4682     0.30359       8.13    1.0816e-13
    x1             -1.2748     0.18274    -6.9759    7.4725e-11


Number of observations: 163, Error degrees of freedom: 161
Root Mean Squared Error: 0.0199
R-squared: 0.232,  Adjusted R-Squared 0.227
F-statistic vs. constant model: 48.7, p-value = 7.47e-11

ans =

    0.2321
```

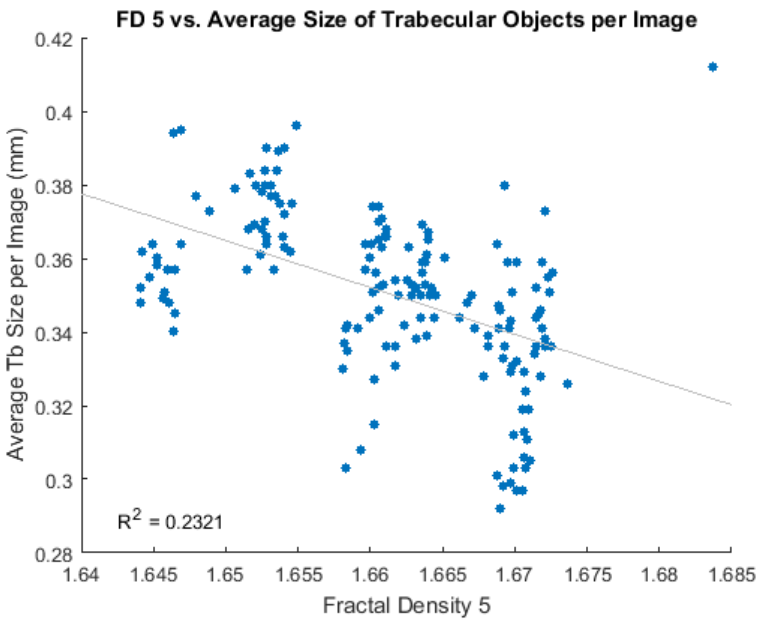

FD5 vs. % Tb Area

```
figure
e5 = FD5;
y5 = Area;
sz=25;
scatter(e5,y5,sz,'o','filled')
title('FD 5 vs. Percent Trabecular Area per Image')
xlabel('Fractal Density 5')
ylabel('Percent Trabecular Area per Image')

mdl = fitlm(e5,y5)
lsline
mdl.Rsquared.Ordinary

rsq = ['R^2 = ',num2str(mdl.Rsquared.Ordinary)];
text(1.675,11.6,rsq,'HorizontalAlignment','right')

hold on
```

```
mdl =


Linear regression model:
    y ~ 1 + x1

Estimated Coefficients:
                   Estimate      SE      tStat       pValue
                   ________    ______    ______    __________

    (Intercept)    -24.972      2.181    -11.45    1.3883e-22
    x1              22.204     1.3128    16.914    1.5372e-37
```

```
Number of observations: 163, Error degrees of freedom: 161
Root Mean Squared Error: 0.143
R-squared: 0.64,  Adjusted R-Squared 0.638
F-statistic vs. constant model: 286, p-value = 1.54e-37

ans =

    0.6399
```

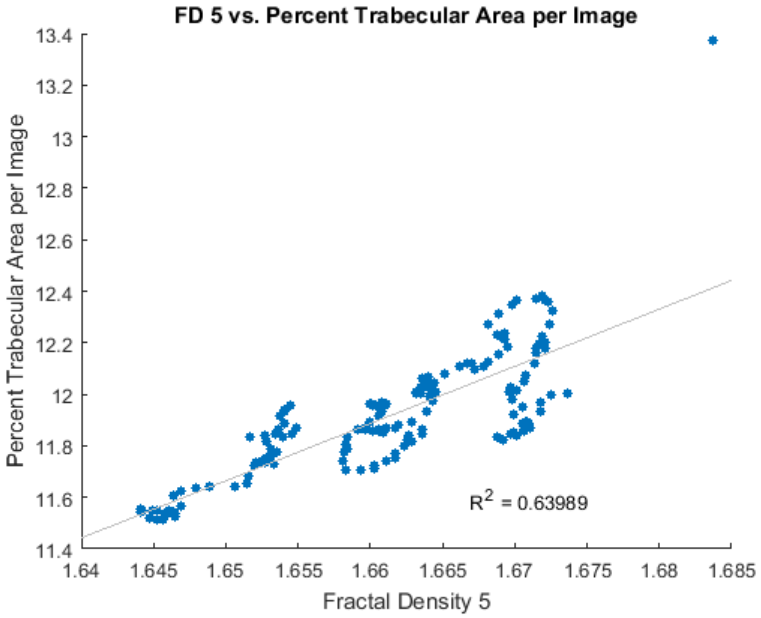

FD5 vs. Avg Spatial Anglular Offset in 2D

```
figure
e6 = FD5;
y6 = AvgAngle;
sz=25;
scatter(e6,y6,sz,'o','filled')
title('FD 5 vs. Average Spatial Angle between Trabeculae')
xlabel('Fractal Density 5')
ylabel('Average Angle Observed per Image')

mdl = fitlm(e6,y6)
lsline
mdl.Rsquared.Ordinary

rsq = ['R^2 = ',num2str(mdl.Rsquared.Ordinary)];
text(1.675,114,rsq,'HorizontalAlignment','right')

hold on
```

```
mdl =


Linear regression model:
    y ~ 1 + x1

Estimated Coefficients:
                   Estimate      SE       tStat      pValue
                   ________    ______    _______    _________

    (Intercept)    93.734      28.001     3.3475    0.0010153
    x1             13.663      16.855    0.81066      0.41876


Number of observations: 163, Error degrees of freedom: 161
Root Mean Squared Error: 1.84
R-squared: 0.00407,  Adjusted R-Squared -0.00212
F-statistic vs. constant model: 0.657, p-value = 0.419

ans =

    0.0041
```

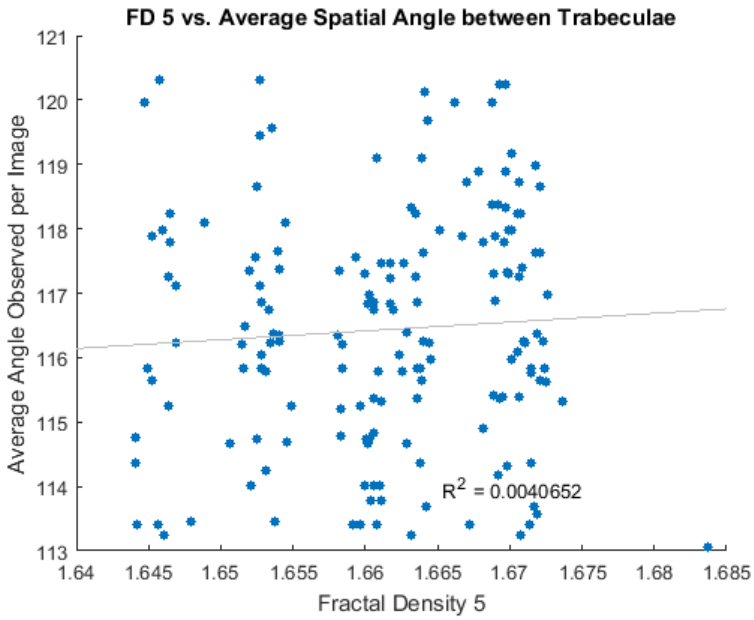

A5. All of the plots for FD5 were generated using the MATLAB code above.

PLOTS FOR FD6

```
%Grid position: 4
%Default Scaling Series
```

```
%36 Degrees Rotation

close all
clc
```

FD6 vs. TbObjectCount

```
figure
f1 = FD6;
y1 = TbObjectCount;
sz=25;
scatter(f1,y1,sz,'o','filled')
title('FD 6 vs. Trabecular Objects per Image')
xlabel('Fractal Density 6')
ylabel('Trabecular Objects per Image')

mdl = fitlm(f1,y1)
lsline
mdl.Rsquared.Ordinary

rsq = ['R^2 = ',num2str(mdl.Rsquared.Ordinary)];
text(1.71,170,rsq,'HorizontalAlignment','right')

hold on
```

```
mdl =


Linear regression model:
    y ~ 1 + x1

Estimated Coefficients:
                   Estimate      SE       tStat      pValue
                   ________    ______    ________    _______

    (Intercept)    3.8682      125.12    0.030915    0.97538
    x1             111.87      75.061      1.4903    0.13809


Number of observations: 163, Error degrees of freedom: 161
Root Mean Squared Error: 13.2
R-squared: 0.0136,  Adjusted R-Squared 0.00748
F-statistic vs. constant model: 2.22, p-value = 0.138

ans =

    0.0136
```

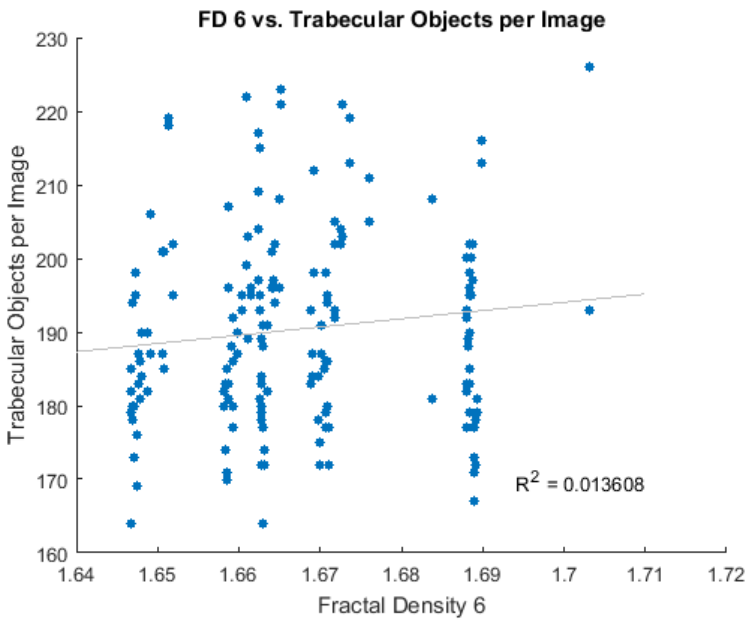

FD6 vs. Plates

```
figure
f2 = FD6;
y2 = Plates;
sz=25;
scatter(f2,y2,sz,'o','filled')
title('FD 6 vs. Number of Plates per Image')
xlabel('Fractal Density 6')
ylabel('Plates Counted per Image')

mdl = fitlm(f2,y2)
lsline
mdl.Rsquared.Ordinary

rsq = ['R^2 = ',num2str(mdl.Rsquared.Ordinary)];
text(1.71,25,rsq,'HorizontalAlignment','right')

hold on
```

```
mdl =


Linear regression model:
    y ~ 1 + x1

Estimated Coefficients:
                   Estimate      SE       tStat      pValue
                   ________    ______    _______    ________

    (Intercept)    -78.898     47.727    -1.6531     0.10026
    x1              66.669     28.631     2.3285    0.021127
```

```
Number of observations: 163, Error degrees of freedom: 161
Root Mean Squared Error: 5.02
R-squared: 0.0326,  Adjusted R-Squared 0.0266
F-statistic vs. constant model: 5.42, p-value = 0.0211

ans =

    0.0326
```

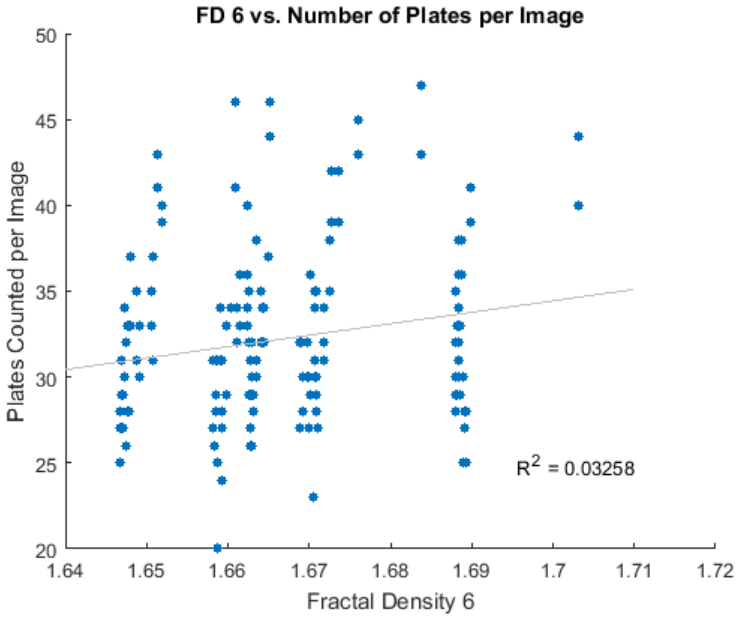

FD6 vs. Rods

```
figure
f3 = FD6;
y3 = Rods;
sz=25;
scatter(f3,y3,sz,'o','filled')
title('FD 6 vs. Number of Rods per Image')
xlabel('Fractal Density 6')
ylabel('Rods Counted per Image')

mdl = fitlm(f3,y3)
lsline
mdl.Rsquared.Ordinary

rsq = ['R^2 = ',num2str(mdl.Rsquared.Ordinary)];
text(1.71,110,rsq,'HorizontalAlignment','right')

hold on
```

```
mdl =


Linear regression model:
    y ~ 1 + x1

Estimated Coefficients:
                   Estimate      SE       tStat     pValue
                   ________    _______    _______    _______

    (Intercept)    38.895      86.609     0.44909    0.65397
    x1             52.605      51.956      1.0125    0.31282


Number of observations: 163, Error degrees of freedom: 161
Root Mean Squared Error: 9.11
R-squared: 0.00633,  Adjusted R-Squared 0.000155
F-statistic vs. constant model: 1.03, p-value = 0.313

ans =

    0.0063
```

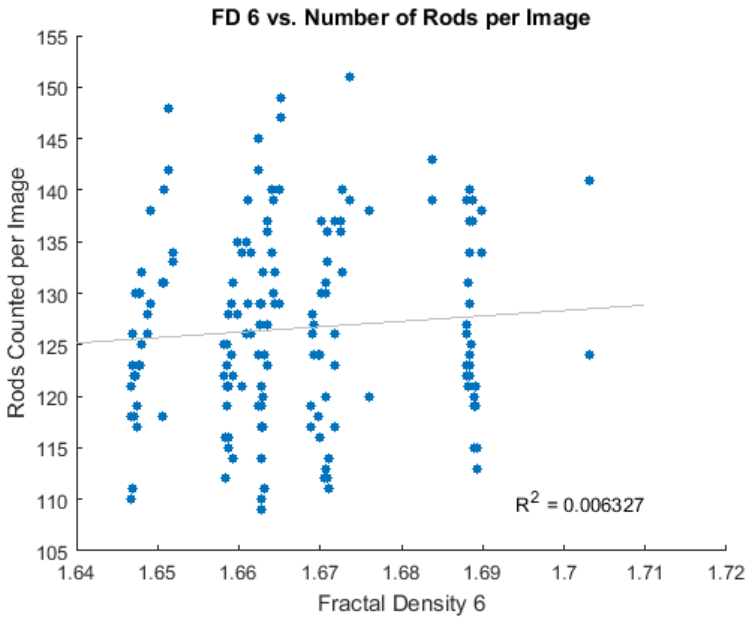

FD6 vs. Avg Tb Size

```
figure
f4 = FD6;
y4 = AverageSize;
sz=25;
scatter(f4,y4,sz,'o','filled')
title('FD 6 vs. Average Size of Trabecular Objects per Image')
```

```
xlabel('Fractal Density 6')
ylabel('Average Tb Size per Image (mm)')

mdl = fitlm(f4,y4)
lsline
mdl.Rsquared.Ordinary

rsq = ['R^2 = ',num2str(mdl.Rsquared.Ordinary)];
text(1.71,0.29,rsq,'HorizontalAlignment','right')

hold on
```

```
mdl =


Linear regression model:
    y ~ 1 + x1

Estimated Coefficients:
                   Estimate      SE        tStat      pValue
                   ________    _______    _______    _________

    (Intercept)     0.59249    0.21505     2.7552    0.0065421
    x1             -0.14524    0.12901    -1.1258      0.26191


Number of observations: 163, Error degrees of freedom: 161
Root Mean Squared Error: 0.0226
R-squared: 0.00781,  Adjusted R-Squared 0.00165
F-statistic vs. constant model: 1.27, p-value = 0.262

ans =

    0.0078
```

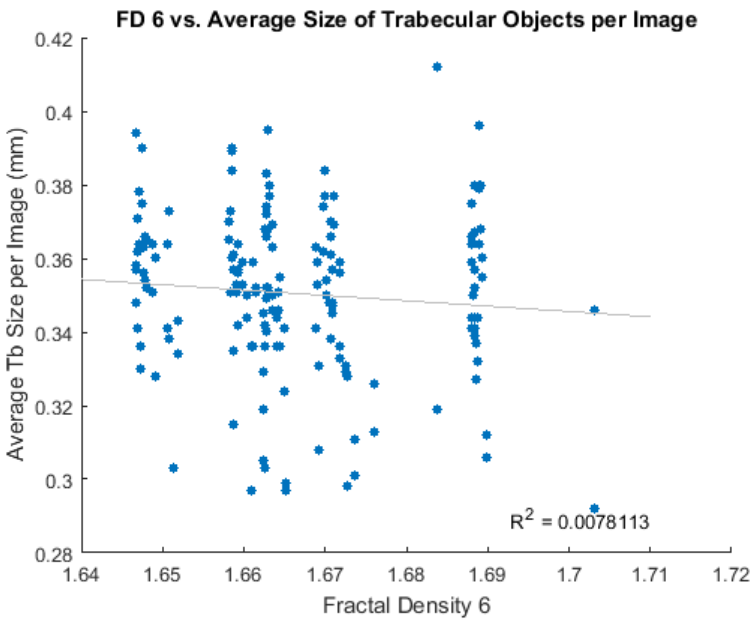

FD6 vs. % Tb Area

```
figure
f5 = FD6;
y5 = Area;
sz=25;
scatter(f5,y5,sz,'o','filled')
title('FD 6 vs. Percent Trabecular Area per Image')
xlabel('Fractal Density 6')
ylabel('Percent Trabecular Area per Image')

mdl = fitlm(f5,y5)
lsline
mdl.Rsquared.Ordinary

rsq = ['R^2 = ',num2str(mdl.Rsquared.Ordinary)];
text(1.71,11.6,rsq,'HorizontalAlignment','right')

hold on
```

```
mdl =


Linear regression model:
    y ~ 1 + x1

Estimated Coefficients:
                   Estimate      SE      tStat      pValue
                   ________    ______    ______    _________

    (Intercept)    9.3508      2.2557    4.1453    5.473e-05
    x1              1.539      1.3532    1.1373       0.2571
```

```
Number of observations: 163, Error degrees of freedom: 161
Root Mean Squared Error: 0.237
R-squared: 0.00797,  Adjusted R-Squared 0.00181
F-statistic vs. constant model: 1.29, p-value = 0.257

ans =

    0.0080
```

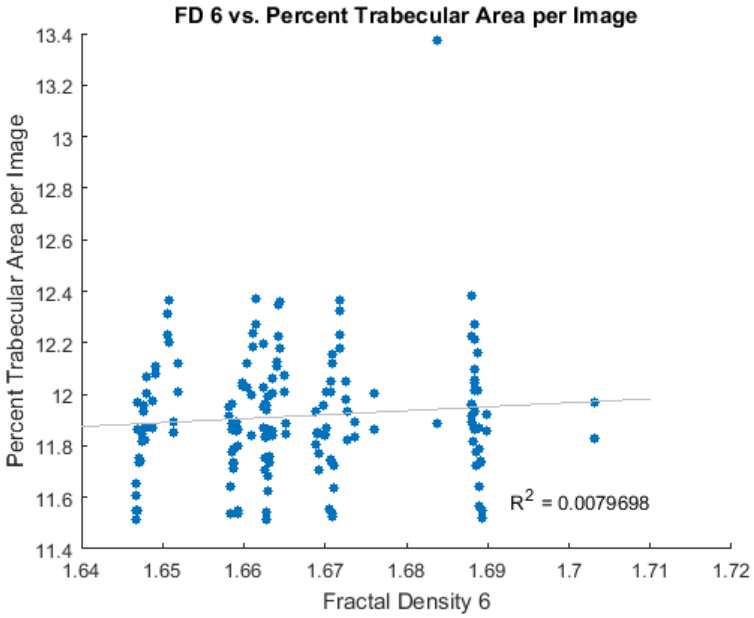

FD6 vs. Avg Spatial Anglular Offset in 2D

```
figure
c6 = FD6;
y6 = AvgAngle;
sz=25;
scatter(c6,y6,sz,'o','filled')
title('FD 6 vs. Average Spatial Angle between Trabeculae')
xlabel('Fractal Density 6')
ylabel('Average Angle Observed per Image')

mdl = fitlm(c6,y6)
lsline
mdl.Rsquared.Ordinary

rsq = ['R^2 = ',num2str(mdl.Rsquared.Ordinary)];
text(1.71,114,rsq,'HorizontalAlignment','right')

hold on
```

```
mdl =


Linear regression model:
    y ~ 1 + x1

Estimated Coefficients:
                   Estimate      SE       tStat        pValue
                   ________    _______    ________    __________

    (Intercept)     118.74     17.484      6.7912    2.0353e-10
    x1             -1.3825     10.489    -0.13181        0.8953


Number of observations: 163, Error degrees of freedom: 161
Root Mean Squared Error: 1.84
R-squared: 0.000108,  Adjusted R-Squared -0.0061
F-statistic vs. constant model: 0.0174, p-value = 0.895

ans =

   1.0790e-04
```

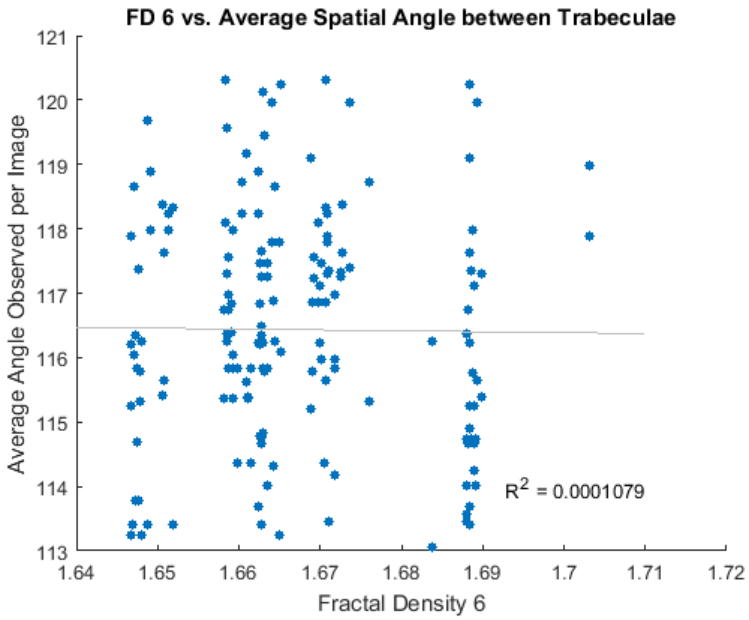

A6. All of the plots for FD6 were generated using the MATLAB code above.

PLOTS FOR FD7

```
%Grid position: 4
%Power Series
```

```
%No Rotation

close all
clc
```

FD7 vs. TbObjectCount

```
figure
g1 = FD7;
y1 = TbObjectCount;
sz=25;
scatter(g1,y1,sz,'o','filled')
title('FD 7 vs. Trabecular Objects per Image')
xlabel('Fractal Density 7')
ylabel('Trabecular Objects per Image')

mdl = fitlm(g1,y1)
lsline
mdl.Rsquared.Ordinary

rsq = ['R^2 = ',num2str(mdl.Rsquared.Ordinary)];
text(1.595,170,rsq,'HorizontalAlignment','right')

hold on
```

```
mdl =


Linear regression model:
    y ~ 1 + x1

Estimated Coefficients:
                   Estimate      SE       tStat       pValue
                   ________    ______    _______    __________

    (Intercept)     2181.8     215.36     10.131    5.7165e-19
    x1             -1247.6     134.92    -9.2472    1.3475e-16


Number of observations: 163, Error degrees of freedom: 161
Root Mean Squared Error: 10.7
R-squared: 0.347,  Adjusted R-Squared 0.343
F-statistic vs. constant model: 85.5, p-value = 1.35e-16

ans =

    0.3469
```

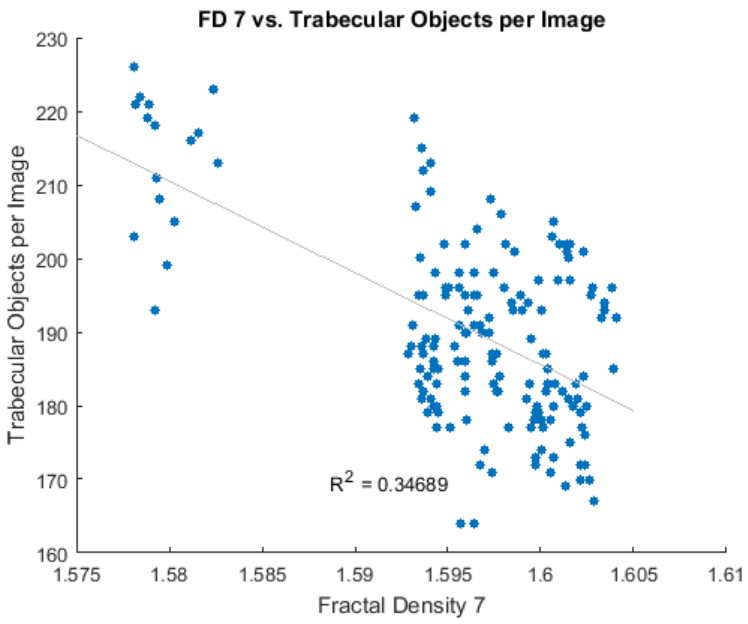

FD7 vs. Plates

```
figure
g2 = FD7;
y2 = Plates;
sz=25;
scatter(g2,y2,sz,'o','filled')
title('FD 7 vs. Number of Plates per Image')
xlabel('Fractal Density 7')
ylabel('Plates Counted per Image')

mdl = fitlm(g2,y2)
lsline
mdl.Rsquared.Ordinary

rsq = ['R^2 = ',num2str(mdl.Rsquared.Ordinary)];
text(1.595,25,rsq,'HorizontalAlignment','right')

hold on
```

```
mdl =


Linear regression model:
    y ~ 1 + x1

Estimated Coefficients:
                   Estimate      SE       tStat       pValue
                   ________    ______    _______    __________

    (Intercept)     726.65      86.83     8.3687     2.658e-14
    x1             -435.05     54.398    -7.9975    2.3411e-13
```

```
Number of observations: 163, Error degrees of freedom: 161
Root Mean Squared Error: 4.32
R-squared: 0.284,  Adjusted R-Squared 0.28
F-statistic vs. constant model: 64, p-value = 2.34e-13

ans =

    0.2843
```

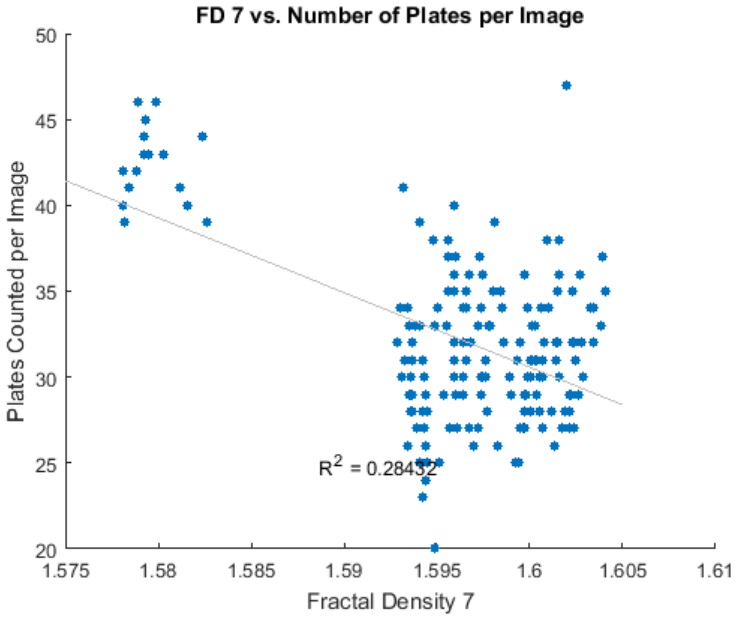

FD7 vs. Rods

```
figure
g3 = FD7;
y3 = Rods;
sz=25;
scatter(g3,y3,sz,'o','filled')
title('FD 7 vs. Number of Rods per Image')
xlabel('Fractal Density 7')
ylabel('Rods Counted per Image')

mdl = fitlm(g3,y3)
lsline
mdl.Rsquared.Ordinary

rsq = ['R^2 = ',num2str(mdl.Rsquared.Ordinary)];
text(1.595,110,rsq,'HorizontalAlignment','right')

hold on
```

```
mdl =


Linear regression model:
    y ~ 1 + x1

Estimated Coefficients:
                   Estimate      SE       tStat       pValue
                   ________    ______    _______    __________

    (Intercept)     941.56     172.19     5.4682    1.7039e-07
    x1             -510.58     107.87    -4.7331     4.813e-06


Number of observations: 163, Error degrees of freedom: 161
Root Mean Squared Error: 8.56
R-squared: 0.122,  Adjusted R-Squared 0.117
F-statistic vs. constant model: 22.4, p-value = 4.81e-06

ans =

    0.1221
```

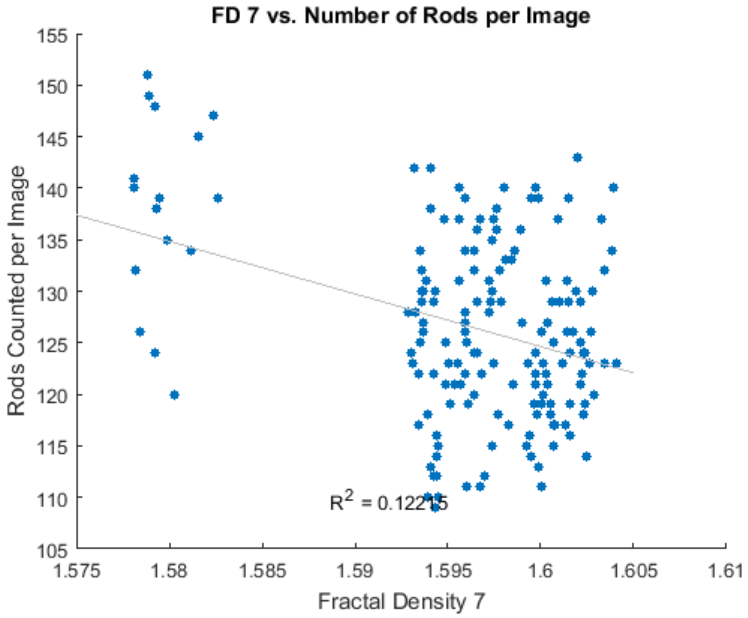

FD7 vs. Avg Tb Size

```
figure
g4 = FD3;
y4 = AverageSize;
sz=25;
scatter(g4,y4,sz,'o','filled')
title('FD 7 vs. Average Size of Trabecular Objects per Image')
```

```
xlabel('Fractal Density 7')
ylabel('Average Tb Size per Image (mm)')

mdl = fitlm(g4,y4)
lsline
mdl.Rsquared.Ordinary

rsq = ['R^2 = ',num2str(mdl.Rsquared.Ordinary)];
text(1.595,0.29,rsq,'HorizontalAlignment','right')

hold on
```

```
mdl =


Linear regression model:
    y ~ 1 + x1

Estimated Coefficients:
                   Estimate      SE        tStat       pValue
                   ________    _______    _______    __________

    (Intercept)    -5.3616     0.34676    -15.462    1.2175e-33
    x1              3.6139     0.21939     16.472    2.3064e-36


Number of observations: 163, Error degrees of freedom: 161
Root Mean Squared Error: 0.0139
R-squared: 0.628,  Adjusted R-Squared 0.625
F-statistic vs. constant model: 271, p-value = 2.31e-36

ans =

    0.6276
```

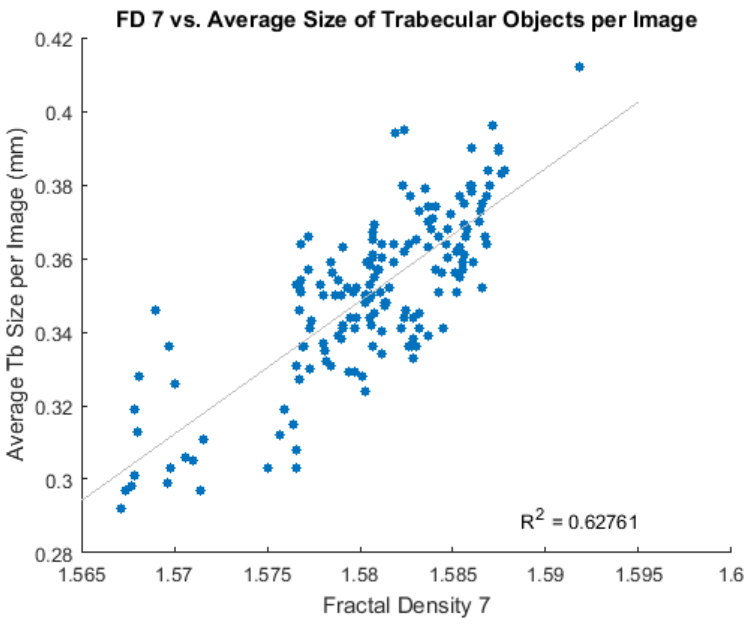

FD7 vs. % Tb Area

```
figure
g5 = FD7;
y5 = Area;
sz=25;
scatter(g5,y5,sz,'o','filled')
title('FD 7 vs. Percent Trabecular Area per Image')
xlabel('Fractal Density 7')
ylabel('Percent Trabecular Area per Image')

mdl = fitlm(g5,y5)
lsline
mdl.Rsquared.Ordinary

rsq = ['R^2 = ',num2str(mdl.Rsquared.Ordinary)];
text(1.59,11.6,rsq,'HorizontalAlignment','right')

hold on
```

```
mdl =


Linear regression model:
    y ~ 1 + x1

Estimated Coefficients:
                   Estimate      SE      tStat       pValue
                   ________    ______    ______    __________

    (Intercept)    -6.0148     4.5773    -1.314       0.1907
    x1              11.234     2.8676    3.9174    0.00013201
```

```
Number of observations: 163, Error degrees of freedom: 161
Root Mean Squared Error: 0.228
R-squared: 0.087,  Adjusted R-Squared 0.0814
F-statistic vs. constant model: 15.3, p-value = 0.000132

ans =

    0.0870
```

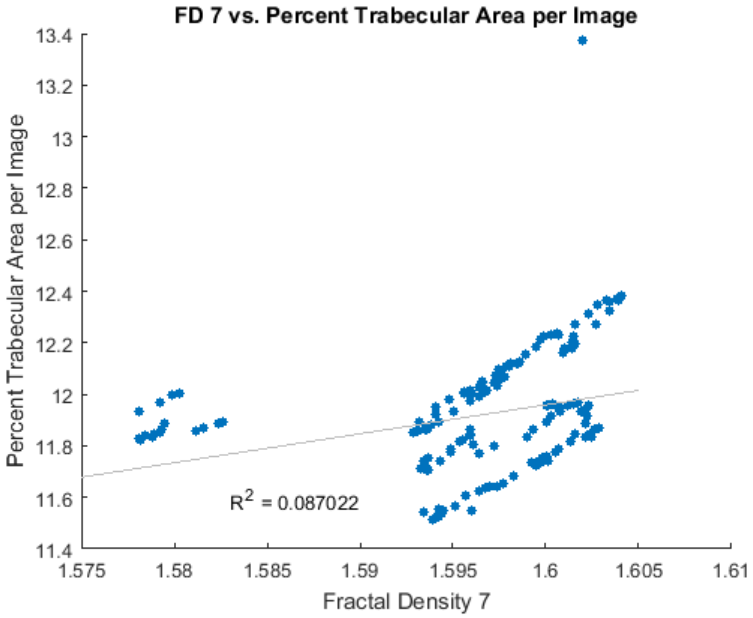

FD7 vs. Avg Spatial Anglular Offset in 2D

```
figure
g6 = FD7;
y6 = AvgAngle;
sz=25;
scatter(g6,y6,sz,'o','filled')
title('FD 7 vs. Average Spatial Angle between Trabeculae')
xlabel('Fractal Density 7')
ylabel('Average Angle Observed per Image')

mdl = fitlm(g6,y6)
lsline
mdl.Rsquared.Ordinary

rsq = ['R^2 = ',num2str(mdl.Rsquared.Ordinary)];
text(1.59,114,rsq,'HorizontalAlignment','right')

hold on
```

```
mdl =


Linear regression model:
    y ~ 1 + x1

Estimated Coefficients:
                   Estimate      SE       tStat       pValue
                   ________    _______    _______    __________

    (Intercept)    227.03      35.942      6.3166    2.5027e-09
    x1             -69.29      22.518     -3.0771     0.0024568


Number of observations: 163, Error degrees of freedom: 161
Root Mean Squared Error: 1.79
R-squared: 0.0555,  Adjusted R-Squared 0.0497
F-statistic vs. constant model: 9.47, p-value = 0.00246

ans =

    0.0555
```

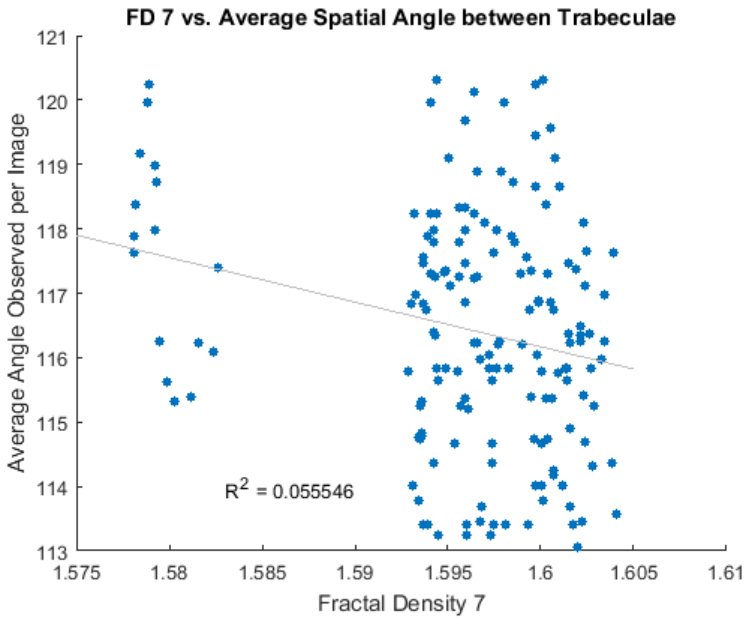

A7. All of the plots for FD7 were generated using the MATLAB code above.

PLOTS FOR FD8

```
%Grid position: 4
%Power Series
```

```
%36 Degrees Rotation

close all
clc
```

FD8 vs. TbObjectCount

```
figure
h1 = FD8;
y1 = TbObjectCount;
sz=25;
scatter(h1,y1,sz,'o','filled')
title('FD 8 vs. Trabecular Objects per Image')
xlabel('Fractal Density 8')
ylabel('Trabecular Objects per Image')

mdl = fitlm(h1,y1)
lsline
mdl.Rsquared.Ordinary

rsq = ['R^2 = ',num2str(mdl.Rsquared.Ordinary)];
text(1.615,170,rsq,'HorizontalAlignment','right')

hold on
```

```
mdl =


Linear regression model:
    y ~ 1 + x1

Estimated Coefficients:
                   Estimate      SE       tStat      pValue
                   ________    ______    _______    ________

    (Intercept)    -309.01     178.84    -1.7279    0.085926
    x1              316.18     113.24     2.7922    0.005869


Number of observations: 163, Error degrees of freedom: 161
Root Mean Squared Error: 12.9
R-squared: 0.0462,  Adjusted R-Squared 0.0403
F-statistic vs. constant model: 7.8, p-value = 0.00587

ans =

    0.0462
```

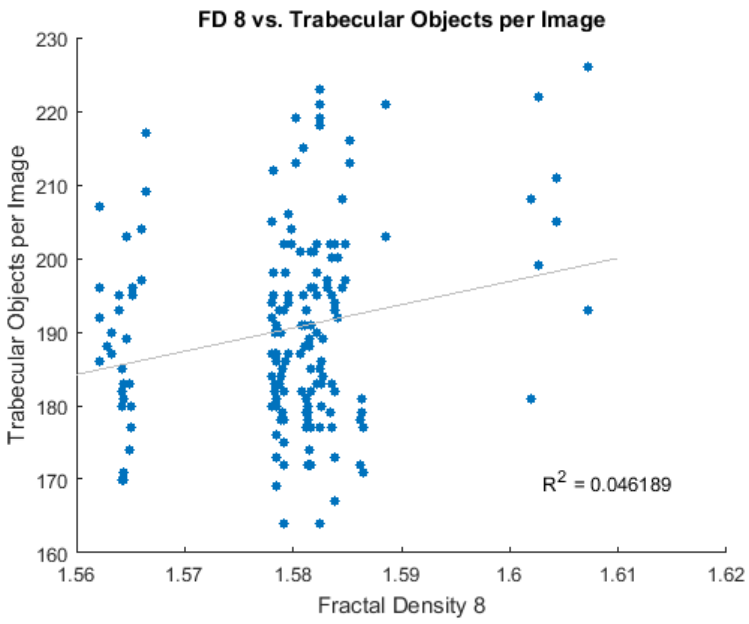

FD8 vs. Plates

```
figure
h2 = FD8;
y2 = Plates;
sz=25;
scatter(h2,y2,sz,'o','filled')
title('FD 8 vs. Number of Plates per Image')
xlabel('Fractal Density 8')
ylabel('Plates Counted per Image')

mdl = fitlm(h2,y2)
lsline
mdl.Rsquared.Ordinary

rsq = ['R^2 = ',num2str(mdl.Rsquared.Ordinary)];
text(1.615,25,rsq,'HorizontalAlignment','right')

hold on
```

```
mdl =


Linear regression model:
    y ~ 1 + x1

Estimated Coefficients:
                   Estimate      SE       tStat       pValue
                   ________    ______    _______    __________

    (Intercept)    -367.76     63.094    -5.8287    2.9633e-08
    x1              253.27     39.949     6.3397    2.2198e-09
```

```
Number of observations: 163, Error degrees of freedom: 161
Root Mean Squared Error: 4.57
R-squared: 0.2,  Adjusted R-Squared 0.195
F-statistic vs. constant model: 40.2, p-value = 2.22e-09

ans =

    0.1998
```

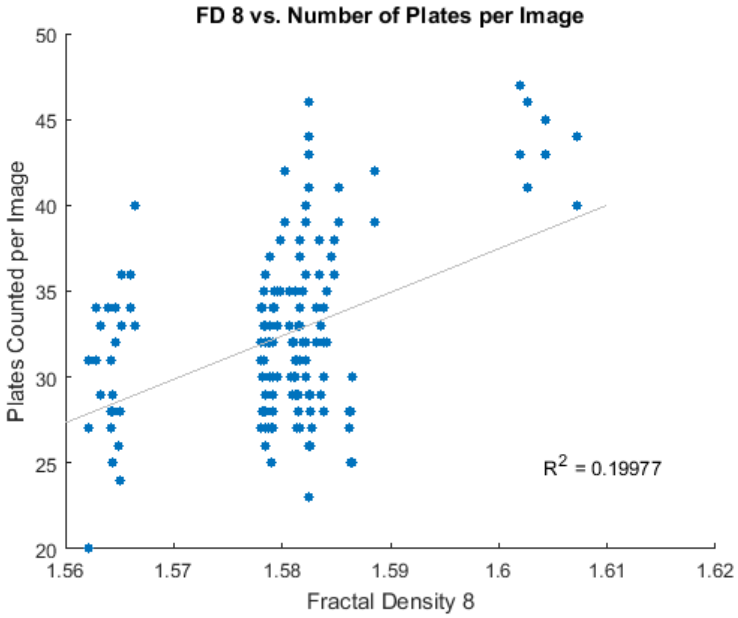

FD8 vs. Rods

```
figure
h3 = FD8;
y3 = Rods;
sz=25;
scatter(h3,y3,sz,'o','filled')
title('FD 8 vs. Number of Rods per Image')
xlabel('Fractal Density 8')
ylabel('Rods Counted per Image')

mdl = fitlm(h3,y3)
lsline
mdl.Rsquared.Ordinary

rsq = ['R^2 = ',num2str(mdl.Rsquared.Ordinary)];
text(1.615,110,rsq,'HorizontalAlignment','right')

hold on
```

```
mdl =


Linear regression model:
    y ~ 1 + x1

Estimated Coefficients:
                   Estimate      SE       tStat       pValue
                   ________    ______    ________    ________

    (Intercept)    -120.75     124.77    -0.96771     0.33464
    x1               156.6     79.003      1.9822    0.049154


Number of observations: 163, Error degrees of freedom: 161
Root Mean Squared Error: 9.03
R-squared: 0.0238,  Adjusted R-Squared 0.0178
F-statistic vs. constant model: 3.93, p-value = 0.0492

ans =

    0.0238
```

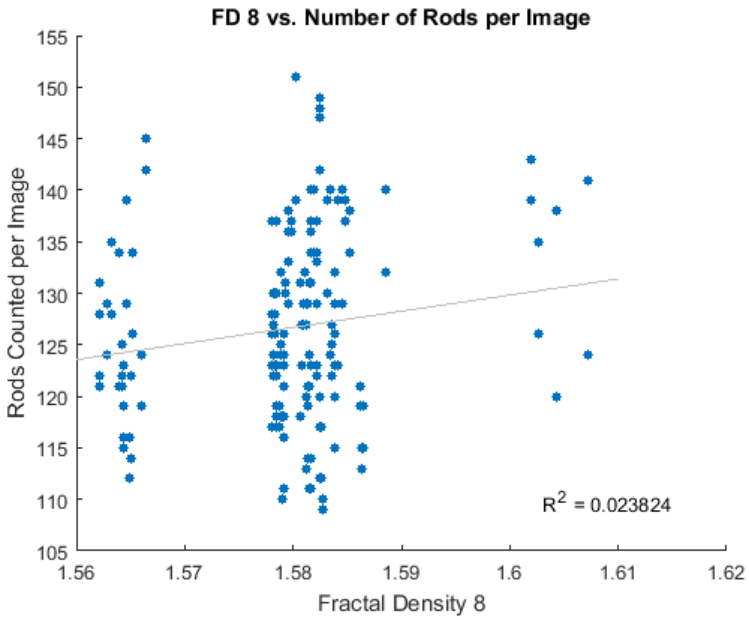

FD8 vs. Avg Tb Size

```
figure
h4 = FD8;
y4 = AverageSize;
sz=25;
scatter(h4,y4,sz,'o','filled')
title('FD 8 vs. Average Size of Trabecular Objects per Image')
```

```
xlabel('Fractal Density 8')
ylabel('Average Tb Size per Image (mm)')

mdl = fitlm(h4,y4)
lsline
mdl.Rsquared.Ordinary

rsq = ['R^2 = ',num2str(mdl.Rsquared.Ordinary)];
text(1.615,0.29,rsq,'HorizontalAlignment','right')

hold on
```

```
mdl =


Linear regression model:
    y ~ 1 + x1

Estimated Coefficients:
                   Estimate      SE       tStat       pValue
                   ________    _______    ______    __________

    (Intercept)      1.0635    0.30873    3.4449    0.00072859
    x1              -0.45154   0.19548     -2.31      0.022161


Number of observations: 163, Error degrees of freedom: 161
Root Mean Squared Error: 0.0223
R-squared: 0.0321,  Adjusted R-Squared 0.0261
F-statistic vs. constant model: 5.34, p-value = 0.0222

ans =

    0.0321
```

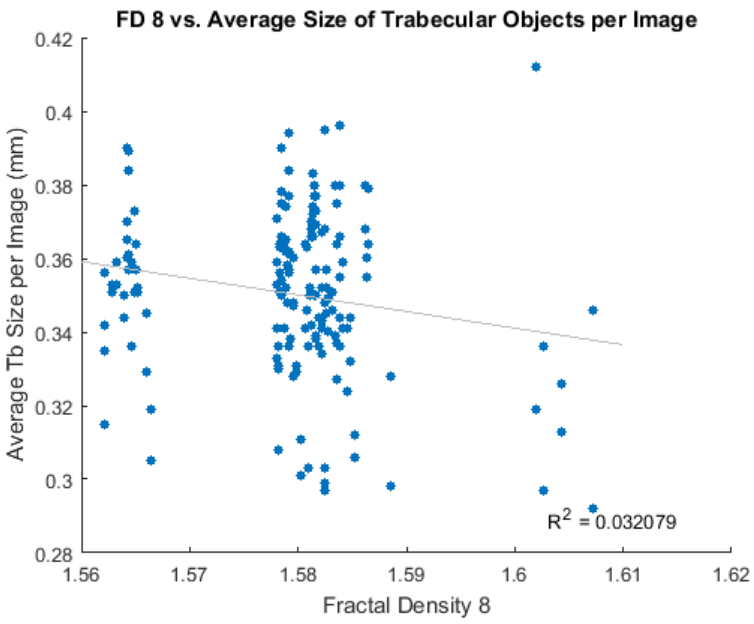

FD8 vs. % Tb Area

```
figure
h5 = FD8;
y5 = Area;
sz=25;
scatter(h5,y5,sz,'o','filled')
title('FD 8 vs. Percent Trabecular Area per Image')
xlabel('Fractal Density 8')
ylabel('Percent Trabecular Area per Image')

mdl = fitlm(h5,y5)
lsline
mdl.Rsquared.Ordinary

rsq = ['R^2 = ',num2str(mdl.Rsquared.Ordinary)];
text(1.615,11.6,rsq,'HorizontalAlignment','right')

hold on
```

```
mdl =


Linear regression model:
    y ~ 1 + x1

Estimated Coefficients:
                   Estimate      SE      tStat      pValue
                   ________    ______    ______    ________

    (Intercept)    8.2369      3.2791    2.5119    0.012993
    x1             2.3297      2.0762    1.1221     0.26351
```

```
Number of observations: 163, Error degrees of freedom: 161
Root Mean Squared Error: 0.237
R-squared: 0.00776,  Adjusted R-Squared 0.0016
F-statistic vs. constant model: 1.26, p-value = 0.264

ans =

    0.0078
```

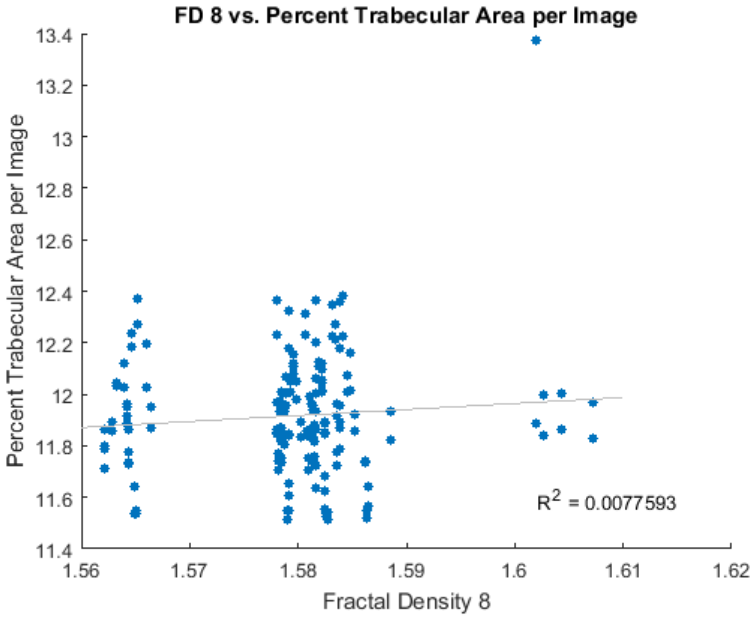

FD8 vs. Avg Spatial Anglular Offset in 2D

```
figure
h6 = FD8;
y6 = AvgAngle;
sz=25;
scatter(h6,y6,sz,'o','filled')
title('FD 8 vs. Average Spatial Angle between Trabeculae')
xlabel('Fractal Density 8')
ylabel('Average Angle Observed per Image')

mdl = fitlm(h6,y6)
lsline
mdl.Rsquared.Ordinary

rsq = ['R^2 = ',num2str(mdl.Rsquared.Ordinary)];
text(1.615,114,rsq,'HorizontalAlignment','right')

hold on
```

```
mdl =


Linear regression model:
    y ~ 1 + x1

Estimated Coefficients:
                   Estimate      SE        tStat        pValue
                   ________    ______    _________    __________

    (Intercept)     118.51     25.414       4.6631    6.5055e-06
    x1             -1.3132     16.091    -0.081607       0.93506


Number of observations: 163, Error degrees of freedom: 161
Root Mean Squared Error: 1.84
R-squared: 4.14e-05,  Adjusted R-Squared -0.00617
F-statistic vs. constant model: 0.00666, p-value = 0.935

ans =

   4.1363e-05
```

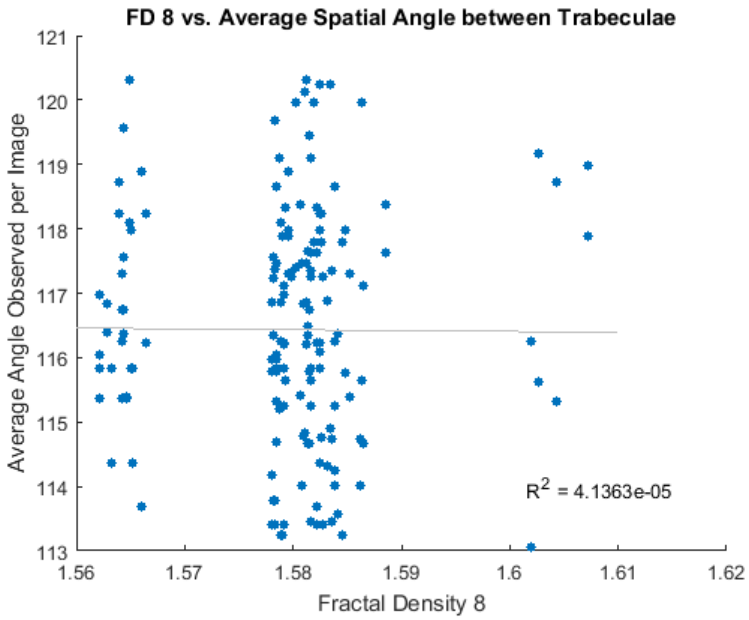

Published with MATLAB® R2015b

A8. All of the plots for FD8 were generated using the MATLAB code above.

FD1 JMP INTERACTIONS MODEL

Reduction Results – FD1

Summary of Fit

RSquare	0.921412
RSquare Adj	0.91839
Root Mean Square Error	0.00198
Mean of Response	1.629596
Observations (or Sum Wgts)	163

Analysis of Variance

Source	DF	Sum of Squares	Mean Square	F Ratio
Model	6	0.00717300	0.001196	304.8414
Error	156	0.00061179	3.922e-6	Prob > F
C. Total	162	0.00778479		<.0001*

Parameter Estimates

Term	Estimate	Std Error	t Ratio	Prob>|t|
Intercept	1.0761623	0.023796	45.22	<.0001*
Tb. Object Count	0.0014585	0.000064	22.80	<.0001*
Avg. Tb. Size	0.7490647	0.035666	21.00	<.0001*
Plate Count	0.0004209	5.37e-5	7.84	<.0001*
(Tb. Object Count-190.337)*(Plate Count-32.2331)*(Rod Count-126.779)	-1.224e-5	2.421e-6	-5.05	<.0001*
(Avg. Tb. Size-0.35039)*(Plate Count-32.2331)*(Rod Count-126.779)	-0.007151	0.001495	-4.78	<.0001*
(% Area-11.9161)*(Plate Count-32.2331)*(Rod Count-126.779)	0.0001791	0.000047	3.80	0.0002*

A9. The table above shows the final reduction for FD1 parameters based on significance.

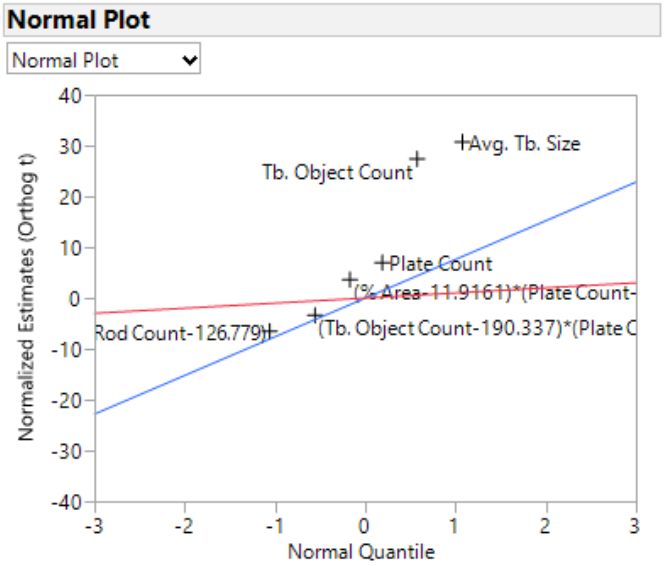

Blue line has slope equal to Lenth's PSE.
Red line has slope 1.

A10. The normal plot for FD1 shows a graphical representation of factor significance. The factors furthest from the center have the most significant effects.

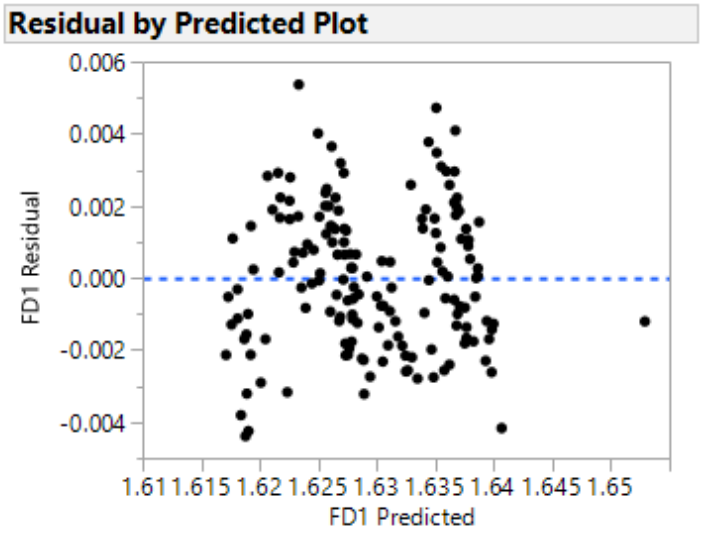

A11. The residual plot for FD1 is shown above. Random, evenly distributed data points indicate a normal data set if they are symmetric across the horizontal line.

Prediction Expression

1.07616225521493
+ 0.00145853098864 * Tb. Object Count
+ 0.74906468692572 * Avg. Tb. Size
+ 0.00042086565003 * Plate Count
(Tb. Object Count - 190.337423312883)
+ (Plate Count - 32.2331288343558) * (Rod Count - 126.779141104294) * -0.0000122375359
(Avg. Tb. Size - 0.35039263803681)
+ (Plate Count - 32.2331288343558) * (Rod Count - 126.779141104294) * -0.0071507392896
(% Area - 11.9161288343558)
+ (Plate Count - 32.2331288343558) * (Rod Count - 126.779141104294) * 0.00017911947197

A12. The prediction expression for FD1 is shown as given by the JMP software after calculation.

FD2 JMP INTERACTIONS MODEL

Reduction Results – FD2

Summary of Fit

RSquare	0.087451
RSquare Adj	0.052353
Root Mean Square Error	0.01373
Mean of Response	1.633875
Observations (or Sum Wgts)	163

Analysis of Variance

Source	DF	Sum of Squares	Mean Square	F Ratio
Model	6	0.00281832	0.000470	2.4916
Error	156	0.02940910	0.000189	Prob > F
C. Total	162	0.03222743		0.0249*

Parameter Estimates

Term	Estimate	Std Error	t Ratio	Prob>|t|
Intercept	1.6336995	0.001105	1479.0	<.0001*
(Tb. Object Count-190.337)*(Tb. Angular Offset-116.433)*(Plate Count-32.2331)	-0.000441	0.00015	-2.94	0.0038*
(Tb. Object Count-190.337)*(Tb. Angular Offset-116.433)*(Rod Count-126.779)	0.0003212	8.954e-5	3.59	0.0004*
(Tb. Angular Offset-116.433)*(Avg. Tb. Size-0.35039)*(Plate Count-32.2331)	-0.26146	0.087977	-2.97	0.0034*
(Tb. Angular Offset-116.433)*(Avg. Tb. Size-0.35039)*(Rod Count-126.779)	0.1908848	0.052384	3.64	0.0004*
(Tb. Angular Offset-116.433)*(% Area-11.9161)*(Plate Count-32.2331)	0.0066572	0.002529	2.63	0.0093*
(Tb. Angular Offset-116.433)*(% Area-11.9161)*(Rod Count-126.779)	-0.004831	0.001382	-3.49	0.0006*

A13. The table above shows the final reduction for FD2 parameters by significance.

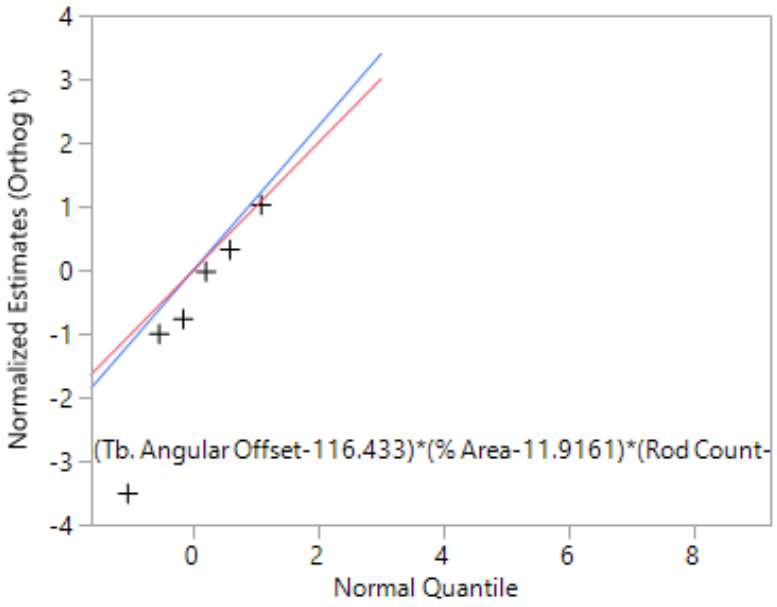

A14. The normal plot for FD2 shows a graphical representation of factor significance. The factors furthest from the center have the most significant effects.

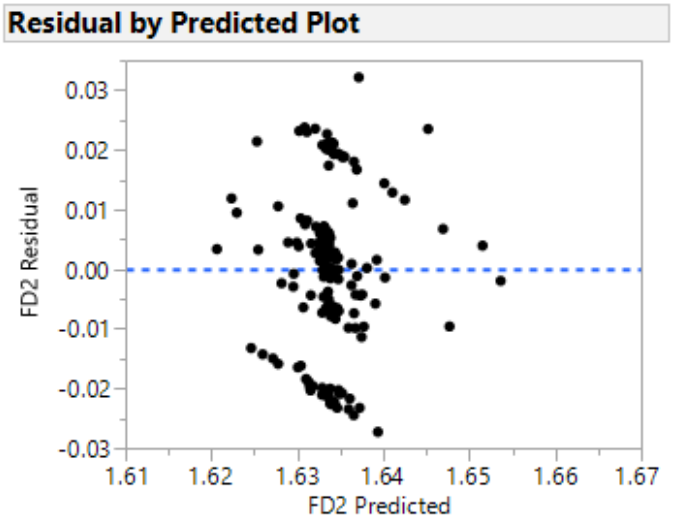

A15. The residual plot for FD2 is shown above. Random, evenly distributed data points indicate a normal data set if they are symmetric across the horizontal line.

Prediction Expression

1.63369954203805
+ (Tb. Object Count - 190.337423312883) * ((Tb. Angular Offset - 116.433368098159) * ((Plate Count - 32.2331288343558) * -0.0004409211076))
+ (Tb. Object Count - 190.337423312883) * ((Tb. Angular Offset - 116.433368098159) * ((Rod Count - 126.779141104294) * 0.00032124665762))
+ (Tb. Angular Offset - 116.433368098159) * ((Avg. Tb. Size - 0.35039263803681) * ((Plate Count - 32.2331288343558) * -0.2614600518419))
+ (Tb. Angular Offset - 116.433368098159) * ((Avg. Tb. Size - 0.35039263803681) * ((Rod Count - 126.779141104294) * 0.19088479038855))
+ (Tb. Angular Offset - 116.433368098159) * ((% Area - 11.9161288343558) * ((Plate Count - 32.2331288343558) * 0.00665720141337))
+ (Tb. Angular Offset - 116.433368098159) * ((% Area - 11.9161288343558) * ((Rod Count - 126.779141104294) * -0.0048306119663))

A16. The prediction expression for FD2 is shown as given by the JMP software after calculation.

FD3 JMP INTERACTIONS MODEL

Reduction Results – FD3

Summary of Fit

RSquare	0.807633
RSquare Adj	0.800234
Root Mean Square Error	0.002218
Mean of Response	1.580558
Observations (or Sum Wgts)	163

Analysis of Variance

Source	DF	Sum of Squares	Mean Square	F Ratio
Model	6	0.00322297	0.000537	109.1585
Error	156	0.00076767	4.921e-6	Prob > F
C. Total	162	0.00399064		<.0001*

Parameter Estimates

Term	Estimate	Std Error	t Ratio	Prob>|t|
Intercept	1.3767638	0.038371	35.88	<.0001*
Avg. Tb. Size	0.2726567	0.094679	2.88	0.0045*
% Area	0.006184	0.002527	2.45	0.0155*
Plate Count	-0.000452	5.64e-5	-8.02	<.0001*
Rod Count	-9.634e-5	2.871e-5	-3.36	0.0010*
(Tb. Object Count-190.337)*(% Area-11.9161)	0.00027	8.638e-5	3.13	0.0021*
Tb. Object Count	0.0003213	0.000173	1.85	0.0655

A17. The table above shows the final reduction for FD3 parameters by significance.

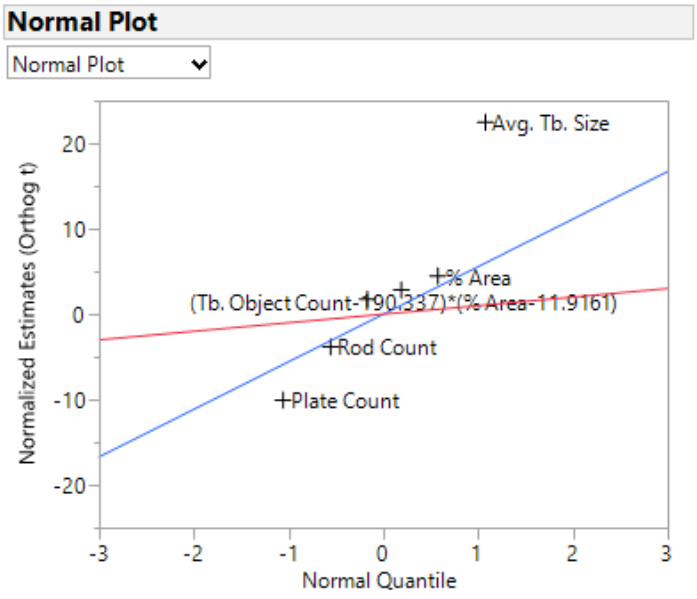

A18. The normal plot for FD3 shows a graphical representation of factor significance. The factors furthest from the center have the most significant effects.

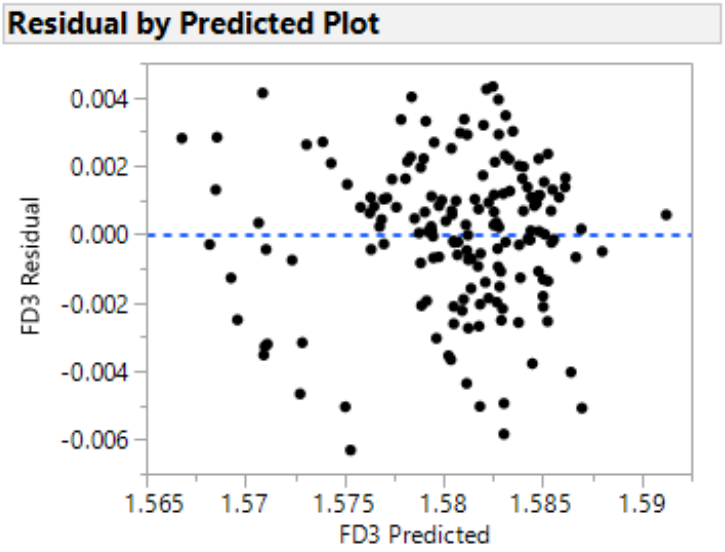

A19. The residual plot for FD3 is shown above. Random, evenly distributed data points indicate a normal data set if they are symmetric across the horizontal line.

Prediction Expression

1.3767638018136
+ 0.27265666334751 * Avg. Tb. Size
+ 0.00618396615367 * % Area
+ -0.0004523463197 * Plate Count
+ -0.0000963374405 * Rod Count
+ (Tb. Object Count - 190.337423312883) * ((% Area - 11.9161288343558) * 0.00027002629552)
+ 0.0003212549372 * Tb. Object Count

A20. The prediction expression for FD3 is shown as given by the JMP software after calculation.

FD4 JMP INTERACTIONS MODEL

Reduction Results – FD4

Analysis of Variance

Source	DF	Sum of Squares	Mean Square	F Ratio
Model	5	0.00278378	0.000557	18.7006
Error	157	0.00467423	0.000030	Prob > F
C. Total	162	0.00745801		<.0001*

Parameter Estimates

Term	Estimate	Std Error	t Ratio	Prob>|t|
Intercept	1.443776	0.092928	15.54	<.0001*
Tb. Object Count	0.0007615	0.000423	1.80	0.0740
Avg. Tb. Size	0.4327152	0.231734	1.87	0.0637
% Area	-0.01474	0.006212	-2.37	0.0189*
Plate Count	0.0010333	0.000139	7.45	<.0001*
Rod Count	-0.000234	6.965e-5	-3.36	0.0010*

A21. The table above shows the final reduction for FD4 parameters by significance.

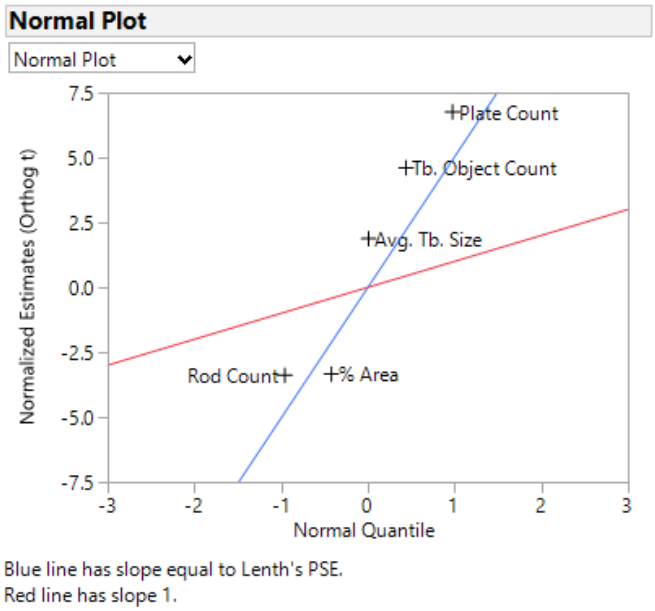

A22. The normal plot for FD4 shows a graphical representation of factor significance. The factors furthest from the center have the most significant effects.

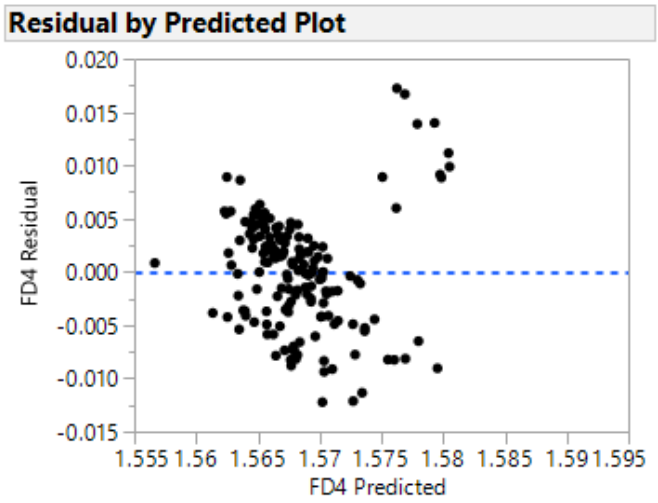

A23. The residual plot for FD4 is shown above. Random, evenly distributed data points indicate a normal data set if they are symmetric across the horizontal line.

Prediction Expression
1.44377603805121
+ 0.00076147173576 * Tb. Object Count
+ 0.43271516437592 * Avg. Tb. Size
+ -0.0147397154696 * % Area
+ 0.00103333069117 * Plate Count
+ -0.0002337184295 * Rod Count

A24. The prediction expression for FD4 is shown as given by the JMP software after calculation.

FD5 JMP INTERACTIONS MODEL

Reduction Results – FD5

Analysis of Variance

Source	DF	Sum of Squares	Mean Square	F Ratio
Model	4	0.01058403	0.002646	327.3637
Error	158	0.00127708	8.083e-6	Prob > F
C. Total	162	0.01186111		<.0001*

Parameter Estimates

Term	Estimate	Std Error	t Ratio	Prob>|t|
Intercept	1.3608553	0.01344	101.26	<.0001*
% Area	0.0232096	0.00118	19.67	<.0001*
Plate Count	0.0007658	0.000053	14.45	<.0001*
(Tb. Object Count-190.337)*(% Area-11.9161)	-0.000597	0.000114	-5.24	<.0001*
(Avg. Tb. Size-0.35039)*(% Area-11.9161)*(Plate Count-32.2331)	-0.023947	0.00255	-9.39	<.0001*

A25. The table above shows the final reduction for FD5 parameters by significance.

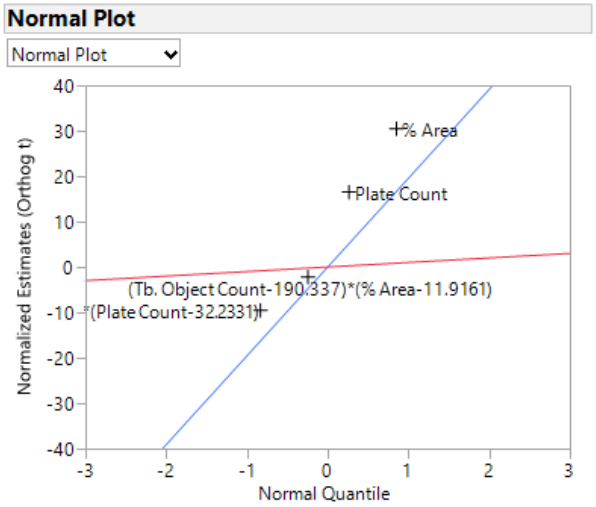

Blue line has slope equal to Lenth's PSE.
Red line has slope 1.

A26. The normal plot for FD5 shows a graphical representation of factor significance. The factors furthest from the center have the most significant effects.

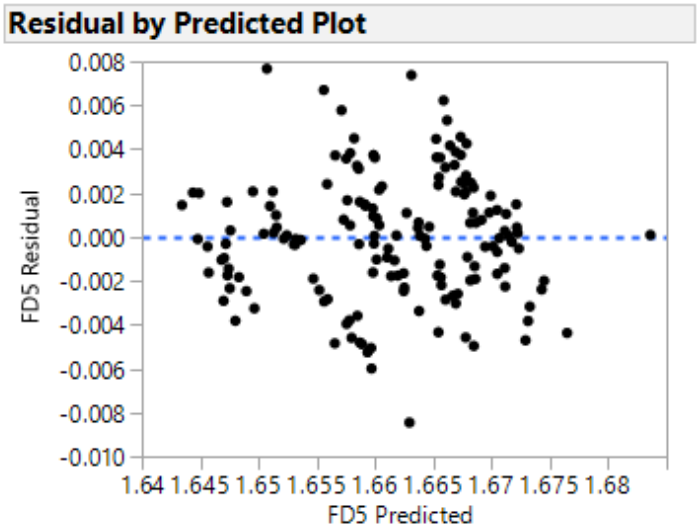

A27. The residual plot for FD5 is shown above. Random, evenly distributed data points indicate a normal data set if they are symmetric across the horizontal line.

Prediction Expression

1.36085533652696
+ 0.023209614441 75 * % Area
+ 0.00076576290082 * Plate Count
+ (Tb. Object Count - 190.337423312883)
* ((% Area - 11.9161288343558) * -0.000596593346)
+ (Avg. Tb. Size - 0.35039263803681)
* ((% Area - 11.9161288343558) * ((Plate Count - 32.2331288343558) * -0.0239465991315))

A28. The prediction expression for FD5 is shown as given by the JMP software after calculation.

FD6 JMP INTERACTIONS MODEL

Reduction Results – FD6

Summary of Fit

RSquare	0.091217
RSquare Adj	0.056264
Root Mean Square Error	0.013384
Mean of Response	1.666905
Observations (or Sum Wgts)	163

Analysis of Variance

Source	DF	Sum of Squares	Mean Square	F Ratio
Model	6	0.00280499	0.000467	2.6097
Error	156	0.02794559	0.000179	Prob > F
C. Total	162	0.03075058		0.0194*

Parameter Estimates

Term	Estimate	Std Error	t Ratio	Prob>|t|
Intercept	1.6667223	0.001077	1547.9	<.0001*
(Tb. Object Count-190.337)*(Tb. Angular Offset-116.433)*(Plate Count-32.2331)	-0.00041	0.000146	-2.80	0.0057*
(Tb. Object Count-190.337)*(Tb. Angular Offset-116.433)*(Rod Count-126.779)	0.0003183	8.729e-5	3.65	0.0004*
(Tb. Angular Offset-116.433)*(Avg. Tb. Size-0.35039)*(Plate Count-32.2331)	-0.243196	0.08576	-2.84	0.0052*
(Tb. Angular Offset-116.433)*(Avg. Tb. Size-0.35039)*(Rod Count-126.779)	0.1897117	0.051064	3.72	0.0003*
(Tb. Angular Offset-116.433)*(% Area-11.9161)*(Plate Count-32.2331)	0.0060585	0.002466	2.46	0.0151*
(Tb. Angular Offset-116.433)*(% Area-11.9161)*(Rod Count-126.779)	-0.004762	0.001347	-3.53	0.0005*

A29. The table above shows the final reduction for FD6 parameters by significance.

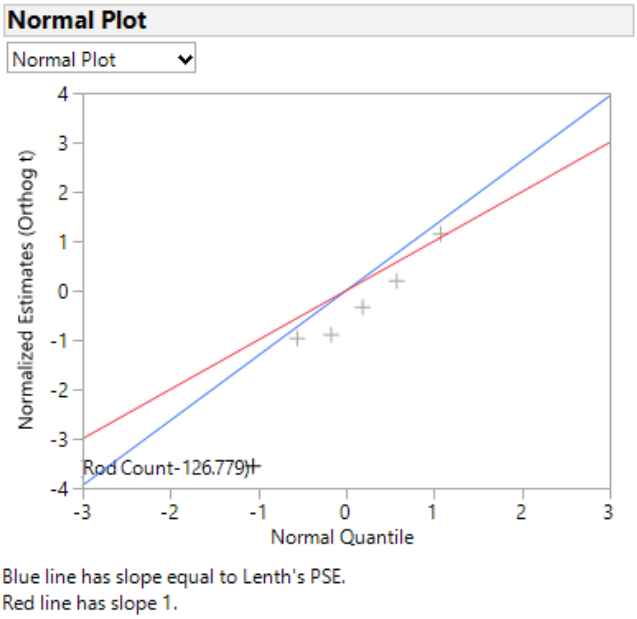

A30. The normal plot for FD6 shows a graphical representation of factor significance. The factors furthest from the center have the most significant effects.

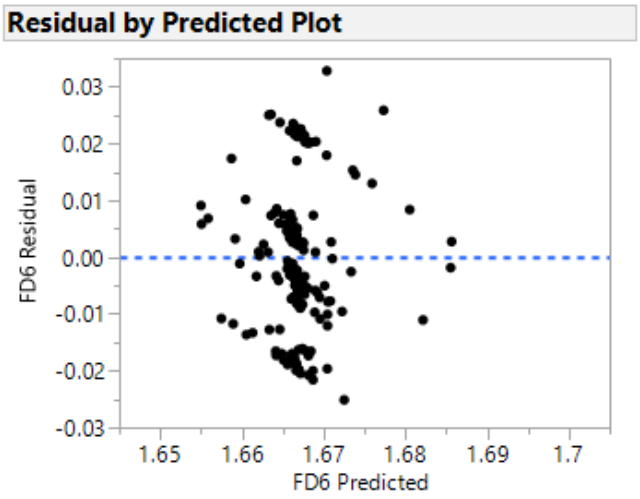

A31. The residual plot for FD6 is shown above. Random, evenly distributed data points indicate a normal data set if they are symmetric across the horizontal line.

Prediction Expression

1.66672226925097
+ (Tb. Object Count - 190.337423312883) * ((Tb. Angular Offset - 116.433368098159) * ((Plate Count - 32.2331288343558) * -0.0004098121963))
+ (Tb. Object Count - 190.337423312883) * ((Tb. Angular Offset - 116.433368098159) * ((Rod Count - 126.779141104294) * 0.00031833752138))
+ (Tb. Angular Offset - 116.433368098159) * ((Avg. Tb. Size - 0.35039263803681) * ((Plate Count - 32.2331288343558) * -0.2431959334308))
+ (Tb. Angular Offset - 116.433368098159) * ((Avg. Tb. Size - 0.35039263803681) * ((Rod Count - 126.779141104294) * 0.18971166744582))
+ (Tb. Angular Offset - 116.433368098159) * ((% Area - 11.9161288343558) * ((Plate Count - 32.2331288343558) * 0.00605852849335))
+ (Tb. Angular Offset - 116.433368098159) * ((% Area - 11.9161288343558) * ((Rod Count - 126.779141104294) * -0.0047621479855))

A32. The prediction expression for FD6 is shown as given by the JMP software after calculation.

FD7 JMP INTERACTIONS MODEL

Reduction Results – FD7

Summary of Fit

RSquare	0.732182
RSquare Adj	0.725402
Root Mean Square Error	0.003268
Mean of Response	1.596175
Observations (or Sum Wgts)	163

Analysis of Variance

Source	DF	Sum of Squares	Mean Square	F Ratio
Model	4	0.00461413	0.001154	107.9882
Error	158	0.00168776	0.000011	Prob > F
C. Total	162	0.00630189		<.0001*

Parameter Estimates

Term	Estimate	Std Error	t Ratio	Prob>|t|
Intercept	1.3835399	0.015295	90.46	<.0001*
% Area	0.0219982	0.001397	15.74	<.0001*
Plate Count	-0.000953	7.111e-5	-13.41	<.0001*
Rod Count	-0.000147	3.951e-5	-3.72	0.0003*
(Avg. Tb. Size-0.35039)*(% Area-11.9161)*(Rod Count-126.779)	-0.006435	0.002461	-2.61	0.0098*

A33. The table above shows the final reduction for FD7 parameters by significance.

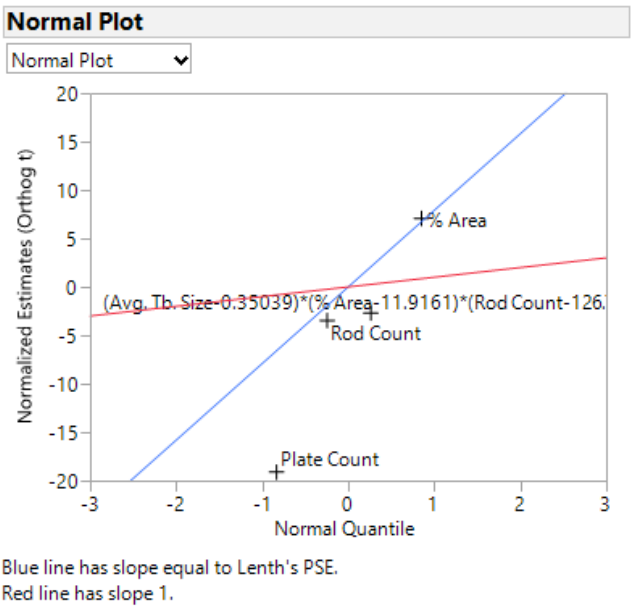

A34. The normal plot for FD7 shows a graphical representation of factor significance. The factors furthest from the center have the most significant effects.

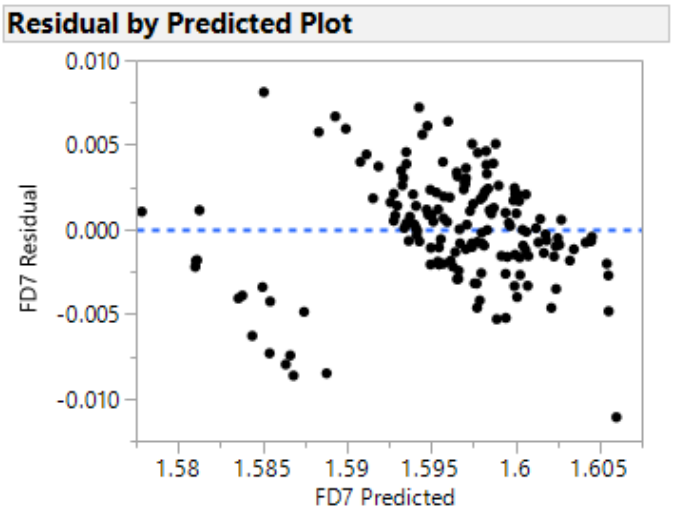

A35. The residual plot for FD7 is shown above. Random, evenly distributed data points indicate a normal data set if they are symmetric across the horizontal line.

Prediction Expression

1.38353992424561
+ 0.02199815257691 * % Area
+ -0.0009533023075 * Plate Count
+ -0.0001470534566 * Rod Count
+ (Avg. Tb. Size - 0.35039263803681)
* ((% Area - 11.9161288343558) * ((Rod Count - 126.779141104294) * -0.0064351335706))

A36. The prediction expression for FD7 is shown as given by the JMP software after calculation.

FD8 JMP INTERACTIONS MODEL

Reduction Results – FD8

Summary of Fit

RSquare	0.272935
RSquare Adj	0.259217
Root Mean Square Error	0.007729
Mean of Response	1.579323
Observations (or Sum Wgts)	163

Analysis of Variance

Source	DF	Sum of Squares	Mean Square	F Ratio
Model	3	0.00356599	0.001189	19.8958
Error	159	0.00949938	0.000060	Prob > F
C. Total	162	0.01306537		<.0001*

Parameter Estimates

Term	Estimate	Std Error	t Ratio	Prob>|t|
Intercept	1.6700044	0.0354	47.17	<.0001*
% Area	-0.010655	0.003179	-3.35	0.0010*
Plate Count	0.001133	0.000149	7.61	<.0001*
(Tb. Angular Offset-116.433)*(Plate Count-32.2331)*(Rod Count-126.779)	-1.421e-5	4.33e-6	-3.28	0.0013*

A37. The table above shows the final reduction for FD8 parameters by significance

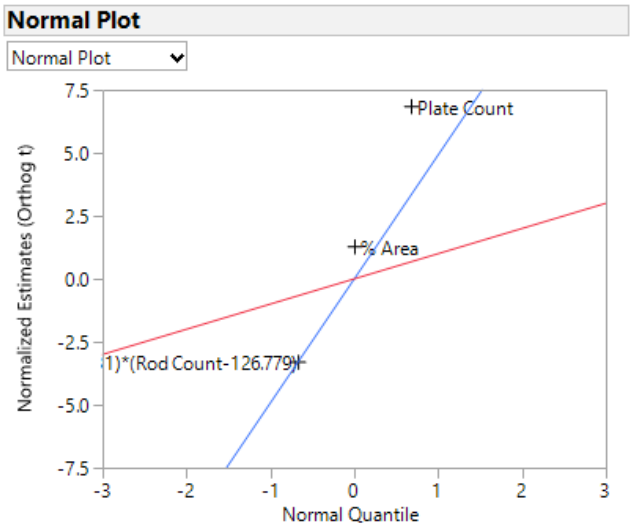

Blue line has slope equal to Lenth's PSE.
Red line has slope 1.

A38. The normal plot for FD8 shows a graphical representation of factor significance. The factors furthest from the center have the most significant effects.

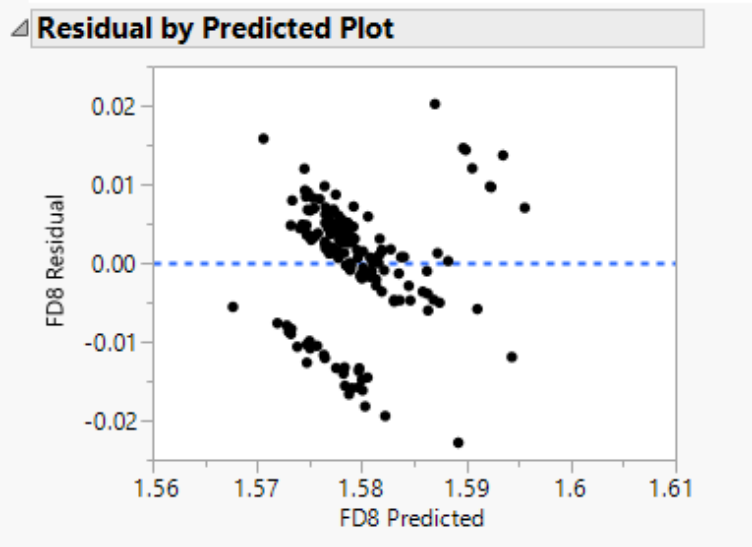

A39. The residual plot for FD8 is shown above. Random, evenly distributed data points indicate a normal data set if they are symmetric across the horizontal line.

Prediction Expression

1.6700043901679
+ -0.0106547902652 * % Area
+ 0.00113296562713 * Plate Count
(Tb. Angular Offset - 116.433368098159)
+ * [(Plate Count - 32.2331288343558)
* [(Rod Count - 126.779141104294) * -0.000014209696]]

A40. The prediction expression for FD8 is shown as given by the JMP software after calculation.